Alma Mater Studiorum- Università di Bologna
in cotutela con Université Claude Bernard, Lyon1

DOTTORATO DI RICERCA IN SCIENZE BIOMEDICHE
CURRICULUM NEUROFISIOLOGIA

XXVII ciclo

Settore Concorsuale di afferenza: 05/D1

Settore Scientifico disciplinare: BIO/09

The posterior parietal cortex: a bridge between vision and action

Presentata da: **Dott. Giulia Dal Bò**

Coordinatore Dottorato
Prof. Lucio Cocco

Relatore
Prof. Patrizia Fattori

Relatore
Dr. Martine Meunier

Esame finale anno 2015

CONTENTS

1. INTRODUCTION **6**

1.1 fMRI and electrophysiology: two methods in the mirror 9

1.2 Visuospatial processing 11

- ✓ The occipito-parietal pathway 14
- ✓ Parieto-prefrontal pathway 15
- ✓ Parieto-premotor pathway 15
- ✓ Parieto-medial temporal pathway 16

1.3 The Posterior Parietal Cortex (PPC) 19

1.4 The perception of motion 21

1.5 Motion visual areas 22

1.6 Lesions of the motion areas in monkeys and humans 25

1.7 The medial motion area V6 27

- ✓ Area V6 in macaque monkeys 27
- ✓ Area V6 in human 37

1.8 Visually Guided Actions 42

1.9 Encoding of 3D space 43

1.10 Lesions of the parietal areas in monkeys and humans 48

1.11 Role of parietal area V6A 58

1.12 Role of parietal area PEc 64

1.13 Aim of the work 67

2 MATERIALS AND METHODS **70**

2.1 Ethics 70

2.2 General and experimental procedures 70

- ✓ fMRI: training and scanning procedures 70
- ✓ Electrophysiology: training and recording procedures 71

2.3 V6 and MT mapping 73

- ✓ Data Analysis 76

2.4 Checking of visual and somatosensory properties 78

- ✓ Visual stimulation 79
- ✓ Somatosensory stimulation 81

✓ Data analysis....83
2.5 Motor Related Activity....85
✓ Data Analysis....88
2.6 Histological Reconstruction of the Recording Sites....91
2.7 Two-dimensional and Three-dimensional Cortical Maps....94
3 RESULTS....97
3.1 V6 and MT Mapping....97
3.2 Visual and Somatosensory properties....107
✓ Visual Properties....108
✓ Somatic properties....113
3.3 Motor Related Activity in 3D Space....125
✓ Tuning for depth and direction in the different task epochs....125
✓ Spatial preference and consistency across epochs....128
✓ Relationship between eye position and arm movement signals....132
✓ Comparison with V6A....135
4 DISCUSSION....138
4.1 Monkey medial PPC: visual motion sensitivity....138
✓ Comparison with human studies....140
✓ Functional role of area V6....140
✓ Activations in surrounding areas....143
4.2 Sensory properties....145
✓ Comparison with other parietal areas....146
✓ Functional Role of area PEc....150
4.3 Motor Related Activity in 3D Space within SPL....153
✓ Role of PEc in arm movements in 3D space....154
✓ Comparison of PEc with V6A and other PPC areas....155
✓ Are PEc and V6A the same functional area?....159
✓ Clarifications....161
5 FUTURE DIRECTIONS....163
6 ACKNOWLEDGEMENTS....164
7 REFERENCES....165

LIST OF FIGURES

Figure 1: *Circuits among brain regions useful for the interactions between the subject and the world.* 7
Figure 2: *Evolution of the "two visual system theory" in time*..... 12
Figure 3: *Anatomy of the three pathways within the dorsal stream, following the model proposed by Kravitz et al. (2011)* 17
Figure 4: *The areas of the medial posterior parietal cortex*. 19
Figure 5: *Example of retinal optic flow*. 21
Figure 6: *Direction selectivity and inputs of area MT*. 23
Figure 7: *MT lesions in monkey and human*. 25
Figure 8: *Location and visual topography of macaque area V6*. 29
Figure 9: *Visual motion sensitivity in area V6.* 29
Figure 10: *RF size versus eccentricity in area V6*. 31
Figure 11: *Visual field representation in V6*. 32
Figure 12: *V6 connections*. 33
Figure 13: *Example of real motion cell of area V6*. 35
Figure 14: *Location and retinotopy of human area V6*. 38
Figure 15: *Retinotopy of eccentricity representation of area V6*. 39
Figure 16: *V6 location in macaque and human brains*. 39
Figure 17: *Motion-selectivity of human V6*. 41
Figure 18: *Perception of distances.* 43
Figure 19: *Impairments in monkey's finger coordination*. 49
Figure 20: *Unilateral visual neglect*. 50
Figure 21: *Patient with optic ataxia*. 51
Figure 22: *Impairments for movements towards different directions and depths*. 54
Figure 23: *Effects of V6A lesions in macaque monkey*. 57
Figure 24: *Visual receptive fields "jumping" in area V6A*. 59
Figure 25: *Spatially tuned modulations in V6A*. 60
Figure 26: *Connections of the ventral (V6AV) and dorsal (V6AD) sectors of area V6A*... 62
Figure 27: *Directional reach neuron of area PEc*. 64
Figure 28: *Anatomical connections of area PEc*. 65
Figure 29: *Experimental fMRI setup*. 74
Figure 30: *Sensory and motor tasks*. 79
Figure 31: *Stimuli used to map the visual receptive fields*. 80
Figure 32: *Somatosensory stimulation*..... 82
Figure 33: *Experimental setup and task sequence.* 87
Figure 34: *Architectural characteristics of area V6, V6A, PEc and PE.* 91
Figure 35: *Bidimensional map of the recording sites*. 95
Figure 36: *Location of area MT*. 98
Figure 37: *Location of area V6*. 99
Figure 38: *Radial-Rings stimulation, first functional session*. 100
Figure 39: *Radial-Rings stimulation, second functional session*..... 101
Figure 40: *Radial-Rings stimulation, average map*. 101
Figure 41: *Flow-Fields stimulation, first functional session*..... 102
Figure 42: *Flow-Fields stimulation, second functional session*. 103
Figure 43: *Flow-Fields stimulation, average maps.* 104
Figure 44: *Sum up of the functional activations for Flow-Fields and Radial-Rings stimuli*. 105
Figure 45: *Incidence and distribution of visual responses*. 108

Figure 46: *Receptive field distribution in the visual field*. 110
Figure 47: *Receptive field center distribution in the visual field.* 111
Figure 48: *Incidence and distribution of somatosensory responses in PEc and V6Ad*. . 113
Figure 49: *Laterality of somatosensory responses.* 115
Figure 50: *Somatosensory submodality.* 115
Figure 51: *Examples of somatosensory responses.* 116
Figure 52: *Incidence and distribution of somatic cells with receptive field in different body parts*. 118
Figure 53: *Somatotopy across area PEc and V6Ad*. 121
Figure 54: *Incidence of unimodal and bimodal visual and somatic cells*. 123
Figure 55: *Depth and direction tuning in an example PEc neuron*. 125
Figure 56: *Depth, direction and combined tuning during each task epoch and comparison between PEc and V6A*. 127
Figure 57: *Spatial preference in single epochs* 128
Figure 58: *Consistency of spatial preference across epochs*. 130
Figure 59: *Combination of eye and hand signals in SPL*. 131
Figure 60: *Population average activity of the main categories of cells*. 133
Figure 61: *Depth and direction coding in the cortical reach-related areas*. 158

1. INTRODUCTION

In everyday life, we constantly interact with other people and objects. We do all these actions in complex environments, in which people and objects are often moving around us and at different distances from us. We move in the world avoiding obstacles and dangers, we look in many different directions searching for what we are looking for and we interact with the object of our interest, reaching, grasping and moving it around the scene. We perform all these actions accurately and automatically without thinking to the direction in which eyes are moving or which muscle is contracting.

In most people's mind, vision has been identified for long time with visual perception ignoring its critical role in the planning and control of movement (cfr, Goodale, 2011). Goodale argued that the reason why this is commonly accepted is the idea that "… *our perception of the world beyond our bodies is such a compelling experience… this must be the main reason vision evolved*…". On the contrary he argued that "… *vision began not as a system for perceiving the world, but as a system for the distal control of movement*…" (Goodale, 2011). In natural conditions, we first visually capture the objects of our interest and only later, although imperceptively, we guide an action towards them. Simple and complex visually guided actions imply the existence of a link between the vision of the target and the desired state of the limb actions. This link integrates visual and proprioceptive information with motor signals to program an appropriate action, as outlined in the schema of Figure 1.

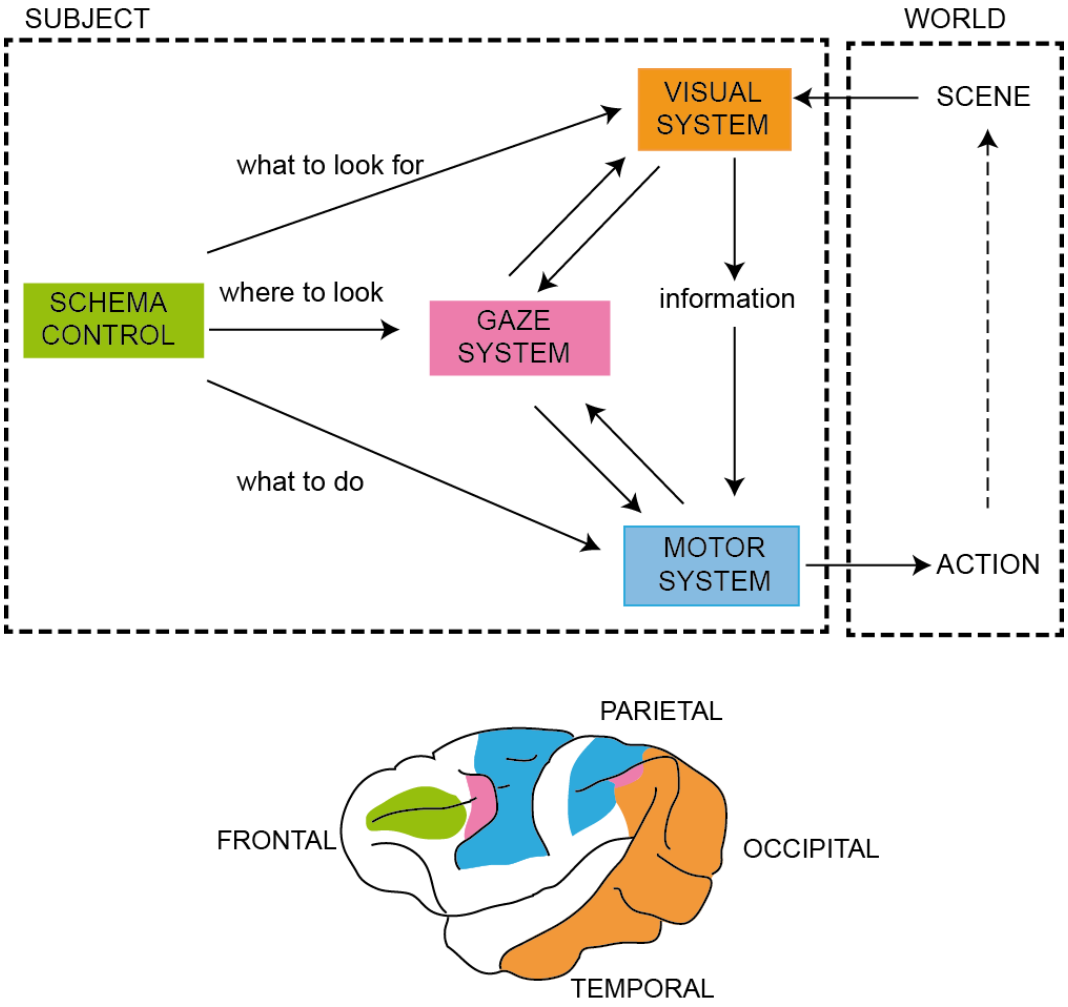

Figure 1: Circuits among brain regions useful for the interactions between the subject and the world.

Top) Relations of the schema, gaze, visual and motor systems during the performance of a visually guided action.

Bottom) Regions of the macaque cortex (shown on the left hemisphere) involved in the control of the systems outline in the schema above.

The schema system is mainly associated with the dorsolateral prefrontal cortex, the gaze system with frontal eye field and the lateral intraparietal cortex, the motor system with the frontal premotor and motor cortices and parts of the posterior parietal cortex and the visual system with occipital, parietal and temporal lobes. *Modified from (Land, 2009).*

This link is represented by the parietal lobe and more importantly by the posterior parietal cortex (PPC), located posteriorly to the postcentral gyrus and anteriorly to the occipital lobe. The PPC, the main argument of this dissertation, receives, among other signals, visual information form the striate and extrastriate areas of the occipital cortex, and is reciprocally connected to the cortical outputs-areas of the premotor and motor cortices (Archambault *et al*., 2014; Vingerhoets, 2014; Rizzolatti *et al*., 2014; Kravitz *et al*., 2011; Goodale, 2011; Filimon, 2010). A constellation of areas lie in this brain region, each of them involved in specific stages of the visuomotor transformation. These brain areas have been identified on the basis of their functional repertoire and cortico-cortical connections in non-human primates and in human brain thanks to the development of different neurophysiological methodologies. The PPC' areas operate on a multiplicity of signals as visual, somatosensory, auditory, vestibular and attentional, to cite only few of them. In this work, I will focus on visual, somatosensory and motor related signal used in the analysis of motion and in the arm movement control.

During the years different methods have been developed to study the brain behavior and functionality. First, the single cell recordings from awake animal, including the non-human primates, which correlates the activity of single cells with specific behavioral activities carried out by the animal; studies on lesions in brain regions in order to correlate specific dysfunctions to the brain region involved in the lesion. Using these techniques, it has been discovered that the mechanisms on the basis of perception of non-human primates were the same of human. Secondly, another informative technique is the study of patients with lesions in a particular region of the brain suffering specific cognitive deficit. The consequences of these lesions are more or less relevant on the basis of the functions carried out by the brain region involved in the lesion. Finally the most recent and useful techniques for exploring visuomotor function are imaging techniques, as PET (Positron Emission Tomography), and fMRI (Functional Magnetic

Resonance Imaging) that allowed to correlate directly *in vivo* on human brain, the changes on the activity of neural population in accordance with particular behavior. In this work I will preset data coming from all these techniques focusing particularly on data from single cell recording in non-human primates and fMRI both in human and non-human primates.

1.1 fMRI and electrophysiology: two methods in the mirror

Currently, microelectrode recordings provide the most precise recordings from single neuron, defined as a single firing neuron whose spike potentials (voltage change with respect to time) are distinctly isolated by a recording microelectrode placed near to the neuron body. The principle advantage of this method is the high spatiotemporal resolution but the disadvantage is that it is restrict to small sample of cells. During microelectrode recordings in fact, it is practically impossible to monitor every relevant neuron in the cortex so data resulting from this type of method report only the properties of the most active neurons that constitute a minority. Moreover, it is an invasive methodology and it requires a lot of time in recordings and analysis of data.

fMRI is based on the detection of oxygen levels in blood (blood oxygen level detection, BOLD), in this way it is sensible to the increasing of blood flow associated to the increasing of neuronal activity. The principal advantages is its non-invasive nature, the high spatiotemporal resolution compared to other imaging techniques (but very low if compared to single cell recordings), and its capacity to demonstrate the entire network of brain areas engaged when subjects undertake particular tasks. One disadvantage is that it measures a surrogate signal whose spatial specificity and temporal response are subject to both physical and biological constraints (Logothetis, 2008).

From this brief summary of the two techniques, it emerges that the accurate and detailed information arising from the registration of individual cortical neuron is sometimes difficult to compare with the indirect measures of activity in large neuronal populations. To this it must be added also the comparison between data coming from these two techniques is sometimes hard because of the anatomical differences between the two species (human and non-human primates) due to the evolutionary development of the brain (as in the case of area V6, later in the introduction). The most logical step to ride out the question of homologies between humans and non-human primates has been the development of monkey fMRI, which bridges the technical gap between human functional imaging and monkey single-cell studies in the knowledge of the brain by applying the same experimental protocol (Vanduffel *et al*., 2001).

A part of my experimental work is the result of a collaboration during my PhD project in co-supervision between the laboratory of the University of Bologna and the INSERM Unit 1028, F-69500 affiliated with University Claude Bernard, Lyon1 in France. The greatest benefit of this collaboration is to build a bridge between two great resources that we have in the study of the brain: the single cells recordings on non-human primates and the fMRI on human. Awake monkey fMRI emerged at the end of the twentieth century as a unique tool to bridge the gap between human whole brain and monkey single cell data (Stefanacci *et al*., 1998; Logothetis *et al*., 1999).

Of course, fMRI on non-human primates passed through difficult challenges because of the difficulty in controlling eye position, attention and, above all, motion during scanning of awake monkeys (Orban, 2002; Goense *et al*., 2010). Over the years motion control as well as distortions have been minimized by improving, on one hand, MRI sequences, coils and head restraint methods, on the other hand by improving the eye-movement tracking system and animal training procedures (Wandell *et al*., 2007; Chen *et al*.., 2012; Stoewer *et al*., 2012; Hadj-Bouziane *et al*., 2014).

Only a multimodal and combined approach in humans as well as in non-human primates will be the best strategy for understanding brain (Logothetis, 2008).

1.2 Visuospatial processing

The dominant model about the neural framework for visuospatial processing has been for long time that proposed by Ungerleider and Miskin (Ungerleider & Mishkin, 1982), shown in Figure 2A. They identified in monkeys two anatomically and functionally distinct pathways that originate in the striate cortex (V1). The ventral stream was described as running through the occipito-temporal cortex to its anterior temporal target, area TE. The dorsal stream originated from the primary visual area (V1) extended across the occipito-parietal cortex reached the posterior half of the inferior parietal lobule (IPL), area PG. These streams were extended from area TE into the ventrolateral prefrontal cortex and from area PG into the dorsolateral prefrontal cortex (Macko *et al*., 1982). Lesions of ventral and dorsal streams in monkeys produced selective deficits in object vision and spatial vision, respectively, leading to their famous characterization of 'What' and 'Where' pathways (Mishkin *et al*., 1983). Later Milner and Goodale (Milner *et al*., 1991) extended the interpretation of these two visual streams. They studied a patient with a visual form of agnosia (D.F.), who had a large bilateral lesion of the occipito-temporal cortex and a small left sided lesion of the occipito-parietal cortex. This patient had impaired perception of objects but intact ability to reach to objects, including shaping her grasping hand to reflect the size, shape and orientation of the object. Moreover, patient D.F. could no longer recognize everyday objects or faces of her friends but she had no difficulties to recognize object's color or texture. At the same time, she had no trouble to identify the shape of objects by touch. What was surprising was that patient D.F. showed accurate

guidance of her hand movements when she attempted to pick-up the objects she cannot identify (Goodale *et al*., 1991; Goodale *et al*., 1994a; Goodale, 2014). For Milner and Goodale it was interesting the dissociation between the deep deficit in the discrimination of object's form and shape and the intact capacity to interact with the same objects. The authors suggested that the principal difference between the two streams consisted in the use that higher hierarchical brain center did of this information, and they proposed that the dorsal stream was more appropriately characterized as a 'How' than as a 'Where' pathway (Goodale *&* Milner, 1992; Goodale, 1994b; Goodale *et al*., 1994c), shown in Figure 2B. In the same years, other authors proposed a similar view of the two visual streams (Jeannerod, 1994). The model proposed by Goodale and Milner was the first that recognized a motor value beyond the perceptive value in the organization of the visual system, but the dichotomy hypothesis appear too simple to explain other pathological situations. Recently it has been propose that the dorsal stream gives rise to three distinct pathways; a parieto-prefrontal, a parieto-premotor and a parieto-medial temporal pathway, see Figure2C, which primarily support spatial working memory, visually guided actions and spatial navigation, respectively (Kravitz *et al*., 2011, for a review).

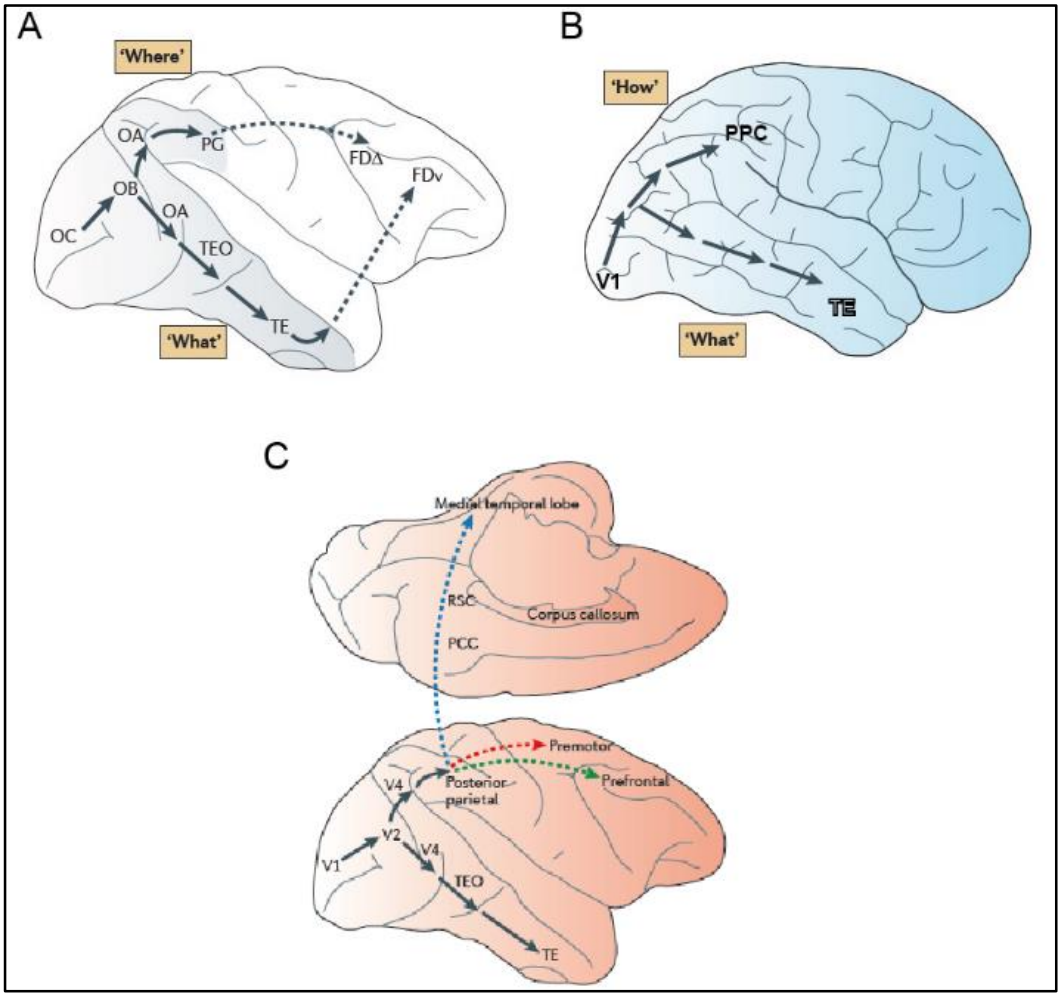

Figure 2: Evolution of the "two visual system theory" in time.

A) The original formulation of the dorsal and ventral streams in the macaque monkey proposed by Ungerleider and Mishkin in the 1982. The dorsal stream projects from striate cortex (named OC) to area PG in the inferior parietal cortex, with a further projection to FDΔ. The ventral stream projects from the striate cortex to area TE in the inferior temporal cortex, with a further projection to FDv. The ventral stream was termed 'What' pathway supporting object vision, whereas the dorsal stream was named 'Where' pathway supporting spatial vision. (Ungerleider & Mishkin, 1982).

B) The proposal of Milner and Goodale of the two visual streams. The dorsal stream was more accurately characterized as a motoric 'How' pathway controlling visually guided actions, whereas the ventral stream remained a perceptual 'Where' pathway. (Goodale & Milner, 1992).

C) The new neural framework proposed by Kravitz in 2011. Three distinct pathways originate from posterior parietal cortex. One pathway, indicated with the green dashed line, targets the prefrontal cortex and supports the spatial working memory; a second pathway, indicate by the a dashed red line, targets the premotor cortex and supports the visually-guided actions; and a third one, shown by a dashed blue line, reaches the medial temporal lobe and supports navigation. (Kravitz et al., 2011).

FDΔ, dorsolateral prefrontal region; FDv, ventral prefrontal region; OA and OB, prestriate cortex; OC, primary visual cortex; PCC, posterior cingulate cortex; PG, area PG; PPC, posterior parietal cortex; RSC, retrosplenial cortex; TE, rostral inferior temporal cortex; TEO, posterior inferior temporal cortex; V1, primary visual cortex; V2 and V4, extrastriate visual areas.

Modified from (Kravitz et al., 2011).

- ✓ *The occipito-parietal pathway*

The common anatomical antecedent of all the three pathways proposed for the dorsal stream by Kravitz et al. (2011), is the occipito-parietal circuit. This circuit is shown in Figure 3A, gray arrows. Portions representing both central and peripheral visual field of V1 project to area V6, which receives projections from other visual areas in the preoccipital region (area V2/V3 and V3A) (Colby *et al*., 1988; Galletti *et al*., 1999a; Galletti *et al*., 2001). Two main projections take place from V6 to the parietal lobe: one medial, projecting to the bimodal areas V6A, MIP (medial intraparietal area) and VIP (ventral intraparietal area), the other runs laterally to LIP (lateral intraparietal area), MT (middle temporal area) and MST (medial superior temporal area) (Galletti *et al*., 2001). The V1 is also strongly connected with MT and with area V2, V3 and V4. All these areas of the circuit are strongly interconnected each other and with the caudal and rostral portions of the inferior parietal lobule (cIPL and rIPL), for detail in the

IPL subdivisions see the close-up view in Figure 3A (Blatt *et al*., 1990; Rozzi *et al*., 2006).

This circuit integrates information about the central and peripheral visual field and represents the space in egocentric frames of reference. Although initial visual signals are entirely retinotopic, this circuit transforms those signals into additional frames of reference relative to the eye and part of the body. The parietal neurons provide information about many egocentric aspects of vision as optic flow and stimulus depth (Duffy, 1998; Genovesio *&* Ferraina, 2004; Orban *et al*., 2006). In humans, egocentric hemispatial neglect arises from damages the IPL (Verdon *et al*., 2010), whereas allocentric neglect (relative to objects) is associated with damages to ventral cortical areas including the MTL.

I will describe briefly the main characteristic of the three pathways lingering on their involvement on motion perception and the visually guided action.

- ✓ *Parieto-prefrontal pathway*

Its strongest sources are areas LIP, VIP, MT and MST, and it links the occipito-parital circuits with two areas, 8A and 46, in the pre-arcuate region and in the caudal portion of principal sulcus, respectively (Cavada *&* Goldman-Rakic, 1989b; Schall *et al*., 1995). See Figure 3B green arrows. This circuit is involved in the control of eye movements and in the spatial working memory (Curtis, 2006).

- ✓ *Parieto-premotor pathway*

This pathway, represented in Figure 3B with red arrows, has two main sources. One originates in area V6A and MIP and reaches the dorsal premotor cortex (areas F2 and F7) (Matelli *et al*., 1998; Gamberini *et al*., 2009). The other source is area VIP that projects to the ventral premotor

cortex (areas F4 and F5) (Rozzi *et al*., 2006). All the regions of this circuit maintain the continuously aligned representations of visual coordinates relative to the location of body parts that is necessary for visually guided actions in the peripersonal space. As I will discuss later on the introduction, posterior parietal damages both in monkeys and humans
are associated with deficits in visually guided reaching and grasping (Goodale *et al*., 1994a).

- ✓ *Parieto-medial temporal pathway*

This pathway is the most complex of the three. It links the cIPL with the medial temporal lobe (MTL), including the hippocampus, through both direct and indirect projections, see Figure 3B blue arrows (Vogt *&* Pandya, 1987; Kravitz *et al*., 2011). The ultimate target of this complex pathway is the hippocampus which is implicated in the complex spatial processing required for navigating through the environment (O'Mara *et al*., 1994). Recent study reported that the response of the posterior parietal cortex during navigation in a virtual environment might be consistent with a representation of absolute distance (Doeller *et al*., 2010). The representation of egocentric depth seems to involve area V3A, V6 and V6A as well as the IPs. Posterior parietal lesions can also be associated with a form of topographic disorientation characterized by impairments in navigation and landmark memory; subjects are unable to orient themselves in the environments also in familiar locations (Stark, 1996; Guariglia *et al*., 2005). This observation suggests that posterior parietal cortex is a source of the egocentric signals needed for navigation (Kravitz *et al*., 2011).

There are strong evidences that the posterior parietal cortex in both monkeys and humans participates in different levels of the visuospatial processing. In the next chapters, I will discuss the functional role of the PPC in motion processing and in the control of arm reaching movements in the three-dimensional space, aim of the present study.

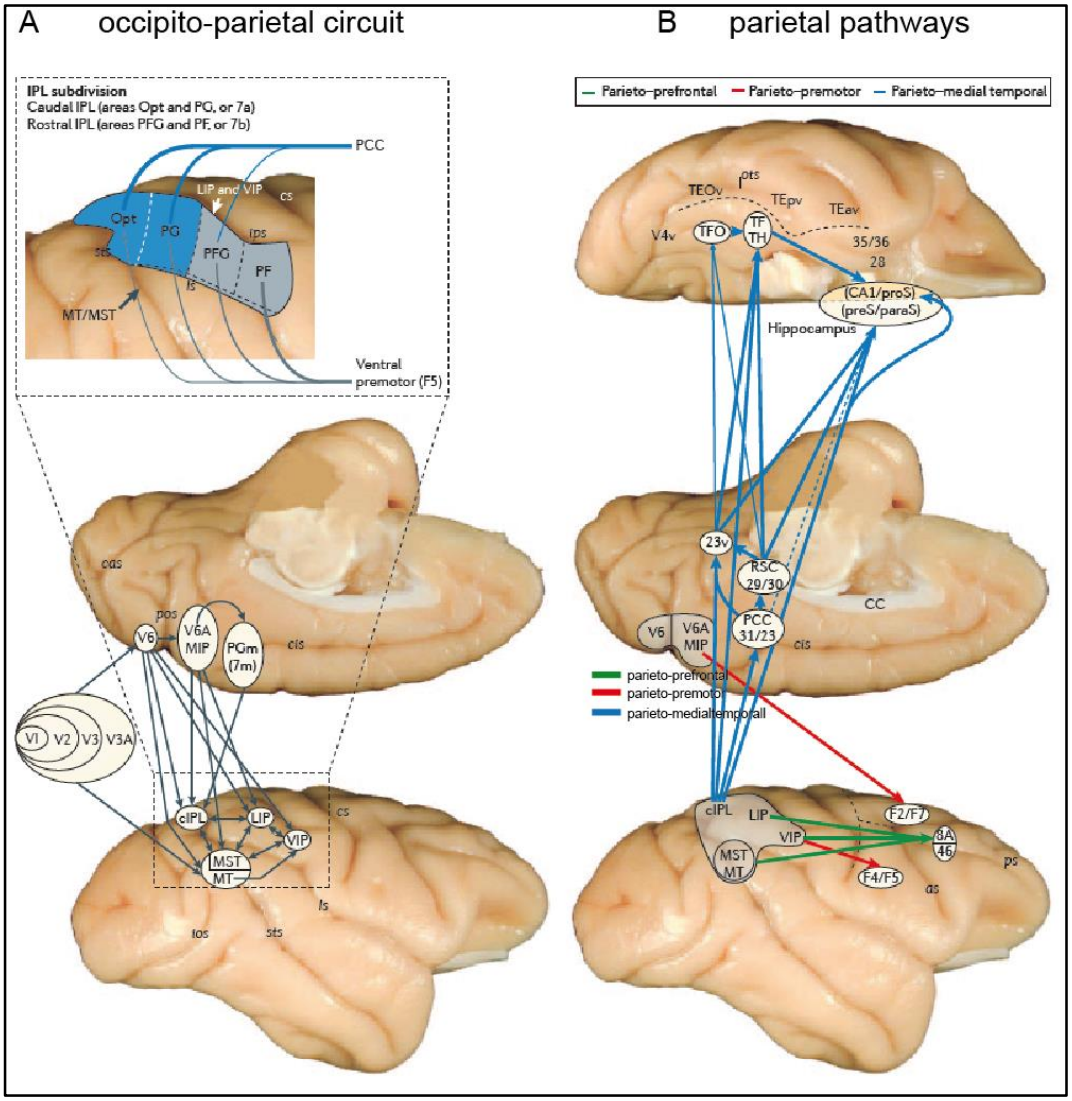

Figure 3: Anatomy of the three pathways within the dorsal stream, following the model proposed by Kravitz et al. (2011)

A) Occipito-parietal circuit on medial and lateral views of a rhesus monkey brain. The visual area V1 projects to area MT through visual areas V2, V3 and V4 and to area V6 through visual areas V2, V3 and V3A. The visual information from area V6 reaches the parietal lobe through two main channels: one projecting medially to areas V6A and MIP; and the other projecting laterally to areas LIP and VIP in the IPs and to areas MT and MST in the caudal part of the STs. All these posterior parietal areas are strongly connected each other and with the surface cortex of the IPL.

B) Parietal pathways, sources and targets. The parieto-prefrontal pathway, shown in green, links areas LIP, VIP and MT/MST with a pre-arcuate region (area 8A, FEF) and the caudal part of the principal sulcus in the lateral prefrontal cortex (area 46). This pathway underlies the eye movements control and the spatial working memory. The parieto-premotor pathway, shown in red, links areas V6A and MIP with the dorsal premotor cortex (areas F2 and F7) and area VIP with the ventral premotor cortex (areas F4 and F5), targets implied in the control of visually guided movements. The parieto-medial temporal pathway, in blue, originates in the cIPL (areas Opt and PG), see the close-up view, and projects to subdivisions of the hippocampus and presubiculum directly and indirectly via the posterior cingulate cortex (PCC), retrosplenial cortex (RSC) and the posterior parahippocampal cortex (areas TF, TH and TFO), targets that enable navigation and route learning.

23v, ventral subregion of the posterior cingulate; 28, entorhinal cortex; 35 and 36, perirhinal cortex; CA1/proS and preS/paraS, hippocampus subdivisions presucIPL, caudal IPL; TE, rostral inferior temporal cortex; TEav, anterior ventral subregion of TE; TEOv, ventral subregion of TEO; TEpv, posterior ventral subregion of TE; TF and TH, areas of the rostral portion of the posterior parahippocampal cortex; TFO, area in the caudal portion of the posterior parahippocampal cortex.

Sulci are also shown: as, arcuate sulcus; cas, calcarine sulcus; CC, corpus callosum; cis, cingulate sulcus; cs, central sulcus; ios, inferior occipital sulcus; ips, intraparietal sulcus; ls, lateral sulcus; ots, occipitotemporal sulcus; pos, paritooccipital sulcus; ps, principal sulcus; sts, superior temporal sulcus.

From (Kravitz et al., 2011).

1.3 The Posterior Parietal Cortex (PPC)

All the anatomical circuits described above have a common core: the posterior parietal cortex (PPC).

The associative areas of the PPC are able to integrate different types of sensory signals such as somatosensory, visual and auditory, and this integration constitutes a fundamental process for the perception of tridimensional shape of objects and for planning their manipulation. Lesions of the PPC do not originate simple sensory deficits as blindness or the loss of tactile sensibility. However, lesions in this brain region cause *agnosia,* the incapacity to perceive objects (visual, auditory or tactile), which are perceived as “presences”. Complex impairments are associated to the *agnosia*, as deficits in the spatial perception, in the visuomotor integration and in the attentional level.

The present dissertation will focus on the crucial role played by the PPC in different aspect of visuomotor transformations. As shown in Figure 4, the medial sector of the superior parietal lobule (SPL) consists in a castellation of different areas each of which is characterized by peculiar functional properties, anatomical connections set or cytoarchitecture pattern. At the caudal pole of this brain region (area V6 in yellow) visual information prevail; on the contrary, moving in the rostralmost part of the SPL (area PE in orange) hand information dominates eye signals. In the intermediate levels, eye and hand signals coexist (areas V6A, MIP, PGm and PEc, pink, light-blue, violet and green respectively) (Battaglia-Mayer *et al*., 2006).

This thesis will take into account three of these areas, area V6, V6A and PEc. The first (with area MT for comparison) will be taken into account for its involvement in the perception of motion, whereas area V6A and PEc will be considered for their implication in the reaching movement. At the beginning of each section, I will briefly describe the processes underlying the perception of motion and the visually guided actions taking into account

the cortical areas involved and the pathological deficits occurring after lesions on these cortical regions.

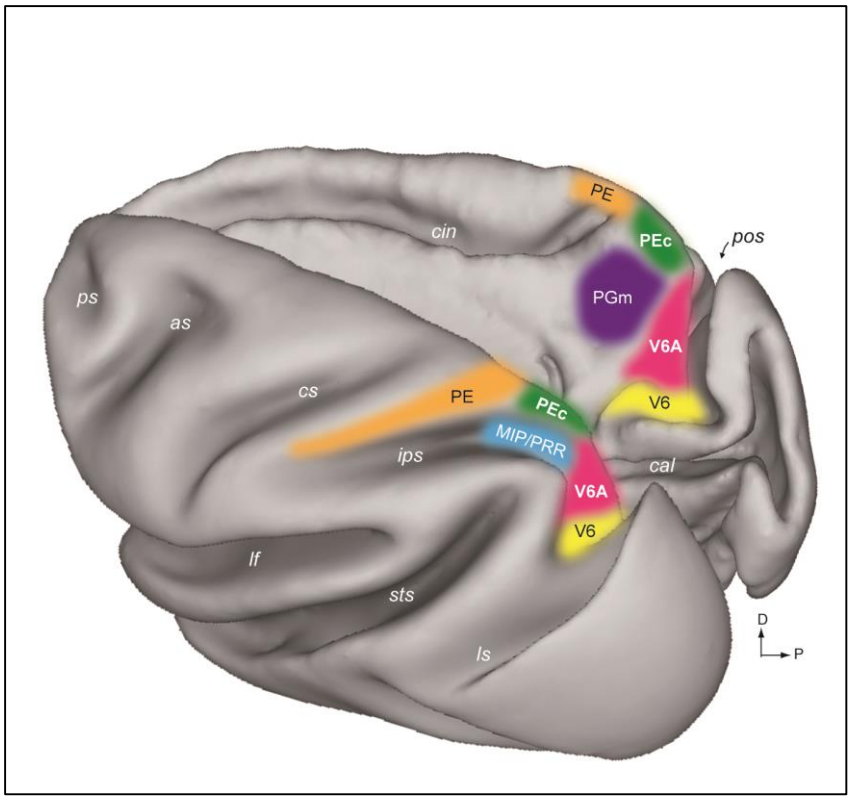

Figure 4: The areas of the medial posterior parietal cortex.

Dorsal view of left hemisphere (left) and medial view of right hemisphere (right) view of left (left) and right (right) hemispheres reconstructed in 3D using Caret software (http://brainmap.wustl.edu/caret/), showing the location and extent of PEc (green), V6A (pink), and V6 (yellow).

The other medial PPC areas are also shown: orange: PE (Pandya & Seltzer, 1982); light-blue: MIP/PRR, medial intraparietal area/parietal reach region (Colby & Duhamel, 1991; Snyder et al.,1997); violet: PGm (Pandya & Seltzer, 1982).

as, arcuate sulcus; cal, calcarine sulcus; cin, cingulate sulcus; cs, central sulcus; ips, intraparietal sulcus; lf, lateral fissure; ls, lunate sulcus; pos, parieto-occipital sulcus; ps, principal sulcus; sts, superior temporal sulcus;. D: dorsal; P: posterior.

1.4 The perception of motion

When moving around the environment, we integrate visual, somatosensory, auditory, and vestibular cues that allow us to determine and monitor the speed and direction in which we are heading. Visual motion has a crucial role in everyday life, it allows a human (as well as an animal) to predict the visual trajectory of moving objects so to facilitate their grasping or avoid a potential danger approaching. For a successful action, the visuomotor system must recognize if a movement is due to an object displacement in the environment or to a self-movement. When we are moving in the environment, we have the perception that it is the visual field moving around us. This perception is called “egomotion”. A key cue to egomotion is optic flow, and its neural representation has been studied in humans and macaque monkeys. The concept of optic flow was introduced by James Gibson to describe the visual stimulus provided to animals moving through the world (Gibson, 1950). Gibson stressed the importance of optic flow for affordance perception, the ability to discern possibilities for action within the environment.

The schema in Figure 5 represents the physical motion while an observer is moving forward through the environment. This motion generates an expanding pattern of flow on the retina and, with the eyes fixed centrally, the direction of heading corresponds to the center of expansion. Each arrow represents the speed and direction of motion for each little patch of the visual field. Near points move fast (long arrows) and far points move slowly (short arrows). The first step in motion perception is for the visual system to estimate optical flow from the changing pattern of light in the retinal image. Then the 3D motion of the observer and objects can be inferred from the optical flow. Optic flow then provides information about observer’s heading and the relative distance to each surface in the world.

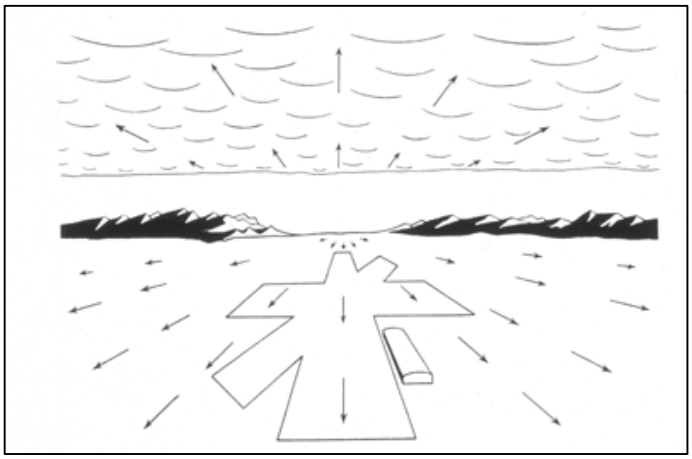

Figure 5: Example of retinal optic flow.

Typical retinal optic flow during a landing (forward motion). The landing field, the mountains and the clouds are visible. The arrows indicate the optic flow direction, arrows length is proportional to the speed of motion. *Adapted from (Bruce et al., 1996).*

1.5 Motion visual areas

The analysis of the optic flow gives two important information: information about the environment, object closer to us seem to move faster than the furthest one, and information about the control of our posture, lateral movement of the visual field induces body oscillations.

Consistent with the evolutionary importance of movement detection for safety, several brain regions in the primate dorsal visual stream are specialized for different aspects of the visual motion processing. As described above, the dorsal visual stream takes origin in the primary visual cortex (V1), extends through several extrastriate areas and ends in higher hierarchical areas of the parietal and temporal lobes. In the primary visual cortex (V1), neurons respond well to a stimulus moving in a certain direction

but not in the opposite one. This direction sensitive property is particularly evident in neurons of layer IVB.

Two areas in monkey, the middle temporal area (MT/V5) and the middle superior temporal area (MST), located in the temporal lobes in the dorsal part of the superior-temporal sulcus (STs), are commonly accepted as the key motion regions of the dorsal visual stream. Neurons belonging to both of these two areas are strongly responsive to visual stimuli in motion and selective for the direction and speed of movement (Felleman *&* Kaas, 1984; Allman *et al*., 1985; Tootell *et al*., 1995; Treue *&* Andersen, 1996; Morrone *et al*., 2000).

Area MT is a small visuotopically organized area on the posterior bank of the STs which receives a direct input from V1 (Ungerleider *&* Desimone, 1986b). The receptive field (RF) of this area are 10 times larger than those of V1 and it has a more-or-less complete retinotopic map of the contralateral visual field. It has a high percentage of neurons selective for direction, speed and binocular disparity of moving stimuli, suggesting its important role in the analysis of visual motion. An example of these neurons is shown in Figure 6A (Maunsell *&* Van Essen, 1983a; b; Maunsell *&* Van Essen, 1983c; Born *&* Bradley, 2005). MT is reciprocally connected with other extrastriate areas like V2, V3, V3A, V4, V4T, V6 and with area MST, VIP, LIP, FEF and FST (Maunsell *&* Van Essen, 1983c; Ungerleider *&* Desimone, 1986a). Some of them are key output structures implicated in the analysis of optic flow (MST and VIP) and the generation of eye movements (LIP and FEF). Figure 6B shows the MT's major inputs highlighting that the most important one comes from the magnocellular projection originated from layer IVb of V1 (Born *&* Bradley, 2005).

Area MST contains neurons sensitive to moving stimuli and it has been proposed that it is involved in the analysis of the optic flow. Neurons of area MST have RF of large dimensions, which cover all the visual field and respond preferentially to movements of large part of the visual field itself. These neurons are also sensitive to the changes of position of the point from

which the global moving of the visual field takes place and to the differences of velocity between the center and the periphery of the visual field (Graziano *et al*., 1994; Duffy *&* Wurtz, 1995).

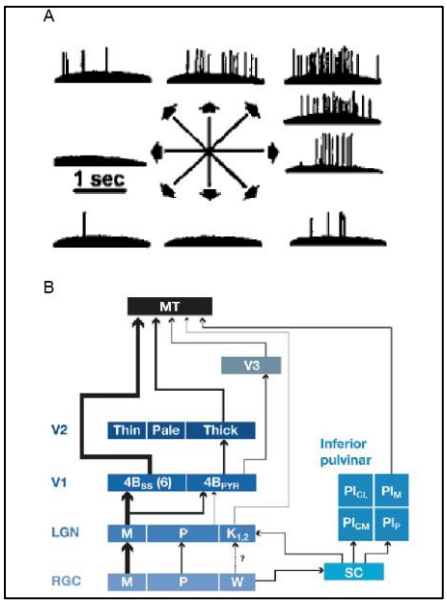

Figure 6: Direction selectivity and inputs of area MT.

A) First demonstration of direction selectivity in macaque MT by Dubner & Zeki (1971). Neuronal responses to a bar of light swept across the RF in different directions. Each trace shows the spiking activity of the neuron as the bar was swept in the direction indicated by the arrow. The preferred direction is the up-right one.

B) Map of the major routes involving area MT. Lines thickness is proportional to the magnitude of the inputs, on the basis of a combination of projection neuron numbers and the charateristics of their axon terminals. The thickest lines represent the direct cortical pathway.

4Bss, spiny stellate neurons in layer 4B; 4BPYR, pyramidal neurons in layer 4B; LGN, lateral geniculate nucleus; M, magnocellular stream; P, parvocellular stream; K, koniocellular layers of LGN; PICL, central lateral nucleus of the inferior pulvinar; PICM, central medial nucleus of the inferior pulvinar; PIM, medial nucleus of the inferior pulvinar; PIP, posterior nucleus of the inferior pulvinar; RGC, retinal ganglion cells; SC, superior colliculus; VP, ventral posterior area.

Adapted from (Born & Bradley, 2005).

1.6 Lesions of the motion areas in monkeys and humans

Lesions well localized in small regions of MT of monkeys caused impairments in judging the velocity of the moving images in the regions of the visual field controlled by the injured regions. These lesions, on the contrary, do not modify either the smooth pursuit eye movements in other regions of the visual field either the fixation of motionless objects. Lesions in area MT cause “blind spot” or scotoma for the movement. Newsome and Pare in 1988 (Newsome *&* Paré, 1988) studied the behavior of MT neurons in normal and impaired monkeys. They trained a monkey to indicate the direction of movement in a cloud of points moving casually. When the correlation was zero, all the points moved randomly, conversely when it was 100% the movement of all the points was coherent in a specific direction, as reported in Figure 7A, top part. A normal monkey needed about the 10% of points moving in a specific direction to detect correctly the direction of movement and execute the task correctly. Instead, monkeys with lesion in area MT needed about the 100% of coherence to obtain the same positive results, as reported in Figure 7B, bottom-left part. Using the same experimental protocol, it was observed the loss of movement perception also in a human subject with a bilateral brain lesion. As illustrated in Figure 7C, bottom-right part, the graphs of monkey and human subject are identical (Baker *et al*., 1991).

Lesions of area MT give only transitory effects, so we could hypotize that cells selective for direction of movement presented in other cortical areas could replace those of MT. The functional recovery is more difficult and slow if lesions are not circumscribed in MT but implicate also the neighboring area MST.

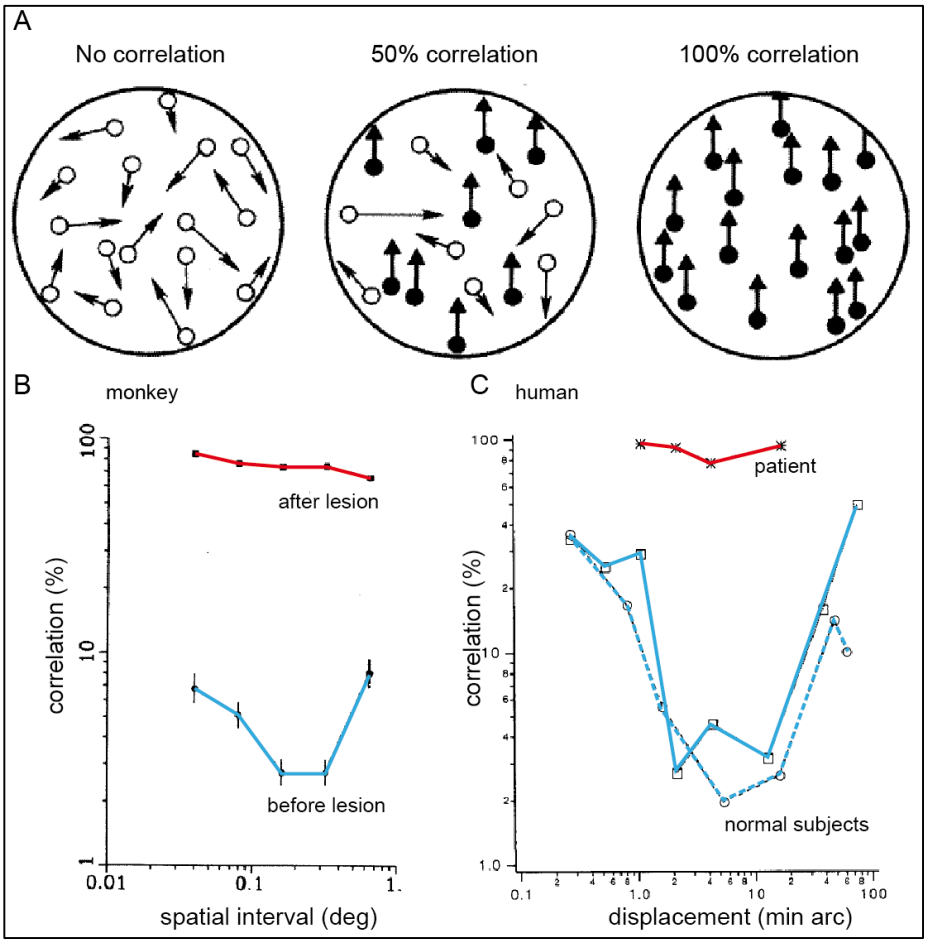

Figure 7: MT lesions in monkey and human.

A) Images used in the perception of motion. In the no correlation image, there is no perception of motion; in the 100% of correlation all the points move in the same direction; in the intermediate case (50% of correlation) half points moves in the same direction whereas the other half in a random order. (Newsome & Paré, 1988).

B) Monkey perception of motion before (light blue) and after (red) a lesion of area MT. (Newsome & Paré, 1988).

C) Human perception of motion in normal subjects (light blue) and in a patient with bilateral brain lesion (red). (Baker et al., 1991).

It is evident the overall similarity between human subject and monkeys and the strong impairment after MT lesion. Horizontal axis, index of motion; vertical axis, percentage of the correlation of motion necessary to perceive the motion of points. *Adapted from (Newsome & Paré, 1988 and Baker et al., 1991).*

Damages in the occipito-parietal circuit described above severally impaired the detection of movement in the visual field (Zihl *et al*., 1983). These patients describe the perceptual experience of looking at a moving object as if the object remains stationary but appears at different successive points. Selective impairments in motion detection have been described after bilateral lesions of the extrastriate cortex in human (Haarmeier *et al*., 1997). The patient suffered from a false perception of motion, due to his inability to take into account eye movements when judging whether a retinal slip was self-induced or due to an actual movement. The patient interpreted any retinal image motion as object motion. Magnetic resonance imaging revealed that the lesion involved the parieto-occipital cortex in and around the IPs. This brain region could include the human homologues of monkey areas V3A, MT, MST and V6, all areas involved in the occipito-parietal circuit.

The presence and the functional involvement in the encoding of motion of area V6, was initially described based on single cell activity in macaque brain (Galletti *et al*., 1996; Galletti *et al*., 1999a). Recently, researchers from the University of Rome described the human homologue area V6 using fMRI technique (Pitzalis *et al*., 2006; Pitzalis *et al*., 2010). Area V6 is a visual extrastriate area involved in both object and self-motion recognition. In the following sections, I will first report a separate and detailed description of area V6 in both monkey and human brain.

1.7 The medial motion area V6

- ✓ *Area V6 in macaque monkeys*

Area V6, the yellow area in Fig. 4, has been described in macaque monkeys based on functional, cytoarchitectual and connectional criteria

(Galletti *et al*., 1996; Galletti *et al*., 1999a; Galletti *et al*., 2001; Galletti *et al*., 2005; Luppino *et al*., 2005). Macaque V6 is located in the depths of the parieto-occipital sulcus (POs) and partially corresponds to area PO, according to its last definition (Colby *et al*., 1988) and Brodmann's area 18 (Brodmann, 1909). As shown in Figure 8, area V6 occupies a 'C-shaped' belt of cortex oriented in the brain in a coronal plane. The upper branch of this 'C-shaped' is located in the POs and the lower one in the medial parieto-occipital sulcus (POM), with the medial surface of the brain as conjunction zone between the two (Galletti *et al*., 1999a). Dorsally and anteriorly, area V6 borders on area V6A, from the medial surface of the hemisphere through the anterior bank and fundus of POs. Ventrally and posteriorly, V6 borders on area V3 (Galletti *et al*., 1999a; Galletti *et al*.,1999b). Functionally area V6 contains only visual neurons very sensitive to moving luminance borders (see Figure 9A). The majority of V6 neurons are both motion and direction selective and respond to stimuli of low spatial frequency (Galletti *et al*., 1996; Galletti *et al*., 1999a; Galletti *et al*., 2001). In 70% of cells, the same stimulus moving with the same velocity but in the opposite direction of movement does not evoke any discharge. An example is shown in Figure 9B and the relative incidence of direction-selective cells in the V6 population in the right part of Figure 9B.

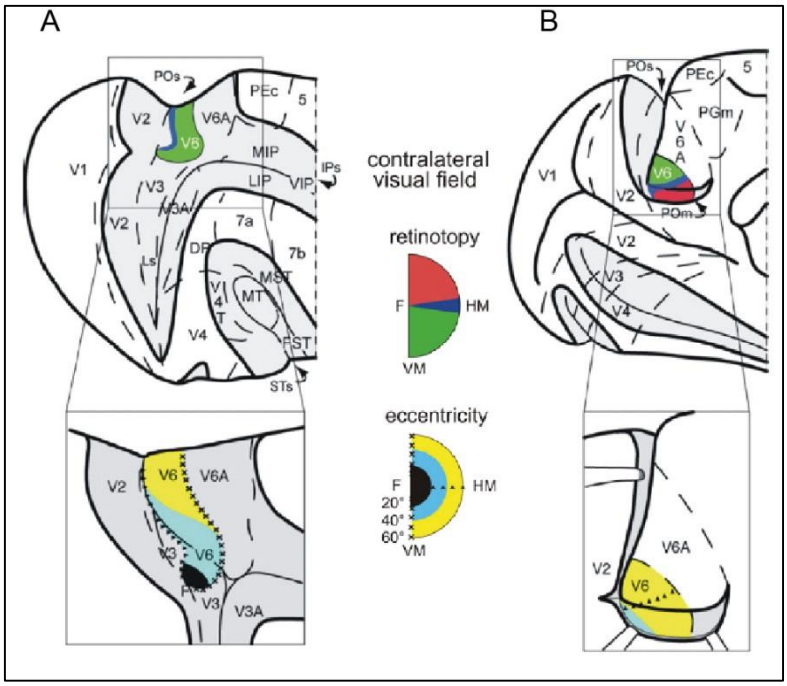

Figure 8: Location and visual topography of macaque area V6.

A) Dorsal view of caudal half of right hemisphere of macaque. Below: close-up of the parieto-occipital region. The parieto-occipital (POs), lunate (Ls) and intraparietal sulci (IPs) are open to reveal the cortex buried within them (dark gray area).

B) Medial view of the caudal half of left hemisphere. Below: close-up of the parieto-occipital region. The POs is open.

Note that V6 represents point to point the entire contralateral visual field with an emphasis in the representation of the peripheral visual field.

Area V6 is shown in color, according to the part of visual field it represents. Conventions reported between A and B. Triangles and crosses indicate the representation of the horizontal (HM) and vertical (VM) meridians of area V6 respectively; F, center of gaze. Dashed lines are the borders between different cortical areas.

From (Pitzalis et al., 2012a).

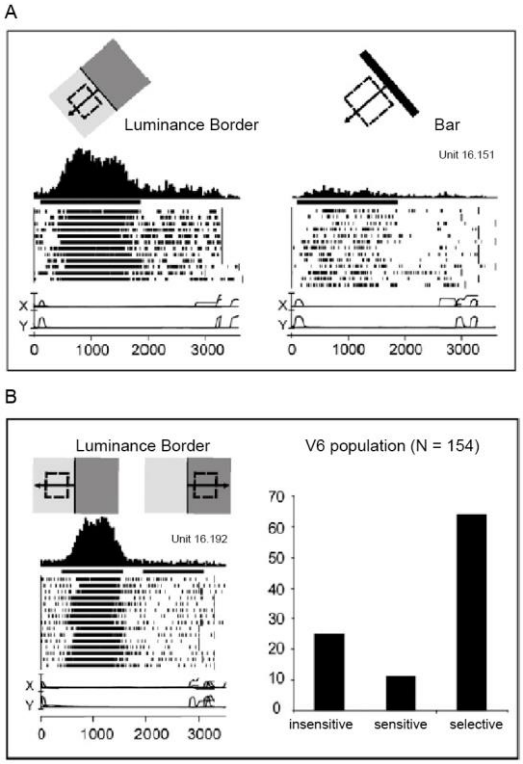

Figure 9: Visual motion sensitivity in area V6.

A) Example of a V6 neuron better activated by the motion of a Luminance Border (left) than by a bar of the same orientation and direction of motion (right). Each insert contains, from top to bottom: schematic representation of the RF (dashed line) and of the stimulus moved across it in the direction indicated by the arrow, peri-stimulus time histogram, bar indicating the duration of visual stimulation, raster plots of spikes recorded during each trial, recording of horizontal and vertical components of eye positions. Scales, bin width: 20ms; eye traces: 60°.

B) Left part: direction selective V6 neuron (all convention as in A). Right part: incidence of direction sensitivity in V6 population. Insensitive: cells whose responses to the stimulus moving in the direction opposite to the preferred one were > 80% of the discharge evoked when the stimulus moved in the preferred direction. Sensitive: cells whose responses in the opposite direction were between 20% and 80% of those in the preferred direction. Selective: cells whose responses in the opposite direction were < 20% of that in the preferred one.

(Adapted from Pitzalis et al., 2010).

Receptive fields (RF) are larger with respect to area V2 and V3 but smaller if compared with V6A, as shown in Figure 10A (Galletti *et al*., 1999a). The size and distribution of RFs in the upper and lower visual fields is unequal in V6: the RFs located in the lower hemifield are smaller and more numerous with respect to those located in the upper visual field (Figure 10B). Area V6 contains a retinotopic map of the entire contralateral hemifield, from the central part of the visual field until the far periphery (80° of eccentricity). From Figure 11 illustrating the visual field representation of V6, it is evident that the inferior hemifiled is more represented with respect to the upper one (Galletti *et al*., 1999). The peripheral lower and upper field representation of area V6, as shown in Figure 9, are visible in the medial surface of the hemisphere and in the dorsal wall of the POM, respectively. The lower field representation is visible in the parieto-occipital cleft. The central visual field, up to 20° of eccentricity, is represented in the lateralmost part of the posterior bank of POs, Figure 8A. This central representation is not emphasized as in the other extrastriate areas. Eccentricities higher than 20° are represented in the fundus of POs, in the ventral part of the anterior bank of POs, on the mesial surface of hemisphere and in the dorsal bank of the medial aspect of POs (Galletti *et al*., 1999a).

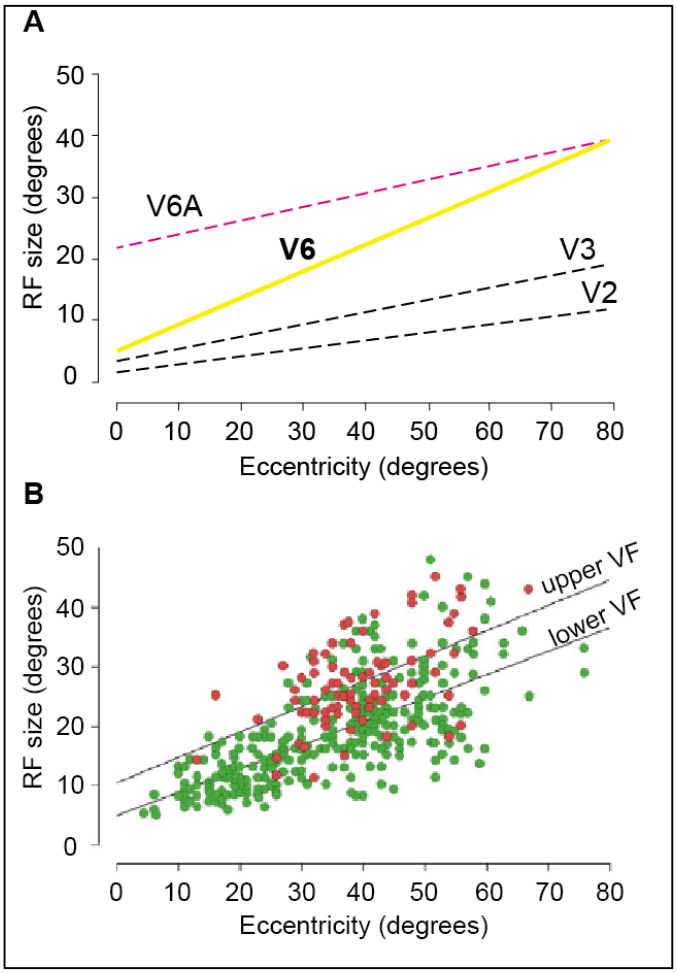

Figure 10: RF size versus eccentricity in area V6.

A) RF size versus eccentricity in V6 and other extrastriate areas. Regression plots of the RF size (square root of area) against eccentricity in degrees (°e) for cells recorded in areas V2 (N=485), V3 (N=353), V6 (N=466), and V6A (N=408). In area V6, RF are larger than in V2 and V3 but smaller than those of area V6A. The regression equations are as follows:

V2, size= 1.2°+0.12°e; R2= 0.63, V3, size= 3.6°+0.19°e; R2= 0.55,

V6, size= 4.8°+0.43°e; R2= 0.45, V6A, size= 21.3°+0.21°e; R2= 0.14

B) Dual regression plot of RF size against eccentricity of V6 cells with the RF in the upper (N= 91, red circles) and lower (N= 375, green circles) visual field (VF), respectively. It is evident that at any eccentricity, RFs are bigger in the upper VF with respect to the lower one. The regression equations are:

Upper, size= 10.2°+0.43°e; R2= 0.31, Lower, size= 4.5°+0.40°e; R2= 0.49

Adapted from (Galletti et al., 1999a).

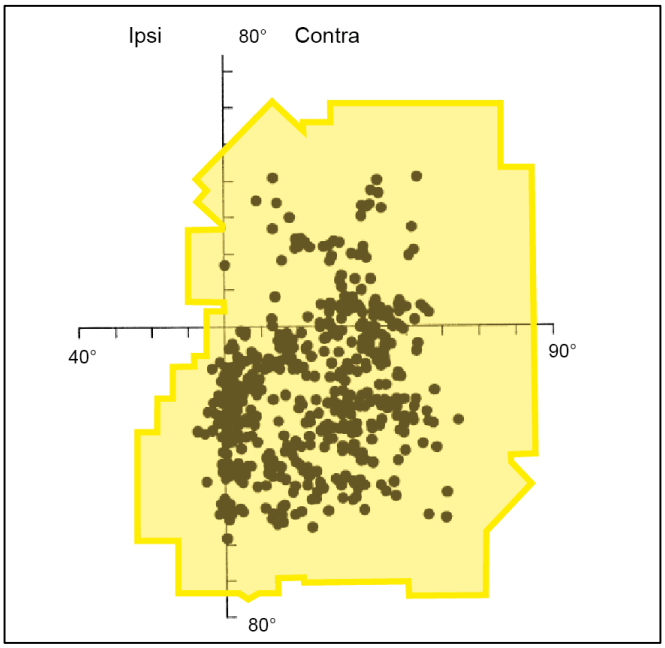

Figure 11: Visual field representation in V6.

The filled circles indicate the retinotopic distribution of RF centers of the same cell population shown in Fig. 10. In yellow, the outline of the most peripheral RF borders. (Adapted from Galletti et al., 1999a).

Area V6 shows a cytoarchitectonic organization typical of occipital areas, for details see the chapter *Histological reconstruction of recording sites*. Briefly, area V6 is characterized by a thick, homogeneous layer IV with densely packed granular cells, a light layer V, populated by small pyramids, and a clear subdivision of layer VI into two sublayers, with a very dense layer VIb, sharply delimited with respect to layer VIa and the white matter (Luppino *et al*., 2005).

Area V6, as shown in Figure 12, like V2 and V3, receives direct input from the primary visual area V1 but, in contrast to the other two, it projects only to the parietal areas of the dorsal visual stream and not to areas of the ventral visual stream (Galletti *et al*., 2001; Kravitz *et al*., 2011). As

summerized in Figure 12, area V6 is strongly connected with the parieto-occipital areas V2, V3 and V3A. The visual information leaving V6 is directed to higher order visual areas of the parietal lobe following two main pathways: a lateral one that reaches the visual area of the dorsal stream (LIP, V4T, V5/MT, MST) and a medial one that reaches the bimodal (visual/somatosensory) areas of the dorsal stream (V6A, MIP, VIP). As all these areas of the dorsal stream are directly connected with the premotor cortex, visual information can reach the frontal cortex following several pathways.

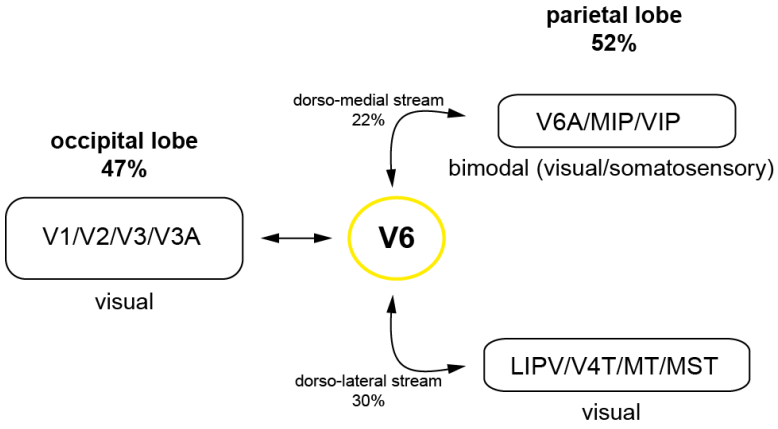

Figure 12: V6 connections.

The occipito-parietal circuit processing visual information. *Modified from (Galletti et al., 2001).*

One characteristic of area V6 is the presence of a particular type of motion sensitive neurons, called “real-motion cells” (Galletti *&* Fattori, 2003). This type of cells has been found, even in a smaller percentage, also in area V1 (Galletti *et al*., 1984; Sugita 2004), V2 (Galletti *et al*., 1988), V3A (Galletti *et al*., 1990), and MT and MST (Thier *&* Erickson, 1992; Ilg *et al*., 2004). The

peculiarity of the real-motion cells is that they discharge vigorously for stimuli moving in a certain direction when the monkey is fixating on a point and the stimulus is moving in the neuron' receptive field. When the same stimulus moves in the same direction on the retina because the monkey's eyes move while the object is stationary, the response of the real-motion cell is attenuated or suppressed, as reported in Figure 13. The visual and motion stimulations are equal in the two situation, but in A there is a real movement of the stimulus and the cell discharges vigorously, whereas in B the stimulus is stationary, the movement of the retinal image is self-evoked by the movement of the eyes and the cell is silent. The peculiar behavior of the real-motion cells indicates that they are processing additional information and not only the retinal ones. These cells allow one to recognize the actual movement of an object across a structured visual background or in complete darkness. They could act as a sensor of a real movement in a neural network that sub-serve an internal map of the visual field (Galletti *&* Fattori, 2003). This internal map would continuously evaluate whether something changes its location or moves in the visual environment. One hypothesis is that the real-motion cells could signal the actual object movements and since V6 is strongly connected with bimodal areas (like V6A), the final goal is to orient animal's attention/alertness toward moving objects, in order to be ready interact/avoid them (Pitzalis *et al*., 2012a).

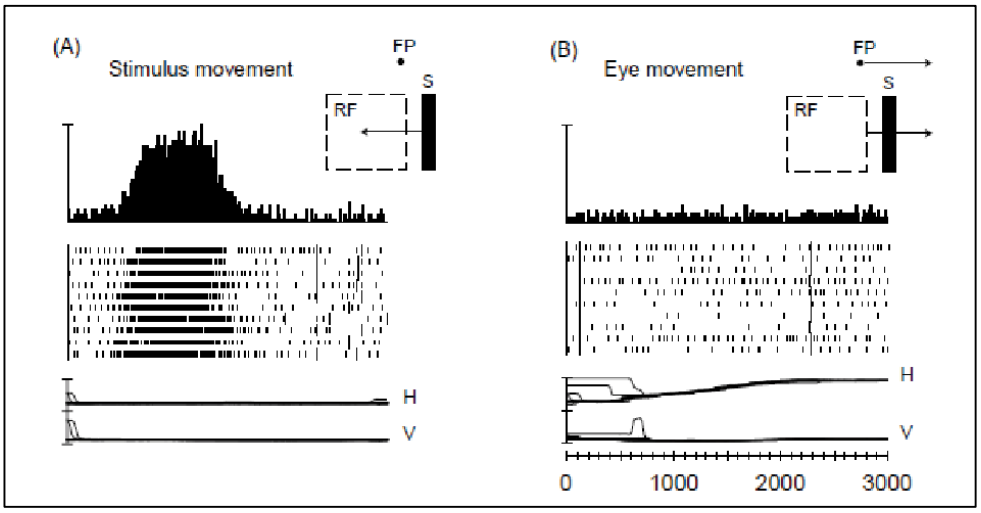

Figure 13: Example of real motion cell of area V6.

A) Neural responses evoked by sweeping the optimal visual stimulus (S) across the RF while the monkey looked at a stationary fixation point (FP).

B) Neural activity evoked by sweeping the RF across the stationary visual stimulus as consequence of pursuit eye movements made to follow the moving fixation point.

The two retinal stimulations are identical, but the neuron's discharge discriminate between real and self-evoked motion.

Scales: neural activity, 150 spikes/s; eye position, 30° per division.

(From Galletti & Fattori, 2003).

Several neuroimaging studies in humans have shown that medial parieto-occipital cortex is activated by tasks involving visual motion perception (Cheng *et al*., 1995; Galati *et al*., 1999; Sereno *et al*., 2001), but none of these studies directly related the activated region to area V6. Pitzalis and collaborators were the first to identify the homologue human area V6 (Pitzalis *et al*., 2006; Pitzalis *et al*., 2010).

- ✓ *Area V6 in human*

The retinotopic organization of human area V6 was described in Pitzalis et al. (2006) using the fMRI technique. Area V6 was found in all 34 subjects that were mapped. It represents the contralateral visual hemifield in both hemispheres with the upper fields located anterior and medial to areas V2/V3, and lower fields medial and anterior to areas V3/V3A, as shown in Figure 14 by the yellow circles/boxes. It contains a representation of the center of gaze and a large representation of the visual periphery, as in monkeys, as illustrated in Figure 15. Area V6 is located within the POs in both humans and macaques, however the folded reconstruction of the medial surface (Figure 16, left) shows that human V6 is superior to macaque V6. Also other visual areas occupy different locations in human and macaque as a consequence of the expansion of laterally placed non primary areas and of the movement of human V1. As illustrated in the Figure 16, the superior/inferior extent of V1 is reduced at the occipital pole because the V1 central representation moves into the posterior calcarine and the peripheries of V1 and V2 are pushed anteriorly, overflowing the calcarine cortex onto the medial wall (Pitzalis *et al*., 2006).

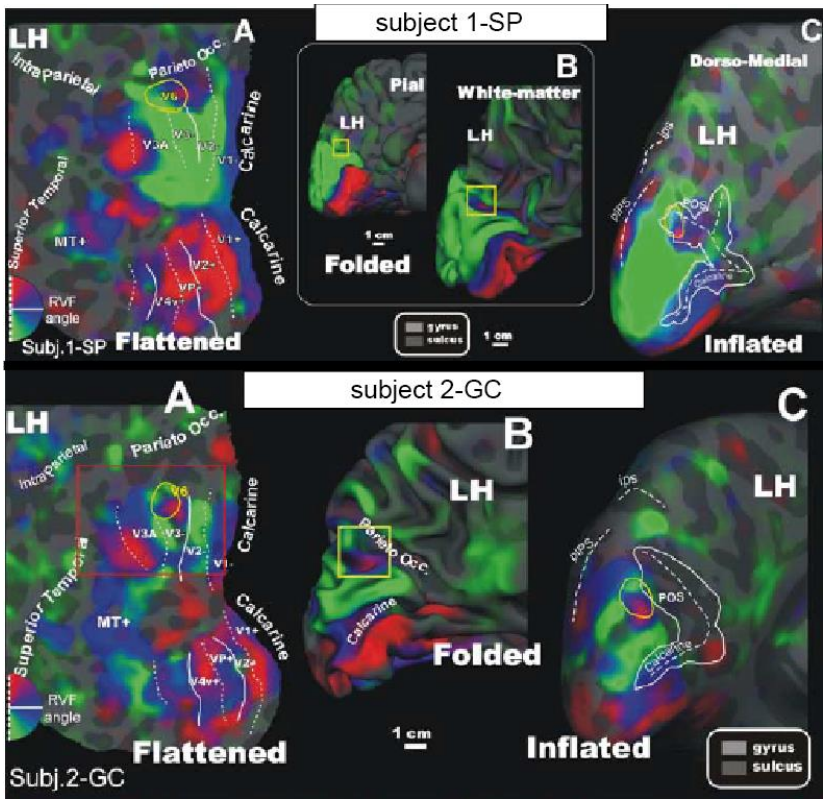

Figure 14: Location and retinotopy of human area V6.

Flattened (A), folded (B), and inflated (C) reconstruction of the left hemisphere (LH) of two participatnts (Subj 1-SP and Subj 2-GC) are shown. Yellow outlines indicate location (in folded) or borders (in flattened/inflated) of the human area V6. It is evident that area V6 contains a clear map of the contralateral hemifield.

The folded cortex is shown in two versions: pial and white matter. Red, blue, and green areas represent preference for upper, middlem and lower parts of the contralateral visual field, respectively. On the flattened map, dotted ad solid white lines indicate vertical and horizontal meridians.The sale bar (1 cm) on the bottom refers to the cortical surface of A and C. RVF, right visual field.

Modified from (Pitzalis et al., 2006).

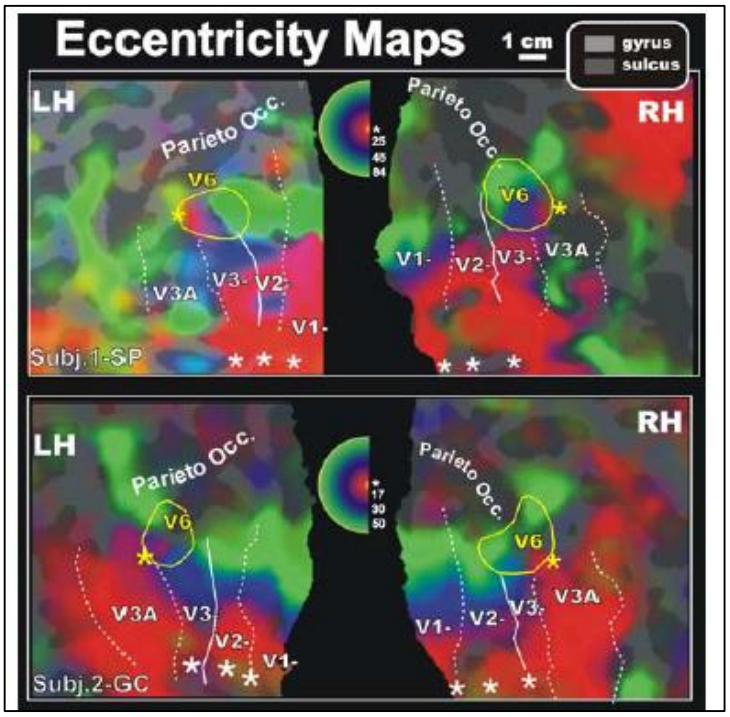

Figure 15: Retinotopy of eccentricity representation of area V6.

Eccentricity maps rendered on a close-up views of the left and right flattened hemispheres in the same two subjects of Figure 14. The representation of eccentricities, from the center to the periphery, is represented by colors, from red to green, respectively (see pseudocolor inset, located in between left andright hemispheres of each participant). Each inset indicates the maximal periphery used in the study. The representations of the center of gaze are indicated with asterisks. *Modified form (Pitzalis et al., 2006).*

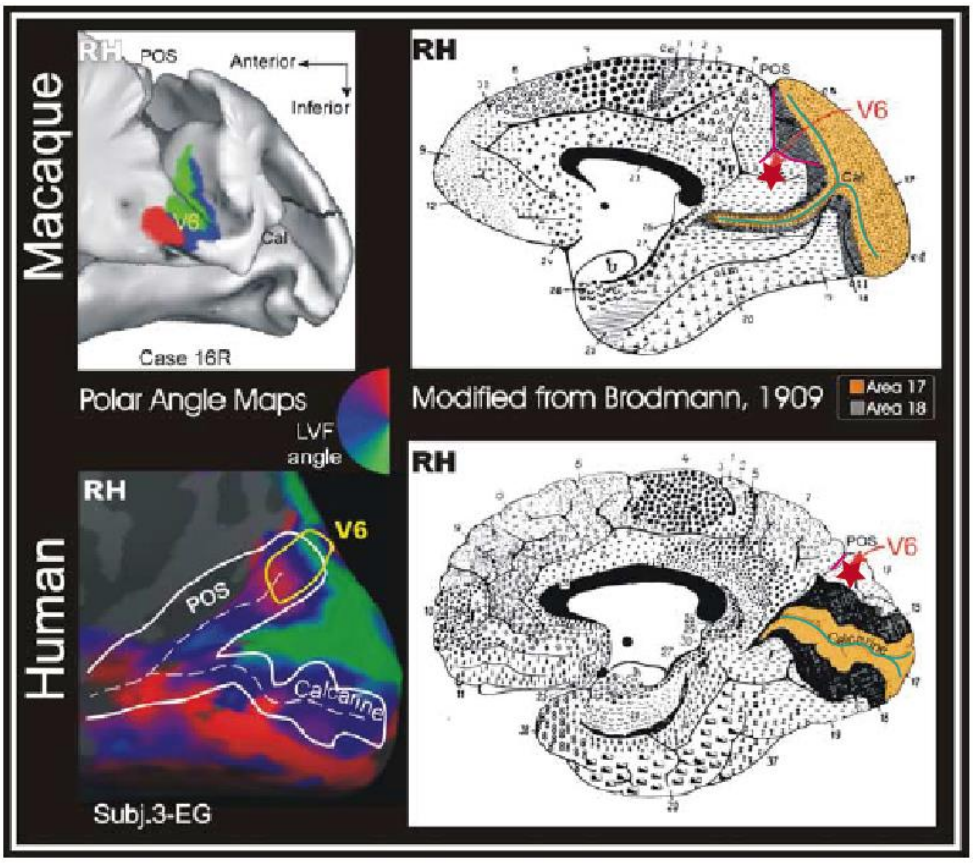

Figure 16: V6 location in macaque and human brains.

Left, retinotopic maps of polar angle representation of area V6 in macaque (top) and human (bottom) brains. Polar angle maps are rendered on the folded (top) and inflated (bottom) cortical surface reconstructions of the caudal part of the right hemisphere (RH), respectively. Both macaque and human retinotopic data show a clear and similarly arranged map of the contralateral left hemifield. Red, upper left visual field; blue, left horizontal; green, lower left.

Right, medial views of macaque (top) and human (bottom) right hemisphere, showing the Brodmann's parcellation of the cortical surface. Areas 17 and18 are color-coded, orange and dark gray respectively. A red arrow and a red star on both brains indicates the location of area V6. The parieto-occipital and calcarine sulci are highlighted in pink and light blue, respectively.

Adapted from (Pitzalis et al., 2006).

Human V6 is a motion area activated by moving stimuli. It is also sensitive to flickering stimulation and shows a high selectivity for coherent Flow-Field motion, a stimulus used for the first time by Pitzalis et al. (2010) and not previously tested in macaque V6 by single unit recordings. The Flow-Fields stimulus is a type of complex coherent motion stimulation similar to the continuously changing optic flow generated when a subject moves through in a complex environment (Koenderink, 1986). As illustrated in Figure 17 (bottom part), human V6 was powerfully activated by Flow-Fields stimulation but not by Radial-Rings stimulation, which on the contrary activated area MT (Figure 17, top part).

Optic-flow, as above-mentioned, is the most important cue for perception of 'egomotion' (i.e., the sensation to be moving in space). The Flow-Fields stimulus becomes an excellent human V6 localizer (Pitzalis *et al*., 2010). The strong activation of area V6 due to Flow-Fields stimulus suggested that area V6 could be involved in the analysis of egomotion (Pitzalis *et al*., 2012a). In agreement with this hypothesis, human clinical studies reported that lesions of human POs produce motion-related visual disturbance (Blanke *et al*., 2003), and epileptic attacks within the precuneus produce self-motion perception (Wiest *et al*., 2004). Human V6 could be implicated in the analysis of egomotion and may be able to distinguish between different 3D flow fields.

To confirm this hypotheses, the first aim of this work was to apply the same fMRI experimental protocol used in human studies to fMRI study in macaque monkey. We used the same stimuli used in human in order to test the selectivity of V6 neurons to Flow-Fields in macaque monkeys, a stimulus never tested in elettrophysiological studies.

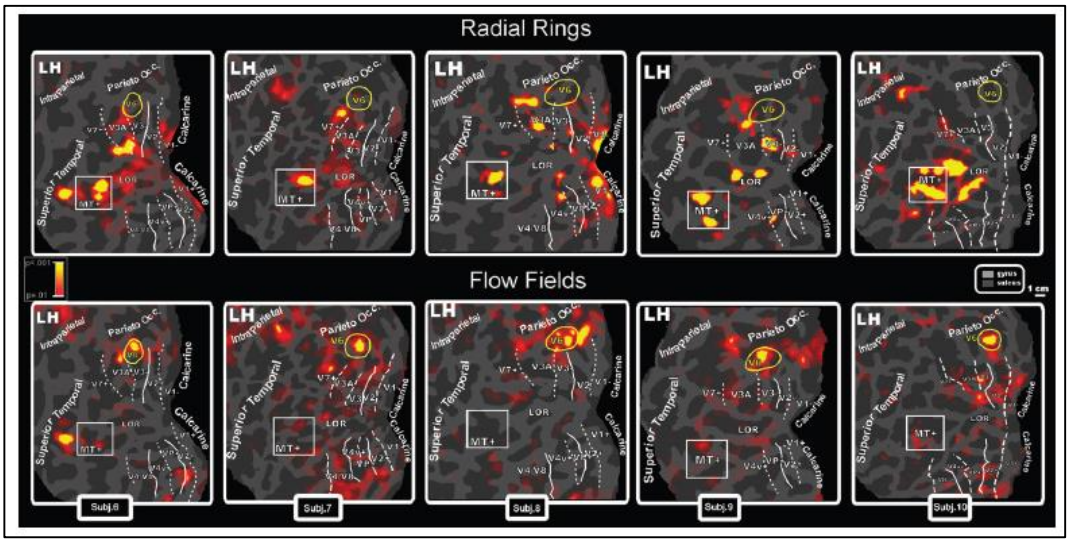

Figure 17: Motion-selectivity of human V6.

Topograpghy of motion-sensitive activity by fMRI mapping from Radial-Rings (Top) and Flow-Fields (Bottom). It is evident that area V6 (indicated by yellow circles) is powerfully activated only by the Flow-Fields stimulus; on the contrary, Radial-Rings stimulus activates area MT (white boxes) but not V6.
Results are displayed on flat maps from the left hemispheres of 5 subjects.
From (Pitzalis et al., 2010).

1.8 Visually Guided Actions

Much of human and non-human primates' behavior regards the manipulation of objects and other movements directed at targets located in the environment. They are capable of reaching and grasping objects with great dexterity and vision plays a critical role in this. To execute these actions, the information about target location is necessary to process the hand trajectory and the corresponding motor program that guides muscles. Goodale in his review (2011) makes the example of picking up a cup of coffee. The author described the several consecutive steps we must

perform to pick up the cup: firstly, we have to identify our cup amongst other objects; secondly, we begin to reach out with our hand toward the cup avoiding possible obstacles while our fingers begin to conform to the shape of the cup's handle. All these conputations and we did not grasp the cup yet! This example clarifies how many sensory systems and computations are necessary to perform the early stages of a simple act, ignoring what happened as soon as we grasp the cup, such as feeling the weight of the cup, adjust the grip and the strength based on its weight. Generating appropriate movements requires a good estimation of the object's locations as its distance from us in the three-dimensional space. Such behaviors require a particular neuronal control of joints and muscles to achieve the correct hand and digits shape.

The aim of this thesis was to study the sensory properties of areas involved in the control of arm movements as well as the sensory-motor transformations underlying the arm reaching movement toward visual targets placed at different directions and depth in the 3D space.

1.9 Encoding of 3D space

One of the principal goals of the vision system is to bestow on two-dimensional images a three-dimensional value. Psychophysics studies indicate that the transition from a two-dimensional to a three-dimensional vision is based on two types of clues: monocular elements about the depth of field and stereoscopic elements based on binocular disparity. Using the monocular elements, we are able to discriminate different depths for long distances (more than 30 meters). Examples of monocular elements (object familiarity, interposition, linear prospective e motion parallax) are illustrated in Figure 18A.

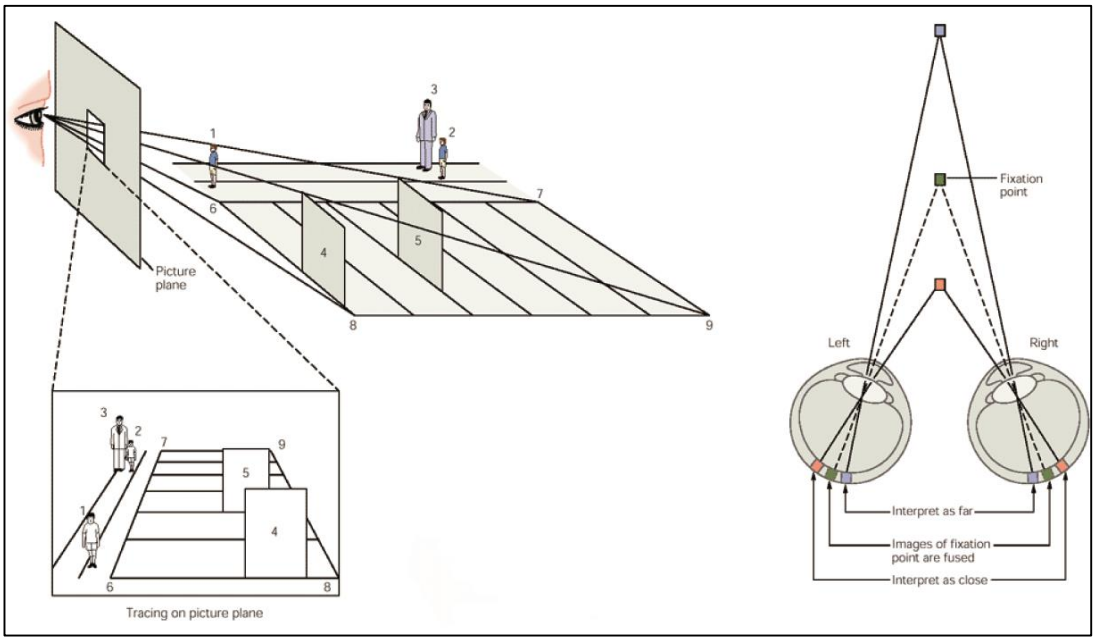

Figure 18: Perception of distances.

Left,monocular elements. Top: side view of a scene. When the scene is traced on a plane of glass held between the eye and the scene (lower drawing) the resulting two-dimensional tracing reveals the cues needed to perceive depth. Occlusion, the rectangle 4 blocks the view of 5 indicates which object is in front, this means that 4 is closer with respect to 5 although we haven't any information about the distance between 4 and 5; Linear perspective, even though lines 6-7 and 8-9 are parallel in reality, in perspective they converge; Size perspective, boy2 appears smaller than boy1, it means that he is farther than boy1; Familiar size, the man3 and the boy1 have the same dimension, but the fact that we know that man are higher than boys, gives us the sensation that man3 is further than boy1.

Right, when we converge the eyes toward an object (fixation point) at distance lower than 30 meters, the images of the object fall into identical part of both retina. Points closer or further with respect to the fixation point, project to different points of the retina of the eye and create the binocular disparity.

Adapted from (Kandel, Schwartz & Jessell, 2000).

The perception of depth for distances less than 30 meters depends on monocular cues but in addition is mediated by stereoscopic vision. The stereoscopic vision is possible because of the distance of the eyes on the horizontal plane that produces the retinal disparity. Since the eyes see the objects with different angles/perspectives (Figure 18B), objects ahead and/or behind of the fixation point project in odd points of the retina. The vergence system uses this retinal disparity to generate the vergence eye movements in which the eyes rotate in opposite directions (dis-conjugated movements) and to provide a measure of the object's distance from the plane of fixation in relation to the body (Poggio, 1995; Cumming *&* DeAngelis, 2001). If the object distance information is combined with the estimation of fixation distance, the brain has sufficient information to calculate the egocentric distance (Pouget *&* Sejnowski, 1994; Genovesio *&* Ferraina, 2004; Crawford *et al*., 2011).

Three important mechanisms are used to estimate the fixation distance: the extra-retinal signals vergence angle, accommodation, and the vertical disparity (Genovesio *&* Ferraina, 2004). While the vertical disparity is used by the visual system for objects with a visual angle greater than 20° (Cumming *et al*., 1991), the vergence angle seems to be the most important mechanism to estimate the fixation distance (Foley, 1980). The vergence system is linked with the accommodation. The accommodation is the changing of the radius of the curvature of the crystalline lens to focus the world on the retina. Blur is the stimulus that induces accommodation; whenever accommodation occurs, the eyes also converge. Similarly, retina disparity induces vergence; whenever the eyes converge, accommodation also takes place. The other important signal to localize an object in the world is the direction of fixation (version angle) that consists in the conjugated eye movement toward the target of interest.

Over the years, several physiological experiments showed that the neuronal activity of many extrastriate and PPC areas is modulated by gaze direction (version angle) (Sakata *et al*., 1980; Mountcastle *et al*., 1981;

Galletti *et al*., 1995). Only few studies have demonstrated that PPC is modulated also by the vergence angle (Sakata *et al*., 1980; Lacquaniti *et al*., 1995; Genovesio *&* Ferraina, 2004; Bhattacharyya *et al*., 2009; Ferraina *et al*., 2009).

The primary visual cortex (area V1) is one of the earliest nodes in which neurons are specifically selective for the horizontal disparity as well as for the direction of gaze. Barlow and coworkers observed that neurons sensitive to a light stimulus recorded in anesthetized cats, (Barlow *et al*., 1967; Trotter *et al*., 1992; Trotter *&* Celebrini, 1999), responded better when the stimulus was in front (near stimulus) or behind the screen (far stimulus). Cells sensitive to the binocular disparity are present also in other extrastriate areas of monkeys as V2, V3, V3A, MT and MST. Importantly neurons modulated by the vergence angle have been found in areas 7a and LIP of the PPC (Sakata *et al*., 1980; Genovesio *&* Ferraina, 2004). In Sakata work, authors reported that 7a neurons were modulated by gaze direction and fixation depth together or alone. More importantly, the study of Genovesio was the first demonstrating that neurons of area LIP were able to combine signals of retinal disparity and the vergence angle to provide an estimate of egocentric distance (Genovesio *&* Ferraina, 2004). A recent study of our group (Breveglieri *et al*., 2012) revealed that the majority of V6A neurons were modulated by both vergence and version signals while monkeys maintained a steady fixation. This finding suggests that the integration of vergence and verison signals is already present in this early node of the dorsal visual stream. Interestingly, the authors observed that during steady fixation the version selectivity decayed more rapidly than the one of vergence, supporting the hypothesis that direction signals are processed before depth information.

The data previously described were mainly collected when monkeys performed fixation task and not during the execution of an arm movements. The most important neurophysiological work in this filed is the one of Lacquaniti and colleagues (Lacquaniti *et al*., 1995). They evaluated in area

5 (PE) the effect of the three spatial coordinates (azimuth, distance and elevation) on the neural responses during reaching movements. The animals performed goal-directed movements towards targets located at similar directions within three different workspaces starting from three initial hand positions. Each of these initial hand positions was located in the middle of an imaginary cube where at each corner a reach target was placed. The authors found that the majority of area 5 neurons was influenced by the spatial location of the hand with subpopulation of neurons coding each of the three (azimuth, distance and elevation) signals (Lacquaniti *et al*., 1995). Recently in a study of our group (Hadjidimitrakis *et al*., 2014) we compared distance and direction coding in area V6A. We found quite opposite results with respect to the Lacquaniti study: distance ad direction information are jointly encoded in the majority of V6A neurons. The opposite results emerging from the two studies not necessarily lead up to contrasting hypothesis, maybe the reason lies in the location of these two areas at the vertexes of the gradient-like network discussed in a previous chapter. To disentangle these contrasting results, we record from area PEc, the intermediate area between V6A and PE.

Cumming and De Angelis (2001) wondered also if the extrastriate responses to disparity can be derived from V1. During years, two differences between striate and extrastriate cortex have been noted. First, neurons in extrastriate cortex tended to be more tuned for disparity than in V1 and second, in extrastriate areas odd-symmetric tuning predominates in contrast to the symmetric tuning behavior of V1 (Cumming *&* DeAngelis, 2001). These two observations suggested that the exstrastriate responses are not derived from the disparity-related neurons of V1 but are constructed *de novo,* but this issue is still unclear (Cumming *&* DeAngelis, 2001). Another long-standing issue concerns if target depth and direction are processed in functionally distinct circuits (Vindras *et al*., 2005) or must be considered as inseparable variables (Crawford *et al*., 2011). In addition, also the temporal evolution of these signals is still in debate. Many studies

suggest that direction is processed before depth (Bhat *&* Sanes, 1998; Breveglieri *et al*., 2012) in contrast with the hypothesis that the processing of direction happens after or at the same time of depth (Rosenbaum, 1980).

1.10 Lesions of the parietal areas in monkeys and humans

Lesions of the parietal cortex, especially on its posterior part, deeply interfere with the awareness of the structure and the size of our body and the space around it. Lesions on the parietal cortex can be subdivided as lesions in the somatosensory areas (S-I, primary somatic area, S-II) and lesions in the posterior parietal cortex (PPC).

Lesions in somatosensory areas of the parietal cortex produce specific sensory deficits. The earliest information about the function of the somatic sensory system came from the analysis of disease states and traumatic injuries of the spinal cord. Additional information about the somatic afferent system has come from studies of the behavioral deficits produced by transection of the dorsal columns of the spinal cord in experimental animals or by trauma in humans. Injury to the afferent somatosensory pathways in the dorsal columns results in a chronic deficit in certain tactile discriminations, such as detecting the direction of movement across the skin. In addition to sensory deficits, lesions of the dorsal columns distort natural hand movements.

A reversible deficit in the execution of skilled movements can be produced experimentally in monkeys by pharmacological inhibition of neural activity in area 2 of the cortex using muscimol. After this transient inactivation, monkey is unable to assume normal functional postures of the hand or coordinate the fingers for picking up small objects as shown in Figure 19 (Hikosaka *et al*., 1985).

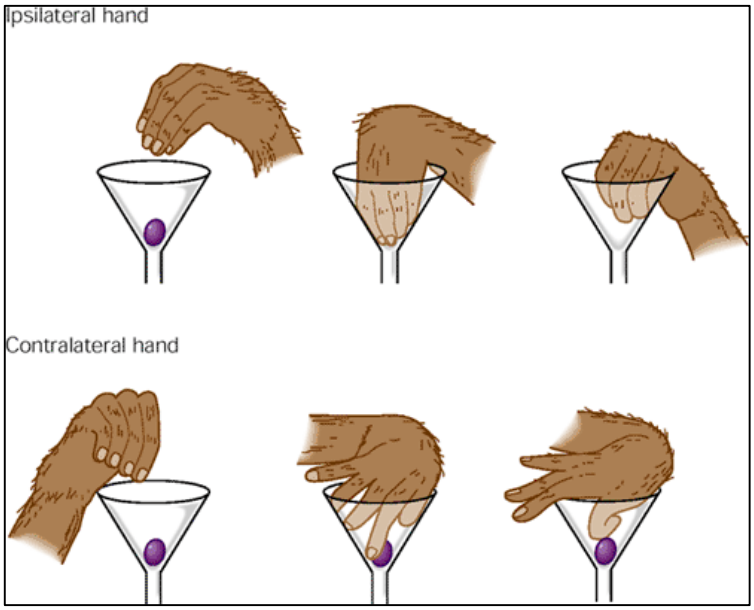

Figure 19: Impairments in monkey's finger coordination.

Muscimol was injected into Brodmann's area 2 on the left hemisphere of a monkey. After some minutes, the finger coordination of the contralateral hand was severely disorganized. The monkey was unable to remove a grape piece from a funnel with the contralateral hand but not the ipsilateral one.

Modified from (Hikosaka et al., 1985).

Experimental lesions of the various somatic areas of the cortex have also provided valuable information about the function of different Brodmann's areas concerned with somatic sensibility. Total removal of the primary somatic cortex S-I produces deficits in position sense and the ability to discriminate size, texture, and shape. Small lesions in the cortical representation of the hand in Brodmann's area 3b produce deficits in the discrimination of the texture of objects as well as their size and shape. Lesions in area 1 produce a defect in the assessment of the texture of objects, whereas lesions in area 2 alter the ability to differentiate the size and shape of objects. This is consistent with the idea that area 3b receives

information about texture as well as size and shape (area 3b, together with 3a, is the principal target for the afferent projections from the ventral posterior lateral nucleus of the thalamus). Area 3b projects to both areas 1 and 2. The projection to area 1 is concerned primarily with texture, whereas the projection to area 2 is concerned with size and shape. Because S-II receives inputs from all areas of S-I, removal of S-II causes severe impairments in the discrimination of both shape and texture and prevents monkeys from learning new tactile discriminations based on the shape of an object.

Damages to PPC produce complex sensorimotor abnormalities. These include the inability to accurately process stimuli in the contralateral visual field or contralateral half of the body. Poor motor coordination and poor eye-hand coordination during reaching, grasping, and hand orientation lead to neglect in usage of the hand (Bisiach & Luzzatti, 1978; Marshall & Halligan, 1995; Andersen, 2011).

A form of *agnosia* particularly interesting is the *astereognosis*, which is the inability to recognize the shape of objects through touch. This deficit is often associated to left-sided paralysis. Patients suffering from this type of *agnosia* have a unique alteration of their left side body image and of the perception of the external world that it is to their left. Some patients (*personal neglect syndrome*) do not care about dressing or cleaning the left side of their body and in the most severe cases, they deny the existence and the belonging of their arm and/or leg. In some patients, this negligence interests also the peripersonal or extrapersonal space (*spatial neglect*). These subjects are unable to recognize or draw the left side of a paint. In Figure 20, the three drawings on the right were made from the models on the left, by patients with unilateral visual neglect following lesion of the right posterior parietal cortex. As shown in the figure, these patients are unable to copy only the left side of the drawings while the right part is identical to the model to copy. The patient may draw a flower with petals on only the

right side of the plant, and when asked to copy a clock, the patient may ignore the numbers on the left.

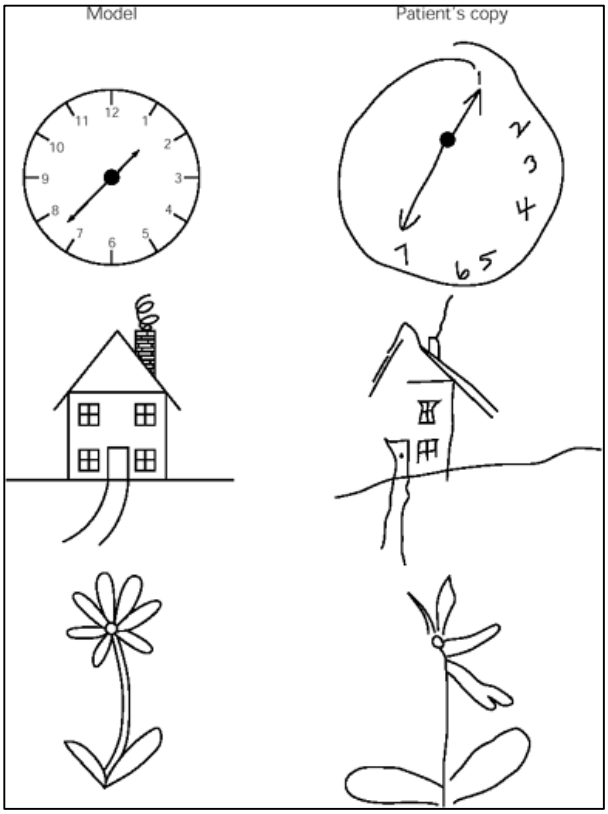

Figure 20: Unilateral visual neglect.

The three drawings on the right were made by patients suffering from unilateral parietal damage. *From (Bloom et al., 1988).*

The Hungarian neurologist Rezso Balint in 1909 first described what he called ‘Optic Ataxia’. The optic ataxia has been studied since it has been discovered and continues to fascinate the researchers. Optic ataxia patients have difficulties in reaching to visually guided targets in peripheral vision, as shown in Figure 21. Moreover, in normal subjects reversible inactivation of PPC through transcranial magnetic stimulation affects the accuracy of hand

movement trajectory (Desmurget *et al*., 1999). Optic ataxia deficit is a result of a lesion to the superior parietal lobule (SPL) and the parieto-occipital junction (POJ). Interestingly, there are no primary sensory or motor deficits involved in lesions in that region. In fact, optic ataxia patients maintain normal vision, stereoscopic vision, voluntary eye movements, proprioception and motor abilities (Perenin *&* Vighetto, 1988). Thus, the problem related to this deficit is at more integrative sensorimotor level. Optic ataxia could be the result of unilateral and bilateral lesions of this brain region and is combined with other disturbances, as misshaping of the hand for the grasping and deficits in the online visuomotor control (Andersen *et al*., 2014a). These impairments occurred more frequently in the peripheral vision but happened also towards foveated targets when the visual feedback is absent (Perenin *&* Vighetto, 1988; Rossetti *et al*., 2003; Battaglia-Mayer *et al*., 2006).

Figure 21: Patient with Optic ataxia.

The patient misreaches beyond the pencil when asked to touch it. From (Andersen et al., 2014a).

Three frameworks have been proposed for optic ataxia: disruption of i) visuomotor processing, ii) visual orientation and iii) online visuomotor control. The visuomotor processing framework posits that the deficit regards the sensorimotor integration (in the case of the patient of Figure 21 regarding vision and reaching movement). Perenin and Vighetto's observations were the basics of Goodale and Milner's (1992) two visual stream hypothesis.

Subjects with lesions to ventral visual areas (the 'What' stream) suffered of agnosia (difficulties in recognizing objects) whereas subjects with lesions of the dorsal visual stream ('How' stream) have optic ataxia.

The second framework ascribes the optic ataxia to a disruption of visual orientation, so subjects cannot correctly judge the location of the target. The British neurologist Gordon Holmes (Holmes, 1918) studied soldiers of the first war world with lesions of the parietal cortex. Importantly this author observed that subjects with bilateral lesions of the postero-lateral parietal lobe, despite having normal visual acuity, were not able not only to localize or grasp objects but also to connect the elements presented in the visual field. Holmes explained the deficits with a perceptual point of view, the loss of visual orientation because of the difficulties of the patients in finding and fixating objects. These defects included perceiving the relative and absolute distances of objects from the body, their shape characteristics and their position. The third hypothesis of framework points out that optic ataxia is the result of a deficit in the mechanism underlying ongoing movements via visual feedback (Andersen *et al*., 2014a). Normal subjects can modify the movement online, unconsciously (Pisella *et al*., 2000) as if they have an "automatic pilot" that plays in case of a perturbation or a jump of the target. In optic ataxia patient this automatic pilot is not working. In a study of 2007, researchers reported also an impaired use of proprioceptive information (Blangero *et al*., 2007). Authors tested the hypothesis of a deficit in extracting the spatial location of the ataxic hand from multi-joint

proprioceptive information. The study revealed misreaching when the ataxic hand pointed toward proprioceptive targets.

The above-mentioned observations confirm the important role of the PPC processing goal directed actions. However, less is known about the involvement of these human regions in the control of movement extent and how much lesions on this brain region could affect the perception of depth. In the work of Baylis and Baylis (2001) it has been reported that optic ataxia patients may have difficulties in detecting the direction of motion and may have severely impaired depth perception. In good agreement with Baylis data, Danckert (2009) studied an optic ataxia patient with damages located in the superior parietal cortex including regions of the IPs and POJ. The authors observed that the patient's movements in the sagittal plane were more impaired than those in the frontoparallel plane, as reported in Figure 22. The authors pointed out that also in normal subjects the movement duration is higher for movements made in the sagittal versus the frontoparallel plane supporting the idea that these movements are more difficult to perform. These authors for the first time pointed out that patients with lesions in PPC show deficits more frequently related to objects placed at different depth than at different direction.

An emerging picture suggests that the heterogeneity of aspects of optic ataxia are the result of damages of an array of functional modules (Battaglia-Mayer *et al*., 2006; Andersen *et al*., 2014a) that human studies cannot completely elucidate. Studies in animals using pharmacological or surgical PPC inactivations have the advantage of confining the inactivation to single anatomically and functionally defined modules. Moffett and coworkers (Moffett *et al*., 1967) studied the tactile discrimination performance in monkeys after the ablation of various subdivisions of PPC. They found that the most severe impairment on the tactile discrimination tended to associated with a severe inaccuracy of reaching.

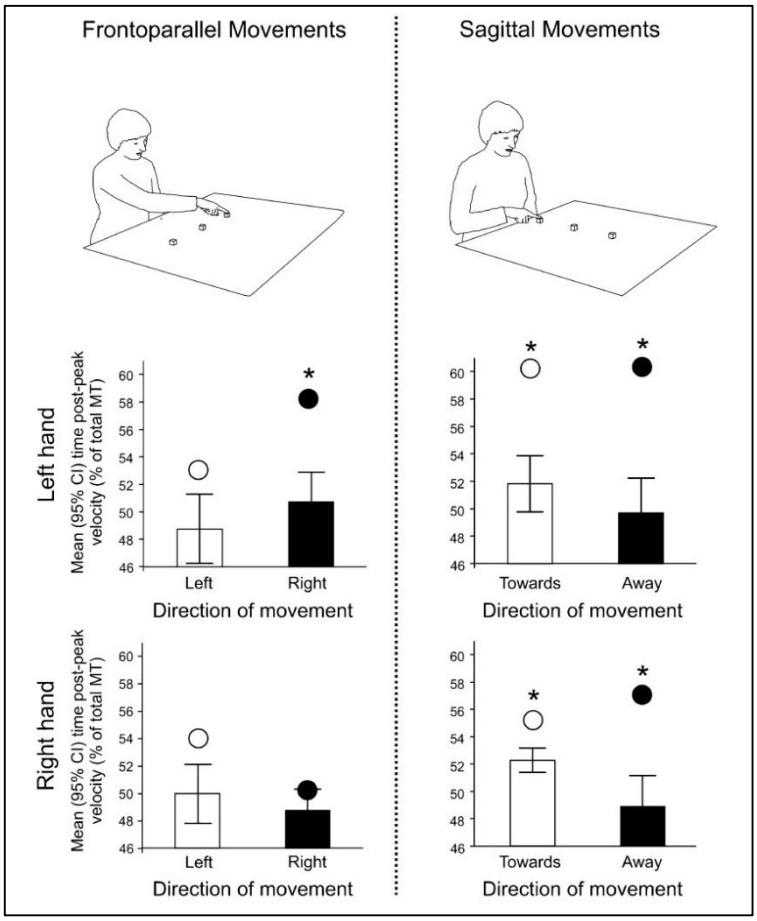

Figure 22: Impairments for movements towards different directions and depths.

Top) experimental setup for frontoparallel movements (left, different directions tested) and sagittal movements (right, different depths tested). Normal subjects and the patient (ME) made reciprocal pointing movement to one of the three targets placed in front.

Bottom) Histograms showing the time spent post-peak velocity (mean and 95% CI's from controls in bars; patient ME means in circles) for each hand (left in the upper panel and right in the lower one) and for each direction of movement.

Significant differences between patient and controls as determined by the one-tailed Crawford t-test ($p<0.05$) are reported by *. Patient ME had more deficits for movements in the sagittal axis than in the frontoparallel plane.

From (Danckert et al., 2009).

Rushworth studies (Rushworth *et al*., 1997a; b; Rushworth *et al*., 1998) on monkeys with lesions on the PPC showed that the ventral part of the posterior parietal lobule (areas 7a and LIP) is essential for the spatial coordination of visual motor transformation, while its dorsal part (areas 5 and MIP) is involved in the spatial coordination of arm movements depending in proprioceptive and efference copy feedbacks. Severe impairments in the visual control of arm movements are also described in animals in which the lesion extended into the medial wall of the SPL affecting area PGm (for its location see Fig. 4, violet patch). In fact, neural activity of this area is deeply influenced by visual feedback signals about hand movement trajectory and hand position in space (Ferraina *et al*., 1997).

The lesions above mentioned covered a quite large portion of cortex and were located mainly in the IPs. Recently, Battaglini and coworkers (2002) studied in two monkeys the effects of lesions of the monkey POs, mainly involving area V6A. Animals were normally reactive to stimuli but their posture was abnormal and both refused to use spontaneously the contralateral arm (with respect to the larger lesion). When the authors forced the animals to use it, the reaching and grasping time increased about 30% with respect to the pre-lesion times. Another important observation was that the position of reaching/grasping target was under- or overestimated (Battaglini *et al*., 2002). The deficit disappeared after some repetitions of the movement but reappeared every time that the food changed in its position, as shown in Figure 23. More importantly, both animals showed abnormality in orienting and conforming the hand, especially the wrist, to the food. These observations confirm the idea that the POs and in particular area V6A is a node of the network underlying visually guided reaching and grasping actions (Battaglini *et al*., 2002). Moving anteriorly in the SPL, Battaglia-Mayer and coworkers (2013) inactivated the superior parietal area 5 (PE/PEa) using muscimol and tested the effect on the jumped target task. After this reversible inactivation, they observed an increase of hand

reaction- and movement-time required to make the correction leading to an elongation of the hand path. They interpreted these findings as a deficit in the online control similar to that observed in optic ataxia patients. Other studies include the inactivation of the parietal reach region (PRR) a region that includes a number of reach-selective cortical areas (Snyder *et al*., 1998; 2000). In this study, animals exhibited increased errors for reach movements to visual stimuli and similarly to human optic ataxia, the errors were seen for extrafoveal but not for foveal targets (Hwang *et al*., 2012).

These results highlight the crucial role played by the PPC especially the SPL in the encoding of target location for the online control of arm movements.

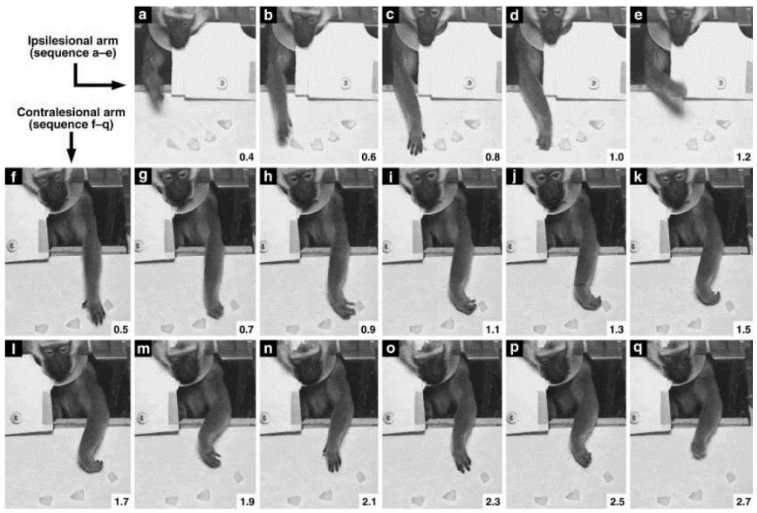

Figure 23: Effects of V6A lesions in macaque monkey.

Single-frame reconstruction of the effect of the second V6A lesion. Frames were recorded every 0.004 s and one every five were sequenced in the figure. Recording was performed the 2nd day after lesion.

It is evident the dysmetria and the impairments in reaching for food. The most important effect is notable when the hand of the animal approaches the piece of food. The monkey rotates its hand abnormally, opening the grip laterally rather than downwards (frames h-m). The defect is evident only with the contralateral hand.

Frames a-e, ipsilesional arm; frames f-q, contralesional arm.

From (Battaglini et al., 2002).

1.11 Role of parietal area V6A

Area V6A, identified by the pink patch in Figure 4, is located in the caudalmost part of the SPL and it extends from the mesial surface of the brain, through the anterior bank of the POs, up to the most lateral part of the fundus of the sulcus (Galletti *et al*., 1996; Galletti *et al.,* 1999b). Area V6A, corresponding to Brodmann's area 19 (Brodmann, 1909), borders ventrally area V6 and dorsally area PEc. Area V6A is a visuomotor area containing visual (~61%) as well as neurons insensitive to visual stimulation or modulated by other type of stimuli (~39%) (Galletti *et al*., 1999b).

Specifically area V6A contains cells modulated: i) by gaze positions in a fronto-parallel plane and in 3D space (Galletti *et al*., 1995; Nakamura *et al*., 1999; Hadjidimitrakis *et al*., 2011; Breveglieri *et al*., 2012), ii) by somatic stimulation (Breveglieri *et al*., 2002) and iii) by reaching and grasping movements (Fattori *et al*., 2001; Fattori *et al*., 2004; Fattori *et al*., 2005; Marzocchi *et al*., 2008; Fattori *et al*., 2009; Fattori *et al*., 2010; Breveglieri *et al*., 2014), as well as iv) by attentional signals (Galletti *et al*., 2010).

Area V6A, contrary to area V6, is a non-retinotopic organized area. Looking at the sequences of RF location shown in Figure 24, it is evident that RFs of this area could remain in the same spatial location for hundreds of microns, and then jump away in an unpredictable direction. In this way, cells near one to another could have RFs either in the same either in a complete different location in the visual field (Galletti *et al*., 1999b). The inferior contralateral hemifield is the most represented in this area thus supporting the idea of its involvement of area V6A in the visuomotor control of arm movements.

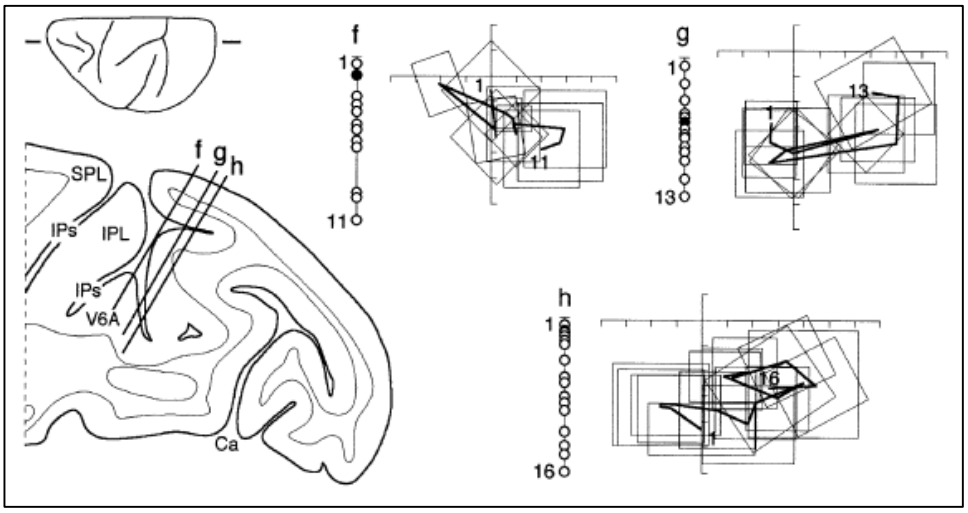

Figure 24: Visual receptive fields "jumping" in area V6A.

Visual RFs plotted in three penetrations made through area V6A.

Left, parasagittal section of the brain of case 16R, taken at the level shown on the brain silhouette placed just above. One inset for each penetration (f, g, h) is shown on the top and right part of the figure.

Right, each of the three insets shows the cell types encountered and their locations along the penetration (empty circles = visual cell; filled circles = non-visual cell), and the RF sequence of visual neurons.

Visual cells are numbered progressively along the penetration and the first and last numbers are reported. The RF centers of visual cells are sequentially connected with a black line, first and last RF encountered are numbered.

Other conventions as reported in above figures.

Adapted from (Galletti et al., 1999b).

This role is supported also by the presence of somatic RFs located mostly in both proximal and distal parts of the contralateral arm. These somatosensory cells could give a feedback on the actual state of the arm while the arm and hand are approaching to the visual target in the peripersonal space (Breveglieri *et al*., 2002). However, the observation that

reach-related activity in V6A is stronger during active than passive arm movements suggests that skeletomotor information could be only partially responsible for the reach signal. As reported in (Galletti *et al*., 1997), neurons modulated by reaching movements increased their firing rate 200 ms before the beginning of the arm movement. This may be due to other information available well before muscles are activated. Preparatory motor activity, as well as a computation of a motor corollary discharge from the premotor dorsal areas (F2 and F7), reciprocally connected with V6A, could explain this observation (Matelli *et al*., 1998; Gamberini *et al*., 2009; Passarelli *et al*., 2011; Breveglieri *et al*., 2014). Neurons of area V6A are very sensitive to the direction of the reaching movement. Fattori and coworkers (2005) studied V6A neuronal response while animals performed a body-out-reaching task toward foveated targets placed in different positions on a frontal panel. They observed that about 40% of V6A cells was modulated by the position/direction of the arm without a strong preference of one target position among the others. Two examples of V6A cells modulated by the direction of the arm reaching movement is shown in Figure 25. These data suggest that area V6A is able to code the direction of an arm reaching movement and the position of the same in the peripersonal space (Fattori *et al*., 2005). As above-mentioned, recently our research team studied the representation of reach depth and direction while the animal performed a reaching task in the 3D space (Hadjidimitrakis *et al*., 2014).

The authors found that, in the majority of single V6A neurons, depth and direction signals were jointly encoded during not only the arm movement phase but also during the fixation and planning phases of the task. These findings support for the first time the existence of a common substrate for the encoding of both target depth and direction during reaches in the medial PPC. Moreover, these data highlight the coexistence within area V6A of several types of neurons that process independently or jointly signals about eye positions and arm status.

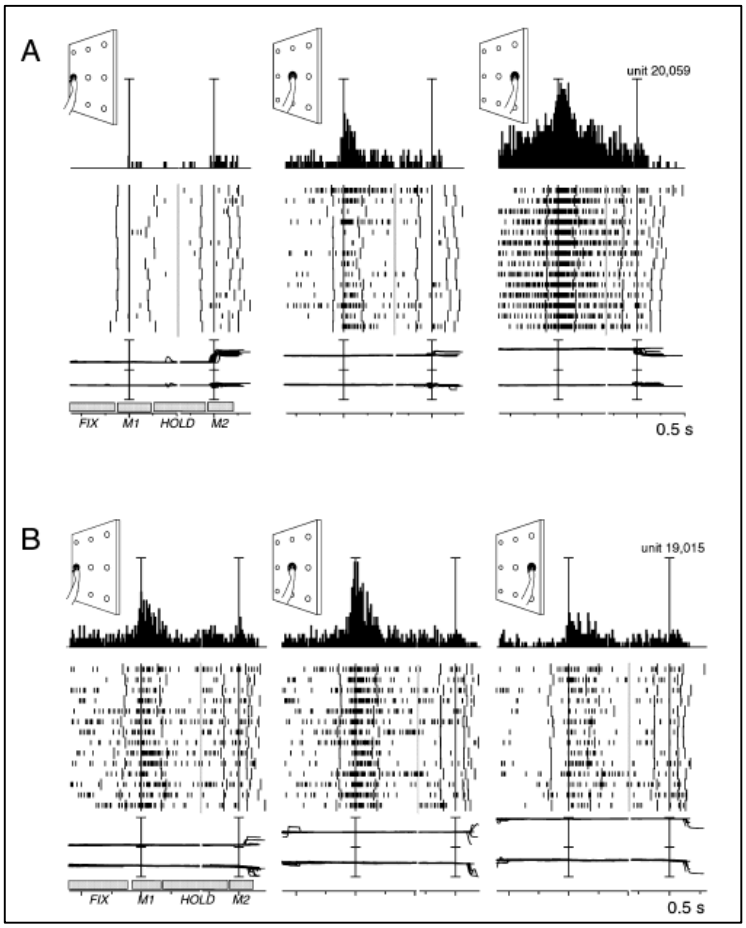

Figure 25: Spatially tuned modulations in V6A.

A) Neuron spatially tuned during the execution of reaching movement, preferring right target position.

B) Neuron spatially tuned during the execution of the movement, preferring reaches directed to the central target position.

Each inset in both A and B contains the peri-event time histogram (PSTH), raster plots and eye traces. Each PSTH is positioned in the same location as the target on the panel, as sketched in the top left corner of each inset. Neural activity and eye traces were double aligned with the onset of outward (first) and inward (second) reach movements. The mean duration of time epochs considered in the analysis is indicated in the bottom left inset. Scale bar, neuron A, 70 spikes/s; neuron B, 100 spikes/s. Time epochs, FIX, steady fixation epoch; M1, outward reach movement epoch; HOLD, holding phase with hand on the target epoch and M2, inward reach movement to return to the starting position.

From (Fattori et al., 2005).

According to a recent study (Luppino *et al*., 2005), area V6A can be subdivided in two subfields: one, ventrally, called V6Av and another, dorsally, called V6Ad. V6Ad is mainly confined to the anterior wall of the POs, slightly extending over the mesial cortical surface and the medial bank of the IPs. Its dorsal border is close to the junction between the anterior bank of the POs and the exposed dorsal surface of SPL. The V6Av extends more rostrally than V6Ad, both in the medial and lateral aspects of the SPL and surrounds anteriorly, medially and laterally area V6. These two cortical sectors show different cytoarchitectural patterns. As discussed later in the next chapter (see Figure 34), the ventral sector of area V6A shows cytoarchitectural pattern more similar to the occipital cortex, whereas the V6Ad a more parietal pattern. Briefly, the ventral part of area V6A is characterized by a well-delineated layer II and a well develop layer V, the dorsal part (V6Ad) is characterized by a poorly defined layer II and a richer layer V with respect to V6Av.

The anatomical connectivity of these two sectors mirrors this different architectural organization. In fact, area V6Av is strongly connected with the occipital extrastriate visual areas, whereas V6Ad shows connections with both parietal and frontal areas (Gamberini *et al*., 2009; Passarelli *et al*., 2011). As illustrated in Figure 26, V6Av receives many of its afferents from the extrastriate area V6 and from regions of V2, V3, V4 and from dorsal stream areas MT and MST. It is evident that V6Av doesn't receive directly projections from V1. The strongest parietal connections are V6Ad, PGm, MIP and PG. On the other hand, the major connections of V6Ad are with areas of the SPL, specifically areas PEc and V6Av, area MIP and LIP of the IPs, and areas PGm, 31 and 23 of the mesial surface. Connections are also directed to the IPL (fields Opt and PG) and to the STs area MST. Importantly, V6Ad unlike area V6Av, is connected with areas of the frontal lobe. The main projections originates from F2 and F7 (Gamberini *et al*., 2009; Passarelli *et al*., 2011). Functional and connections data support the idea that V6A is a single functional area involved in the control of visually

guided actions, with its ventral sector more involved in the visual control of the motor act and the dorsal one in the somatic control of it (Gamberini *et al*., 2011).

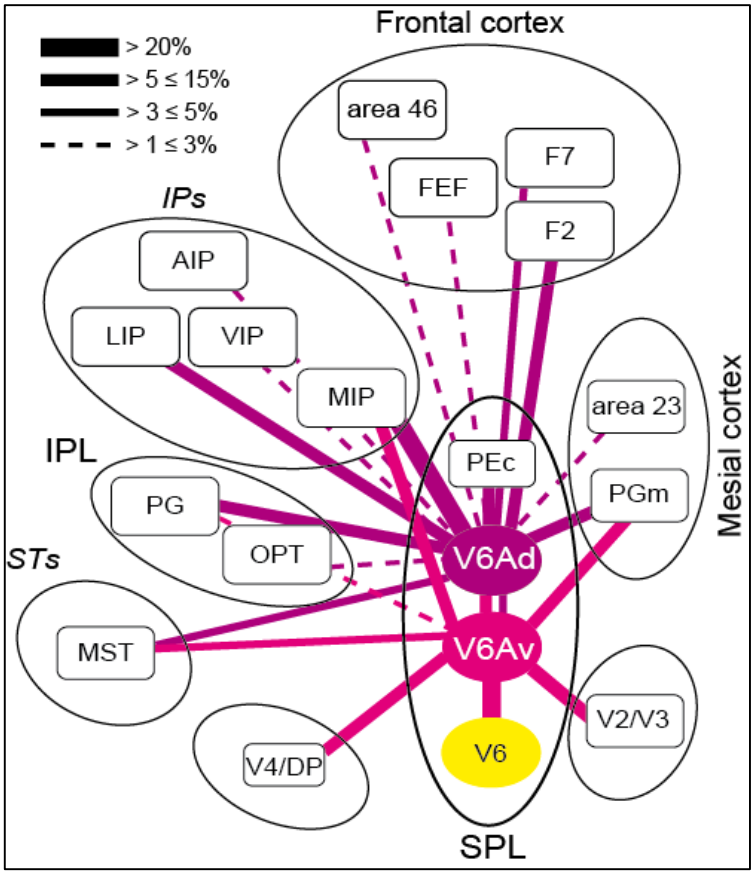

Figure 26: Connections of the ventral (V6Av) and dorsal (V6Ad) sectors of area V6A.

The boxes representing different areas are organized in a caudal to rostral sequence, from the bottom part of the figure to the top. The proportion of neurons forming each connection is illustrated by the thickness of the bars linking different areas. The ventral part of V6A is characterized by visual afferents, and this emphasis is gradually substituted by sensory association and premotor connections as one proceeds toward the dorsal sector.

Adapted from (Passarelli et al., 2011).

1.12 Role of parietal area PEc

In a review of several anatomical studies, Pandya and Seltzer (Pandya *&* Seltzer, 1982) defined the region in the caudal pole of the SPL of rhesus monkey as area PEc. As shown in Figure 4 (green patch) this area occupies the caudalmost third of the exposed cortex of the SPL and extends onto the mesial surface of the hemisphere where it borders area PGm (Pandya *&* Seltzer, 1982; Cavada *&* Goldman-Rakic, 1989a). Its unique architectural profile will be discussed later in the dissertation. Several physiological studies highlight the sensory and motor properties of cells in PEc. Many cells in this area respond to moving visual stimuli and optic flow signals (Squatrito *et al*., 2001; Raffi *et al*., 2002; Breveglieri *et al*., 2008), as well as to tactile stimulation and passive movements (Breveglieri *et al*., 2006; Breveglieri *et al*., 2008). Somatosensory neurons were mostly found in the upper limbs and only a minority of their RFs were located on the lower limbs and/or trunk (Breveglieri *et al*., 2006). In the above studies, no clear retinotopy or somatotopy was discerned. Eye-position and reaching neurons were also found within area PEc (Ferraina *et al*., 2001; Raffi *et al*., 2008) suggesting its involvement in visuomotor behavior and in the internal perception of oneself (Battaglia-Mayer *et al*., 2001; Breveglieri *et al*., 2006). In the work of 2001, Ferraina and coworkers tested the neuronal response of single cells of PEc while the animal performed a reaching task from a central position to eight peripheral foveated targets (Ferraina *et al*., 2001). Similarly to what found in area V6A, a large proportion of PEc cells (60%) displayed a relationship to hand movement direction, in Figure 27 an example of direction selective reaching neuron is shown. Until now, contrary to the nearby area V6A, the involvement of area PEc in the coding of pure depth or both depth and direction has never been investigated. One of the aims of this thesis is to test the presence within PEc of neurons modulated by one or both these two signals.

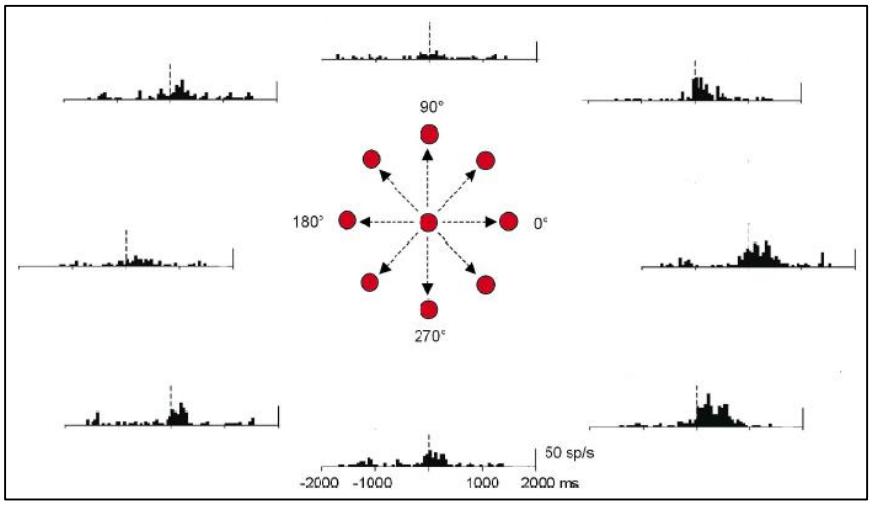

Figure 27: Directional reach neuron of area PEc.

Peri-events time histograms of the activity of PEc neuron in the 8 different directions tested during the center-out reach task. Neuronal activity is aligned to the onset of hand movement (vertical dashed line). Bin size 50 ms. In the center, directional array of the workspace is shown. Vertical scale indicating the spikes per second and time is indicated. *Adapted from (Ferraina et al., 2001).*

The most important source of projections to area PEc, as shown in Figure 28, is the somatosensory-related cortex (areas PE and PEci). Connections were also found in the medial bank of the IPs with a subdivision of area MIP (a region named dMIP) and in the postcentral area 2 (Bakola *et al*., 2010). The main motor connection is represented by areas F2 and F3 in which a high number of neurons responds to passive stimulation of the lower limbs. The only visual input to PEc originates in the dorsal sector of area V6A. Based on connectivity data, it has been suggested that PEc process information about the position of the limbs. The links with between PEc and motor and premotor areas together with the link with the vestibular cortex and areas involved in the analysis of optic flow and spatial navigation, imply a role for PEc in locomotion and limb movement in the environment.

The abundance of projection neurons in zones that represent the lower limbs (Bakola *et al*., 2010) contrasts with the reported involvement of PEc in manual tasks as well as with the reported somatosensory over-representation of the upper limbs (Breveglieri *et al*., 2006; Breveglieri *et al*., 2008). This contract could be due to a limited neuronal sampling in the above-mentioned studies or to the fact that not the entire extension of area PEc has been tested.

The third aim of this thesis is to investigate/reinvestigate visual and somatosensory properties of PEc cells increasing the number of cells to avoid the two methodological biases above discussed.

Considering the proximity and the functional affinity between areas PEc and V6A, we compare both sensory (visual and somatic) and motor (reaching) properties of neurons recorded in area PEc to those of neurons in area V6A, especially in its dorsal part.

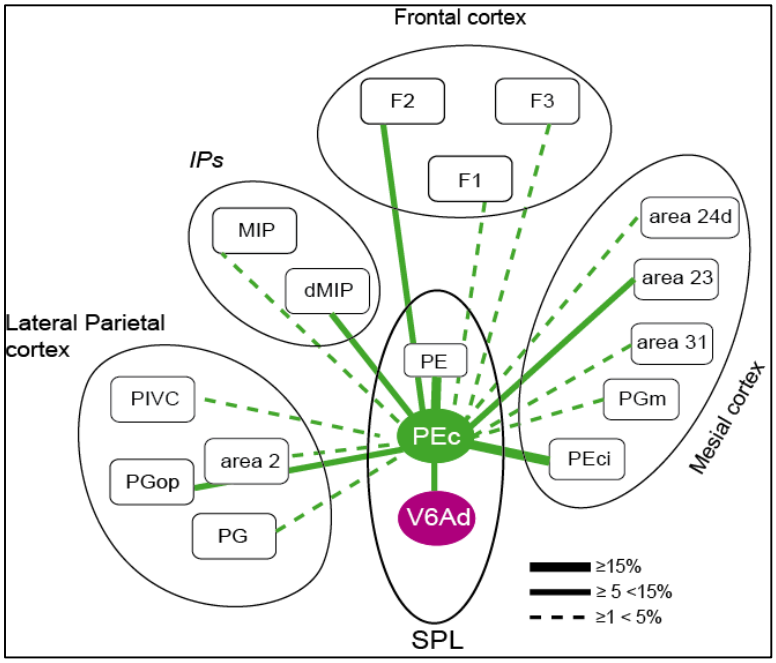

Figure 28: Anatomical connections of area PEc.

Flow chart of the cortical areas that contained significant (≥1%) numbers of labeled cells after PEc injections. *Adapted from (Bakola et al., 2010).*

1.13 Aim of the work

In the posterior parietal cortex, there is a constellation of areas collectively involved in the visuomotor transformations necessary for controlling goal-directed actions. Different cortical areas, identified on the basis of their functional repertoire and cortico-cortical connections, operate on a multiplicity of signals (visual, somatosensory), each of which influences differently cell activity. The PPC is characterized by a gradient-like distribution of properties, with the eye preponderance in its caudal pole, and the opposite arm supremacy in its rostralmost pole. In between, eye and hand signals coexist with different strength relationship. The present work takes into account three PPC areas, V6, V6A, and PEc, each one operating on a different subset of signals (visual, somatic, motor). The work focuses on the study of their functional properties, to better understand their respective contribution in the neuronal circuits that make possible the interactions between subject and external environment.

In the caudalmost pole of PPC there is an extrastriate visual area named V6. Human and macaque results together suggest that this area is related to the encoding of both objects- and ego-motion. The functional visual properties of V6 neurons were studied over years on single-cell recordings on macaque monkeys (Galletti *et al*., 1991; 1995; 1999a). The human homolog of macaque area V6 has been found in the dorsalmost part of the human parieto-occipital sulcus and contains a representation of both the center and the periphery of gaze (Pitzalis *et al*., 2006; 2010; 2012; 2013). Human studies highlighted the role of area V6 in the analysis of flow field resulting from self-motion. However, while the sensitivity of V6 neurons to optic flow stimulations has been tested in human fMRI experiments, the Flow-Fields stimulus has never been tested in monkey. Here we addressed this issue by applying on monkey the same experimental protocol used in human studies. We will able to bridge a gap between human and monkey studies. Animals were trained to perform a fixation task while two visual

stimuli, Radial-Rings and Flow-Fields, were projected on a screen faced the animal located inside the scan bore. The preliminary results discussed in this thesis are in line with those described in human. The visual stimulation obtained with the Flow Fields stimulus was the most effective and powerful to activate area V6 in monkey, highlighting the important role of this area in the analysis of motion.

Two neighboring areas of the caudal part of the superior parietal lobule, V6A and PEc, show different cytoarchitecture and connectivity profiles, but have neurons with similar functional properties that are involved in the control of reaches. In everyday life every arm movement happens in 3D space and there is substantial psychophysical evidence that direction and distance of reaches are processed independently (Gordon *et al*.,1994; Sainburg *et al*., 2003; Vindras *et al*., 2005; Bagesteiro *et al*., 2006; Van Pelt *&* Medendorp, 2008). However, the evidence on their neural substrates in SPL remains fragmentary. Most single unit studies have either employed center-out reaching tasks, or addressed only the coding of hand movements in depth (Bhattacharyya *et al*., 2009; Ferraina *et al*., 2009; Hadjidimitrakis *et al*., 2014). While we have recently demonstrated that during reaches in 3D space both depth and direction information is represented in V6A, the encoding of reach depth has never been investigated in PEc (Battaglia-Mayer *et al*., 2000; 2001; Ferraina *et al*., 2001). From these considerations, arise the aim of this work, to check whether PEc and V6A show different functional properties. We first studied both visual and somatosensory behaviors of 1496 neurons collected from 12 animals over several years, comparing the properties of neurons recorded in area PEc with those of the dorsal sector of V6A. Secondly, we studied the motor related behavior of 288 PEc neurons during reaching in 3D space comparing also the direction and depth tuning of PEc neurons with those of V6A neurons during the several phases of arm movements in 3D space. Single unit activity was recorded from three *Macaca fascicularis* monkeys performing foveal

reaching in darkness towards targets placed at different depths and directions.

The results of the functional properties show that area PEc and V6Ad share several functional properties. Area PEc, however, contains more neurons modulated by somatosensory stimulations with respect to the visual ones; the opposite happened in V6Ad in which visual neurons and somatic neurons are both presented with the same percentage.

Studying the motor properties of area PEc, we observed that the effect of direction was more prevalent than depth before reaching execution, whereas depth modulations and convergence of direction and depth signals became prominent mostly after the start of the arm movement. Comparing the two areas revealed that PEc cells processed mostly the depth information related to the arm movement, whereas V6A neurons processed jointly the depth signals related to eye position and movement execution. These findings are consistent with the involvement of both areas in visuospatial and action representations in 3D peripersonal space. Sensory and motor data together support the idea of the existence of a caudo-rostral trend in the superior parietal lobule, from a representation of both space and action in V6A to action prevalence in PEc.

2 MATERIALS AND METHODS

2.1 Ethics

Electrophysiology experiments were performed in Bologna, following the national laws on care and use of laboratory animals and with the European Communities Council Directive of November 24, 1986 (86/609/EEC) and that of 22th September 2010 (2010/63/EU). The Bioethical Committee of the University of Bologna approved all the experimental protocols. fMRI experiments were carried out in Lyon, in accordance with the French transposition texts of Directive 2010/63/UE and the project was authorized by the French Ministry for Higher Education and Research based on ethical evaluation.

2.2 General and experimental procedures

- ✓ *fMRI: training and scanning procedures*

Each monkey was surgically implanted with a plastic head post in aseptic conditions under anesthesia (glycopyrrolate 0.01 mg/kg, i.m. + acepromazine maleate 0.05ml/kg, i.m. + ketamine 10mg/kg, i.m.) followed by the gaseous anesthesia (2-chloro-2-(difluoromethoxy)-1,1,1-trifluoro-ethane 0.5 to 2% depending on the condition of the animal). The body temperature was controlled throughout the procedure. The animal was intubated and ventilated with a mixture of 30% O2 and 70% N2O. Tidal volume and respiratory rate were tailored according to each animal (approximately 10ml/kg at 20-30 breaths per minute). An intravenous line was placed in the saphenous vein through which a saline solution was delivered at 5 ml/kg/hour. The animal was then placed in a stereotaxic frame before the surgery begins. MRI-compatible (plastic or ceramic) screws and

a plastic headpost were implanted on the skull. After surgery, the animal got under close supervision for a minimum of 20 days before being involved in experimental procedures. Postoperative pain was controlled by buprenorphine hydrochloride (0.01mg/kg, i.m.). Postoperative treatment further consisted of antibiotics (enrofloxacin 5mg/kg, i.m. for 10 days), and anti-inflammatory agent (tolfenamic acid 4mg/kg, i.m. for 3 days). After recovery, monkeys were trained to sit in a sphinx position in a plastic chair with their heads fixed. Monkeys underwent 2-5 training sessions per week in order to optimize the experimental setup and familiarize the animals to the primate chair and the fMRI sound. The implant is cleaned after each training session with betadine and hydrogen peroxide. The scans were performed after injection of an exogenous contrast agent (monocrystalline iron oxide nanocolloid MION, 7-11mg/kg) into the femoral vein to increase the contrast-to-noise ratio and optimize the localization of the fMRI signal (Vanduffel *et al*., 2001). Imaging data were collected on a 1.5T Siemens Magnetom (Sonata, Siemens AG, CERMEP imagerie du vivant, Lyon, France) horizontal scanner (60 cm diameter of the bore). Functional data from the whole brain were acquired with a custom-made 9 cm radial surface coil (1 channel, Rapid Biomed) positioned immediately over the head (Figure 27A). Each run of scanning lasted 257 s (TR 2 s; TE 27; 2x2x2 mm; 132 TRs; phse FOV 100.0). In monkey CE we performed two scanning session collecting 8 runs in the first and 24 runs in the second, in monkey CA we collected 21 runs and 13 runs during 2 scanning sessions. For a detailed description of the scanning procedure see Hadj-Bouziane and coworkers 2008; 2012; 2014 (Hadj-Bouziane *et al*., 2008; 2012; 2014).

- ✓ *Electrophysiology: training and recording procedures*

The head-restraint system and the recording chamber were surgically implanted in asepsis and under general anesthesia (sodium thiopenthal, 8mg/kg*h, i.v.) following the procedures reported in a work of the 1995 (Galletti *et al*., 1995). A full program of postoperative analgesia (ketorolac

tromethamine, 1mg/kg i.m. immediately after surgery, and 1.6 mg/kg i.m. on the following days) and antibiotic care (Ritardomicina, benzatinic benzylpenicillin + dihydrostreptomycin + streptomycin, 1-1.4 ml/10kg every 5-6 days) followed surgery.

The recording chamber, positioned on the midsagittal plane and centered 13-15 mm posterior to the interaural line, provided access to the cortex hidden in the parieto-occipital sulcus of both hemispheres. The microelectrode entered the cortex with an angle between 26° and 45° with respect to the stereotaxic vertical and reached the anterior bank of the parieto-occipital sulcus (area V6A) in the depth and/or the exposed surface of the superior parietal lobule (area PEc).

Single-cell activity was extracellularly recorded using either homemade glass-coated Elgiloy microelectrodes (Suzuki *&* Azuma, 1976) with a tip impedance of 0.8-2 MΩ at 1kHz, or microelectrodes type ESI2ec (Thomas Recording) with a tip impedance of 1-2 MΩ mounted on a five-channel multielectrode recording minimatrix (Thomas Recording). Signals from the electrode were amplified (gain 10,000) and filtered (bandpass between 0.5 and 5 kHz). Action potentials were isolated with a dual time-amplitude window discriminator (DDIS-1; Bak Electronics) or with a waveform discriminator (Multi Spike Detector; Alpha Omega Engineering). Spikes were sampled at 1 KHz in 4 animals and at 100 kHz in 5. Behavioral events were recorded with a 1 ms resolution. Eye movements were monitored continuously using an infrared oculometer (ISCAN, 100 Hz). During training and recording sessions, particular care was taken to avoid any behavioral and clinical sign of /pain and distress. During the training period, animals were manipulated and touched on the entire body by the experimenter and were rewarded with water, juice and fruits during manipulation in order to get them docile and cooperative. Electrophysiological recordings were made 6-7 h per day, between recording sessions, the monkeys lived in their home cage without showing any sign of pain or distress.

2.3 V6 and MT mapping

Two female rhesus monkeys (Macaca mulatta, weight 5-5.5 Kg) participated in this study. Monkeys had a plastic head post secured by plastic screws and bone cement. During training sessions and fMRI scanning, alert monkeys sit in a sphinx position inside a plastic chair (Vanduffel *et al*., 2001) with the head fixed facing a screen on which visual stimuli were presented in complete darkness as shown in Figure 29A. Each stimulus was presented with a small central fixation cross on which the monkeys were required to fixate to receive a liquid reward. To promote long periods of fixation, the frequency of reward delivery increased as the duration of fixation increased. During all the sessions, gaze location was monitored by using an infrared pupil tracking system (ISCAN) centered on the right eye. Stimuli were presented by using a projector (Canon XEED SX60) and displayed on a screen positioned just outside the magnet bore at 90 cm distance from the animal (36° wide of visual field tested). Presentation® program (Neurobehavioral systems) was used to run the fixation task and control the reward; visual stimuli were presented using Mac OS X.

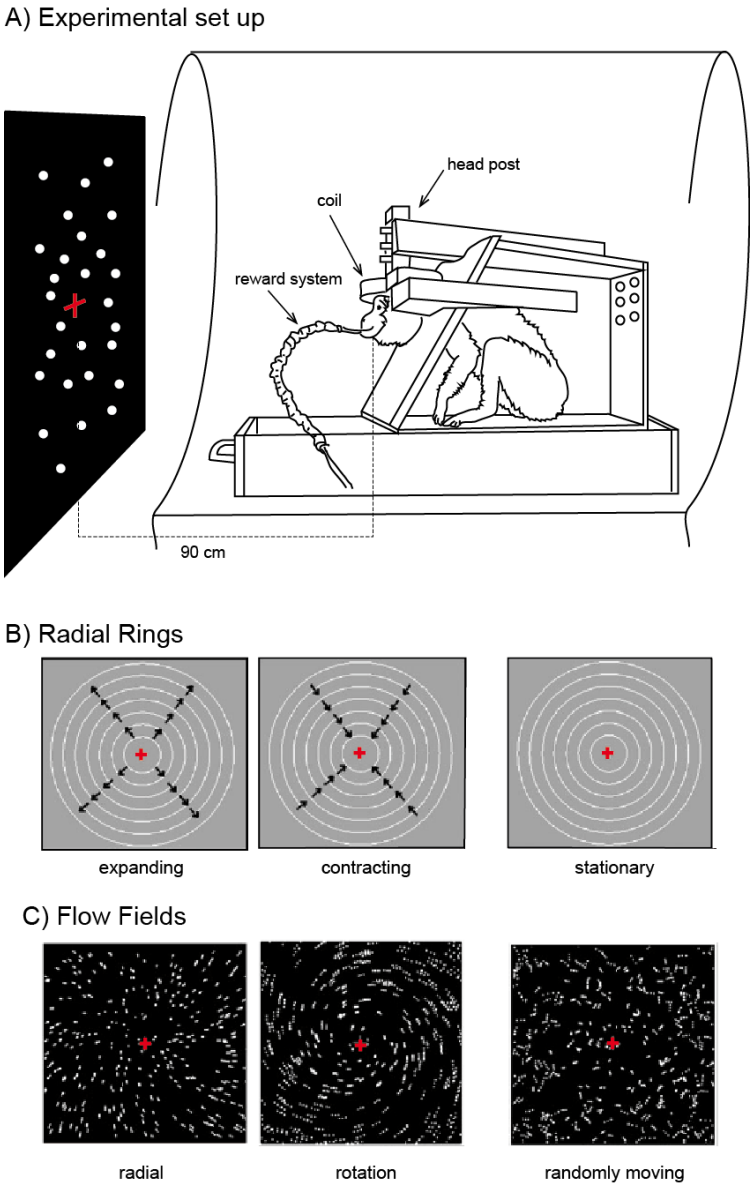

Figure 29: Experimental fMRI setup.

A) Diagram of the monkey in the MR scanner. The monkey sat on its haunches in a plastic restraint box with its head immobilized comfortably but securely. On the monkey head, a surface coil was mounted. Adapted from (Vanduffel et al., 2001).

B) Radial Rings stimulus. The two frames of the moving phase show the two directions of the radial motion (expanding and contracting) that switched every 2 s and that was compared with stationary rings presented during the stationary phase. Adapted from (Pitzalis et al., 2010).

C) Flow Fields stimulus. The two frames on the left show the two different types of coherent motion (radial and rotation) that switched every 500 ms and were compared with a random motion (randomly moving). *Adapted from (Pitzalis et al., 2010).*

Monkeys were trained to maintain steady fixation on the red cross located in the center of the screen. The distance between screen and animal was 90 cm.

We used two different types of stimuli according to those used in fMRI studies in human (Pitzalis *et al*., 2010), Radial-Rings and Flow-Field (Fig. 29B and 29C). These stimuli were either static or moving and were all produced by an X11/OpenGL program.

- "Radial Ring" (Fig. 29B) stimuli were concentric thin light gray rings (0.2 cycles/deg, duty cycle = 0.2) on a slightly darker-gray background, either moving (7 deg/s) or stationary. During the moving period, the concentric rings periodically expanded and contracted (1 s, 1 s). The stimulus luminance contrast was low to better isolate MT as described by (Tootell *et al*., 1995).
- "Flow Fields" (Fig. 29C) was produced by the same software X11/OpenGL and consist in blocks of coherent dot field motion contrasted with scrambled motion. A new field of white dots was generated every 500 ms (dot size 0.4 x 0.4 deg^2). Dots immediately began to move along a trajectory to generate a coherent movement on a plane. The pattern motion was chosen randomly for that 500 ms period from a continuum ranging from dilation to outward spiral, to rotation, to inward spiral, to contraction. The speed varied within a small range. During the randomly moving period the coherence of movement was scrambled but the speed gradient was preserved (central dots continued to move slower than peripheral dots). The average luminance of the stimulus was 31cd/m^2.

In this work, I will present only the results obtained from the first animal scanned.

- ✓ *Data Analysis*

Preprocessing. Data were analyzed using AFNI software (Analysis of Functional NeuroImages, http://afni.nimh.nih.gov/afni/; Cox, 1996) as reported in Hadj-Bouziane and coworkers (2014). Images were realigned to the first volume of the first scanning session and smoothed by using a 2-mm full-width half-maximum Gaussian kernel. The preprocessing included: i) despiking motion correction using 3dvolreg; ii) temporal filtering to extract the spontaneous brain activity (0.01-0.1 Hz); iii) linear regression to remove variables as head motion. Data were aligned onto a MRI-based atlas of the rhesus macaque (McLaren *et al*., 2009) and normalized to the Saleem and Logothetis stereotaxic atlas (Saleem *&* Logothetis, 2012). In both scanning session analyzed the first five TRs were discarded.

Functional image processing. Surface reconstruction of the monkey data were performed using FreeSurfer (http://surfer.nmr.mgh.harvard.edu/), to achieve two separate but important goals: i) the “inflation” of the cortical surface in order to easily visualize the activity occurring inside sulci and ii) the “flattening” of an entire hemisphere so that the activity across the hemisphere may be seen from a single view (Dale, 1999; Dale *et al*., 1999; Fischl *et al* 1999). Analysis methods were similar to those used in previous studies (Sereno *et al*., 1995; Tootell *et al*., 1997; Pitzalis *et al*., 2006). Data were analyzed by Fourier transforming the MR time course from each voxel (after removing constant and linear terms). This generates a vector with real and imaginary components for each frequency that defines an amplitude and phase of the periodic signal at that frequency. To estimate the significance of correlation of BOLD signal with the stimulus frequency, the squared amplitude of the signal at the stimulus frequency was divided by the mean of squared amplitudes at all other noise frequencies (excluding low-frequency signals caused by residual head motion and harmonics of the

stimulus frequency). This ratio of two χ^2 statistics followed the F-distribution and with degrees of freedom equal to the number of time points, can be used to calculate a statistical significance *p* value. Pseudocolor scales were used to represent the amplitude of the response after masking the data with a significance threshold and in order to highlight the phase. We modulated the saturation of the color as a function of the signal amplitude using a sigmoid function. This sigmoid function was arranged so that saturated phase colors began to emerge from the gray background at a threshold of $p < 10^{-2}$. The data at most activated cortical surface points had much higher significance values ($p < 10^{-5}$ to 10^{-10}) as used in previous studies (Tootell *et al*., 1997).

2.4 Checking of visual and somatosensory properties

Twentytwo hemispheres from twelwe macaque monkeys (*Macaca fascicularis,* males, weight range 3-7 Kg) were used in this study as summed up in Table 1. The monkeys sat in a primate chair and were trained to perform visual fixation task and to accept a somatosensory stimulation. A reaching task was also applied in three animals (M 22, M 24 and M 25) but will be presented in a separate section of the dissertation. A schematic view of the tasks used in this work is shown in Figure 30.

CASE	RECORDING SITE	NUMBER OF CELLS
M14L	V6Ad	28
M15L	V6Ad	194
M15R	V6Ad	49
M16L	V6Ad	45
M16R	V6Ad	92
M17L	V6Ad/PEc	84
M17R	V6Ad	35
M18L	V6Ad/PEc	93
M19L	V6Ad/PEc	179
M19R	V6Ad/PEc	141
M20L	V6Ad	122
M20R	V6Ad	82
M21L	V6Ad	8
M21R	V6Ad/PEc	77
M22L	V6Ad/PEc	5
M22R	V6Ad/PEc	5
M23L	V6Ad/PEc	12
M23R	V6Ad	14
M24L	V6Ad/PEc	60
M24R	V6Ad/PEc	57
M25L	V6Ad/PEc	90
M25R	V6Ad/PEc	24
TOTAL		**1496**

Table 1: General information on cases included in the study.

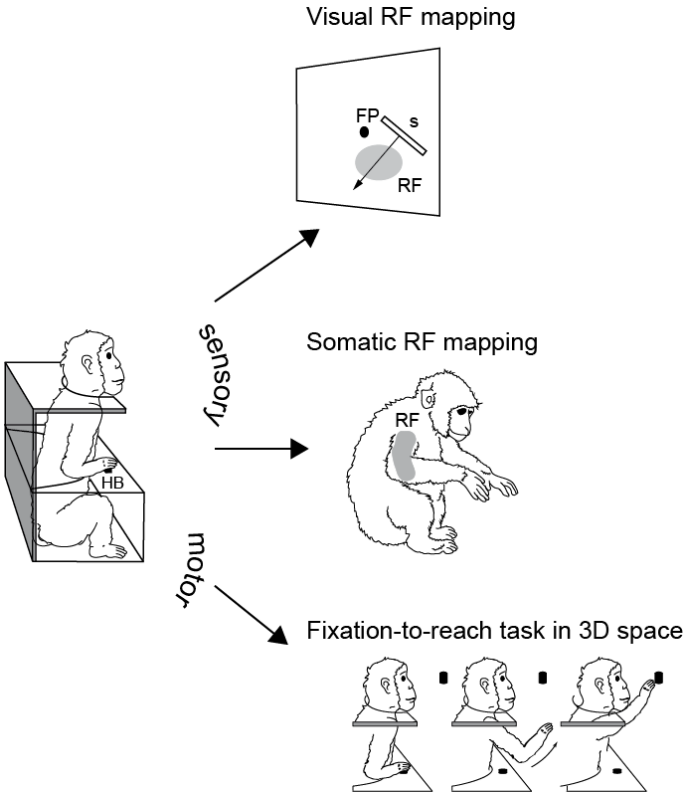

Figure 30: Sensory and motor tasks.

Animals were trained to perform two sensory tasks, focused on mapping the receptive field (RF) of visual (top) and somatosensory (middle) neurons. Animals were also trained to perform a motor task (bottom) requiring reaching arm movements in 3D space. In all cases, animals maintained a steady fixation of a constant location in front of them.

- ✓ *Visual stimulation*

Animals were trained to perform steady gaze fixation in darkness in a behavioral task in which they had to fixate for a variable time (2-6 s) at a small target rear projected on a large (80° x 80°) tangent screen placed 57 cm from the eyes, ignoring any other visual stimulus present or moving across the visual field as shown in the top part of Figure 31. The fixation

target could be projected in different positions of the screen in order to allow visual stimulations also in the far periphery of the visual field. Individual cells' visual sensitivity was first tested with elementary visual stimuli, like light/dark borders, light/dark spots and bars (see Fig. 31A, bottom left part). The stimuli were moved across the neuronal receptive field (RF) with different orientations, directions and speeds of movement. When a neuron responded to this visual stimulation, it was classified as low-level visual cell. If the neuron was unresponsive to elementary visual stimuli, testing was continued using more complex stimuli as light/dark gratings and corners of different orientations, directions and speed of movement as well as shadows with irregular contours and shadows rapidly changing in size and/or shape (see Fig. 31B, bottom right part). When a neuron responded to complex visual stimulation but not to a simple one, it was classified as high-level visual cell. Cells unresponsive to either elementary or complex stimuli were classified as nonvisual cells. Cells with an indefinable responses either to simple either to complex visual stimulation were classified as "unclear cells" and were discarded from all the analysis. A detailed description of the methodologies used to map RFs is reported previous works of our group (Galletti *et al*., 1996; 1999b; Gamberini *et al*., 2011).

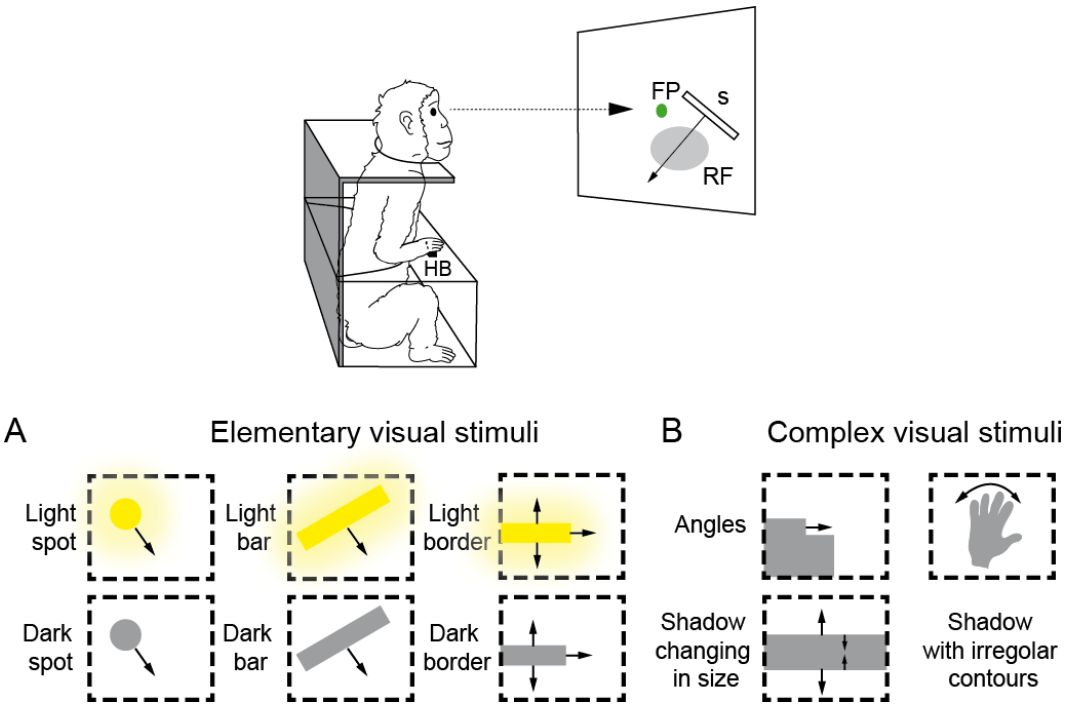

Figure 31: Stimuli used to map the visual receptive fields.

Top, experimental setup. The animal sat in a primate chair in front of a screen where a fixation point (FP) and the stimulus (S) were projected. The animal was trained to maintain steady fixation on the FP while the stimulus moved with different orientations, directions and velocities.

A) Elementary visual stimuli. Light/dark spots, bars and borders.

B) Complex visual stimuli. Dark shadows with irregular shapes or continuously changing in size.

✓ *Somatosensory stimulation*

Passive somatosensory stimulations were applied on the whole body of the monkeys by the experimenters that stood behind the animal. The first somatosensory stimuli applied consisted of a superficial tactile stimulation, such as light touching of hair and skin (Figure 32A, top part). If no response was elicited, we attempted the deep pressure of skin (Figure 32B, middle

part) in order to stimulate subcutaneous tissues, as well as proprioceptive stimulations by slow and/or fast rotations of the joints (Figure 32C, bottom part). When a cell was responsive to joint rotation, we carefully checked whether skin stimulation around the joint was responsible for the observed modulation. We are aware that some somatosensory modulations were not taken into account because of the experimental conditions, as neck rotation that could not be tested because of the monkey's head fixed. Stimuli were delivered on both sides of the body. To exclude visual influences, somatosensory stimulations were performed in complete darkness. Eye positions and eye movements were continuously monitored to exclude the possibility that the observed modulations were due to oculomotor activity. When a neuron responded to somatosensory stimulation, it was classified as skin, deed or joint, according to the type of stimuli that evoked neuronal response; and as arm, trunk or leg according to the location of somatosensory receptive field. When somatosensory stimulations were not effective, the neuron was classified as somatically unresponsive. The occurrence of salient events of the stimulation were signaled pushing a pedal connected to the computer for data acquisition. A detailed description of somatosensory stimulation methods was reported in a previous work (Breveglieri *et al*., 2002).

Single neurons recorded from both area PEc and V6Ad that were tested with both somatosensory and visual stimulations (in a randomized order) were classified in 4 groups (Breveglieri *et al*., 2008): unimodal visual, unimodal somatic, bimodal and unresponsive. Among bimodal cells, we checked their visual and somatosensory properties.

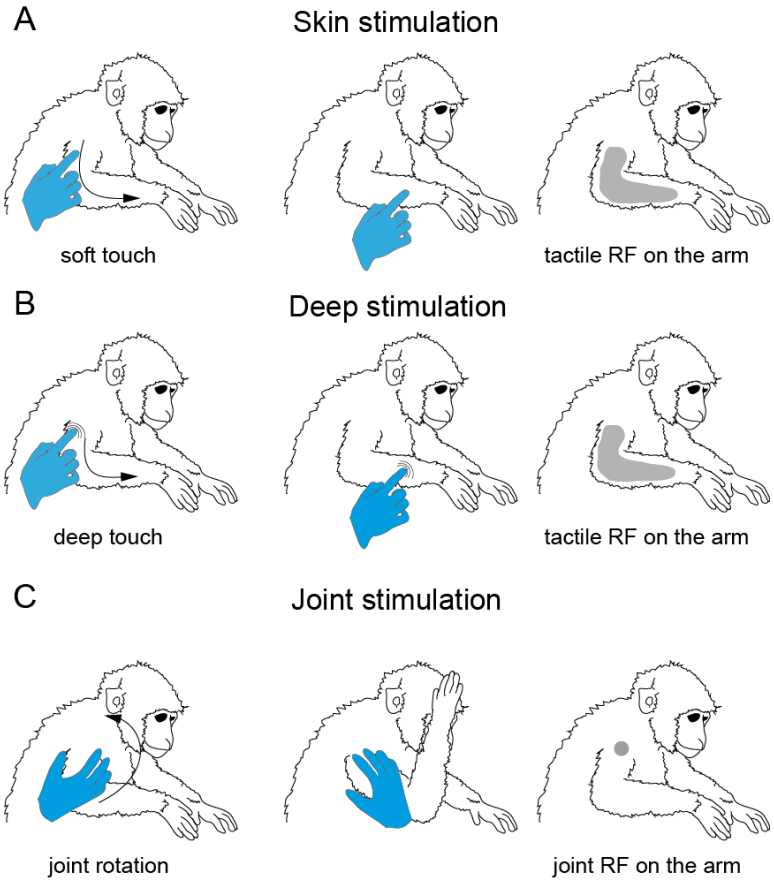

Figure 32: Somatosensory stimulation.

A) Skin stimulation. Superficial tactile stimulation performed by the experimenter (blue hand on the figure).
B) Deep stimulation. Deep pressure of the skin in order to stimulate the subcutaneous tissue.
C) Joint stimulation. Slow/fast rotations of the joints.

Somatosensory mapping was performed in complete darkness all over the animal's body. The experimenter stood behind the animal.

✓ *Data analysis*

The numbers of cells significantly modulated by a specific sensory stimulation was expressed as the percentage of cells sensitive to that

stimulation of the total cells tested for that property. Cells with an uncertain classification were discarded from the analysis. The frequency of cells sensitive or not to a specific stimulation were firstly compared in PEc and V6Ad separately (χ^2, $p< 0.05$) and secondly compared between PEc and V6Ad (two proportion z test, $p< 0.05$) (Zar, 1999) and detailed in (Fluet *et al*., 2010). All the statistical analysis were performed

2.5 *Motor Related Activity*

Three male macaque monkeys (*Macaca fascicularis,* M22, M24 and M25) with a weight ranged between 3.8 Kg and 4.4 Kg were used in this study.

Electrophysiological data were collected while monkeys were performing a fixation-to-reach task. The animal performed arm movement with the contralateral limb (with respect to the recording hemisphere), with the head restrained, in darkness, while maintaining steady fixation of the target. Before starting the movement, the monkey kept its hand on a button (home-button (HB), 2.5 cm in diameter) located next to its trunk (Fig. 33A). Reaches were performed to one of nine Light Emitting Diodes (LED, 6 mm in diameter). The LEDs were mounted on the panel at different distances and directions with respect to the eyes, always at eye level. Target LEDs were arranged in three rows: one central, along the sagittal midline and two lateral, at version angles of -15° and +15°, respectively (Fig. 33B). Along each row, three LEDs were located at vergence angles of 17.1°, 11.4° and 6.9°. The nearest targets were located at 10 cm from the eyes, whereas the LEDs placed at intermediate and far positions were at a distance of 15 cm and 25 cm, respectively. The range of vergence angles was selected in order to include most of the peripersonal space in front of the animal, from the very near space (10 cm) up to the farthest distances reachable by the monkeys (25 cm).

The time sequence of the task is shown in Figure 33C. A trial began when the monkey pressed the button near its chest (HB press). After 1s, one of the nine LEDs was switched on green. The monkey had to fixate the LED while keeping the HB button pressed. Then, the monkey had to wait for 1.7–2.5s for a change in the color of the LED (from green to red) without performing any eye or arm movement. The color change was the go signal (GO) for the animal to release the HB and to start an arm movement (M) towards the target. Then, the monkey reached the target (H) and held its hand on the target for 0.8-1.2s. The switching off of the target (Red-off) cued

the monkey to release the target and to return to the HB (HB press), which ended the trial and allowed the monkey to receive its reward. The presentation of stimuli and the animal's performance were monitored using custom software written in Labview (National Instruments), as described previously (Kutz *et al*., 2005). Eye position signals were sampled with two cameras (one for each eye) of an infrared oculometer system (ISCAN) at 100 Hz, and were controlled by an electronic window (4 x 4 degrees) centred on the fixation target. If the monkey fixated outside this window, the trial was aborted. The task was performed in darkness, in blocks of ninety randomized trials, ten for each target position. The luminance of LEDs was adjusted in order to compensate for difference in retinal size between LEDs located at different distances. The background light was switched on briefly between blocks to avoid dark adaptation.

At the beginning of each recording session, the monkey was required to perform a calibration task gazing at targets on a frontal panel placed at a distance of 15 cm from the eyes. For each eye, signals to be used for calibration were extracted during fixation of five LEDs arranged to a cross, one central aligned with the eye's straight ahead position and four peripheral placed at an angle of +/- 15° (distance: 4 cm) both in the horizontal and vertical directions. From the two individual calibrated eye position signals, we derived the mean of the two eyes (the conjugate or version signal), and the difference between the two eyes (the disconjugate or vergence signal) using the equations: version = (R+L)/2 and vergence = R-L, where R and L were the position of the right and left eye, respectively.

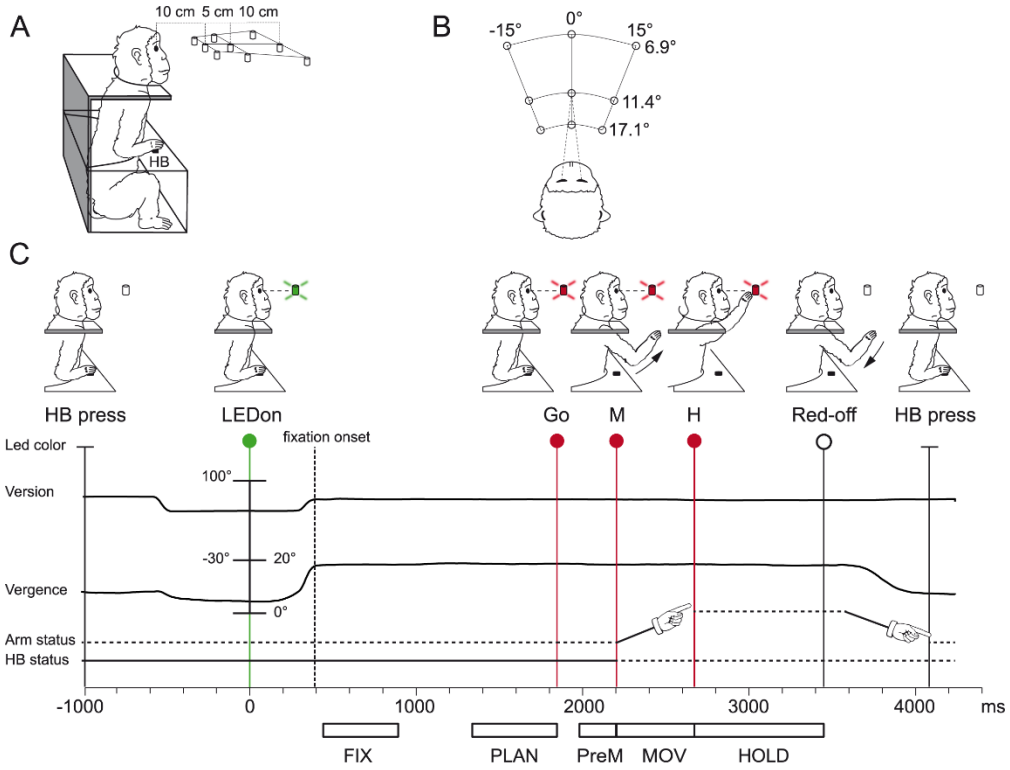

Figure 33: Experimental setup and task sequence.

A) Scheme of the setup used for the reaching task. Nine LEDs located at eye level were used as fixation and reaching targets. The distances of the three LEDs of the central row from mid-eye level are shown. HB, home button.

B) Top view of the target configuration with the values of vergence and version angles.

C) Time sequence of task events with LED status, eye's vergence and version traces, arm status and HB status. From left to right vertical lines indicate respectively: trial start (HB press), target appearance (LEDon), fixation onset (dashed line, end of saccade movement), go signal (GO), start of the arm reaching movement (M), holding phase of the target (H), turning off of the target (Red-off), and trial end (HB press). Arm drawings indicate the forward and backward arm movements. White rectangles below the time axis illustrate time epochs used for the analysis of neural activity. From left to right: FIX, from 50 ms after fixation onset till 450 ms after it; PLAN, the last 500 ms before the Go signal; PreM, the last 200 ms before movement onset; MOV, from the releasing of the home button to the pressing of the target; HOLD, from target pressing till Red-off.

✓ *Data Analysis*

The effect on neural activity of gazing at different target positions was analyzed in different epochs during the task. The task epochs taken into account for the analysis are indicated in the bottom part of Figure 33C. They were: a) the early fixation epoch (FIX), from 50 ms after the end of the saccade performed to catch the LED till 450 ms after it, b) the preparation epoch (PLAN), the last 500 ms of fixation before the GO signal, c) the pre-movement epoch (PreM), the last 200 ms before the movement onset, d) the movement epoch (MOV), from the releasing of the home button to the pressing of the LED target, and e) the hold epoch (HOLD), from the pressing of the LED target till the target offset; this epoch lasted either 800 or 1200 ms, depending on the trial length.

Rasters of spiking activity were aligned on specific events of the task sequence, depending on the epoch analyzed. The effect of target depth and direction on cell activity was analyzed only in those units with a mean firing rate higher than 3 spikes/s and in those neurons that were tested in at least seven trials for each spatial position. The reasons for this conservative choice are connected to the implicit high variability of biological responses and are explained in detail in (Kutz *et al*., 2003).

Significant modulation of neural activity relative to different target locations was studied using a two-way Analysis of Variance (ANOVA) performed separately for each epoch with factors being target's depth and direction. Target depth was defined as the distance of the target from the animal (near, intermediate, far) and target direction as its position with respect to the recording hemisphere (contralateral, central, ipsilateral). Neurons were considered modulated by a given factor only when the factor's main effect was significant ($p < 0.05$). To find whether the incidence of each of the main effects differed significantly between two epochs a two-proportion z test (Zar, 1999) was applied, as detailed in (Fluet *et al*., 2010).

To analyze the spatial tuning of activity, a stepwise multilinear regression model was applied in each epoch considered. Regression methods quantify relationship between dependent (neural activity) and independent (target's depth and direction) variables. Given that the monkeys fixated the target in all epochs of interest, its depth and direction in space were equal to the vergence and version angles of the eyes, respectively. That being said, in the rest of the thesis, when referring to spatial tuning analysis and data, the terms depth and vergence, as well as direction and version, are interchangeable.

In the multiple linear regression model relating the neural activity in the epochs of interest to the different target positions we used this equation for the firing rate:

$$A(X_i, Y_i) = b_0 + b_1 X_i + b_2 Y_i$$

where A was the neural activity in spikes per second for the *i*th trials; X_i, and Y_i the positions of the target defined as vergence and version angles, respectively, of the eyes during target fixation; b_1 and b_2 were regression coefficients and b_0 the intercept. After being tested for their significance, the vergence and version coefficients were normalized with the standard deviation of vergence and version, correspondingly. The standarized coefficients allow a comparison among the independent variables and provide information about its relative influence in the regression equation. In our study, this allowed to compare the vergence and version coefficients and to account for the fact that angle range was different for vergence and version. The regression coefficients were selected using a backward stepwise algorithm (Matlab function *stepwise*) that determined whether the coefficients were significantly different from zero. At the conclusion of the stepwise algorithm, only the coefficients that were significantly different from zero remained ($p < 0.05$). These coefficients were then used to determine the spatial preference only in the cells with a significant main effect (ANOVA $p< 0.05$) in a certain epoch. The linear regression model was used because few neurons displayed their maximal firing rates for intermediate and central

positions. In each neuron, the sign of the linear correlation coefficients (standarized) were used to determine the spatial preference in a certain epoch. In modulated neurons without significant linear coefficients a Bonferroni post-hoc test ($p < 0.05$) was applied to define the preferred position.

Population analysis. For each cell modulated by target depth and/or direction in the epochs of interest, a spike density function (SDF, Gaussian kernel, half width at half maximum 40 ms) was calculated for each trial and averaged across all the trials of the preferred and the opposite depths and directions as defined by the linear regression analysis. The peak discharge of the preferred condition was used to normalize the SDFs. Population SDF curves representing the activity of the preferred and opposite target positions were constructed by averaging the individual SDFs of the cells (Marzocchi *et al*., 2008), aligned at the behavioral event of interest. SDFs curves of preferred and opposite positions were statistically compared pairwise with a permutation test with 10,000 iterations comparing the sum of squared errors of the actual and randomly permuted data ($p< 0.05$). The intervals of the curve we compared were different according to the epoch considered: for cells modulated by depth/direction during FIX, the interval was from 50 to 400 ms after saccade offset; for cells modulated during MOV, the interval was from the movement onset (key-up) to 400 ms after it. In order to describe the time course of the activity of the different functional categories of cells, we performed a sliding window permutation test (width 100 ms). The sliding window was placed at 2000 ms before the SDF alignment event (saccade offset and/or key-up) and was shifted in sequential 20-ms steps. The onset of difference in the activity between the two SDF curves was determined as the time of the first of five consecutive windows where comparisons were statistically significant ($p< 0.05$).

All the analyses were performed using custom scripts written in MATLAB (Mathworks, Natick, MA, USA).

2.6 *Histological Reconstruction of the Recording Sites*

During the last week of recording, electrolytic lesions (40-50µA cathodal current for 30s) were made at different depths along single penetrations carried out at different coordinates within the recording chamber. After the end of the electrophysiological recording session, the animals were anaesthetized with ketamine hydrochloride (15 mg kg i.m.) followed by an i.v. lethal injection of sodium thiopental and perfused through the left cardiac ventricle with 0.9% sodium chloride followed by 4% paraformaldehyde in 0.1 M phosphate buffer (pH 7.4) and by 5% glycerol in the same buffer. The brains were then removed from the skull, photographed, placed in 10% buffered glycerol for three days and then in 20% glycerol for 4 days. Brains were cut on a freezing microtome at 60µm in parasagittal plane except for one hemisphere cut in coronal plane. In all cases, each second section of a series of five was stained with the Nissl method (thionin, 0.1% in 0.1 M acetate buffer, pH 3.7) for the cytoarchitectonic analysis. Procedures to reconstruct microelectrode track and the location of each recording site were those previously described by our group (Galletti *et al*., 1996; 1999a; 1999b; Breveglieri *et al*., 2006; Gamberini *et al*., 2011). Briefly, penetrations were reconstructed on the basis of: 1) marking electrolytic lesions, 2) the coordinates of penetrations within the recording chamber and their distances from the surface of the hemisphere, 3) the type of cortical area passed through before reaching the region of interest, 4) the relative depths of the boundaries between white and gray matter and 5) the cytoarchitectural characteristics. Based on these criteria, neurons were assigned to area PEc according to the cytoarchitectural criteria of (Pandya *&* Seltzer, 1982; Luppino *et al*., 2005).

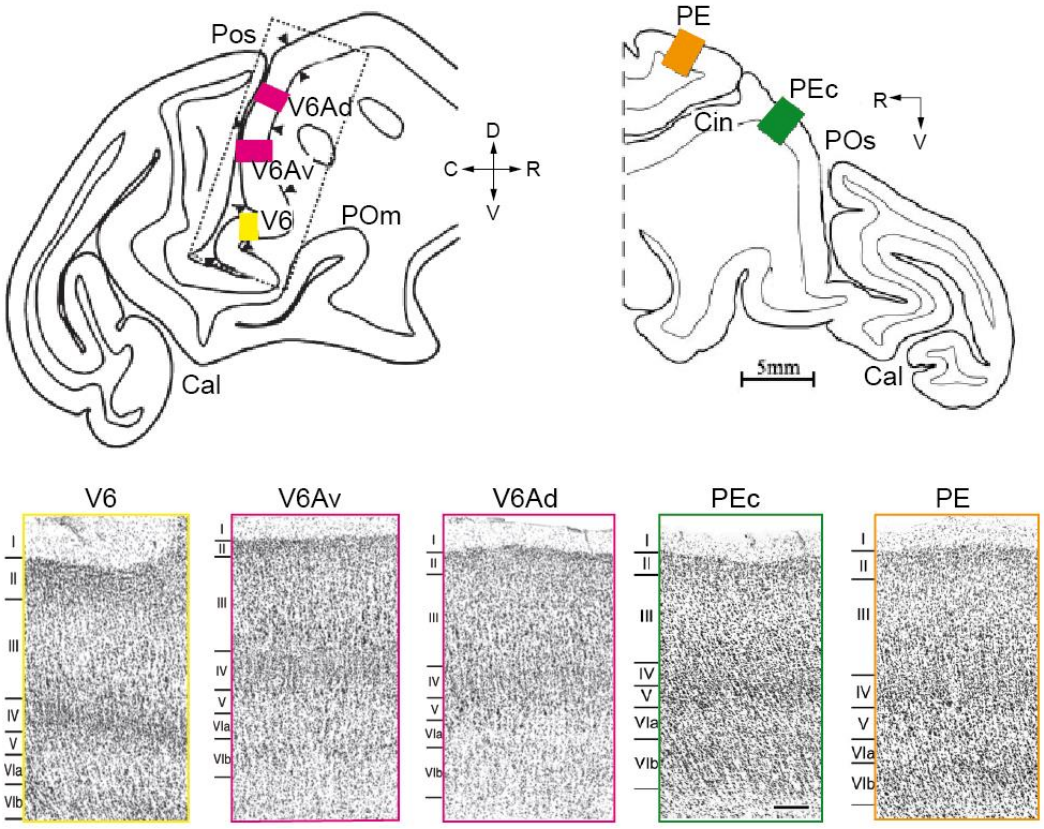

Figure 34: Architectural characteristics of area V6, V6A, PEc and PE.

Left, brain location of areas V6, V6Av and V6Ad. Drawing of a parasagittal section centered on the anterior wall of the POs. Colored boxes on the section indicate the location of the higher magnification yellow and pink views shown in the left-bottom part, corresponding to the cytoarchitectonic areas V6, V6Av and V6Ad. *Adapted from (Luppino et al., 2005).*

Right, brain location of areas PEc and PE. Drawing of a parasagittal section centered on the anterior wall of the POs. The two colored boxes (green and orange) indicate the location of the two high-magnification views shown in the right-bottom green and orange panels, corresponding to the cytoarchitectural pattern of area PEc and PE respectively. *Adapted from (Breveglieri et al., 2006).*

Scale bar of the drawings: 5 mm; photomicrographs scale (shown in PEc), 200 µm. Cin, cingulate sulcus; Cal, calcarine sulcus; POm, medial parieto-occipital sulcus; POs, parieto-occipital sulcus; C, caudal; D, dorsal; R, rostral; V, ventral.

As shown in Figure 34, area PEc is characterized by the presence of a clear size gradient in layer III, which is densely populated by medium-sized pyramids in its lower part, and by a dense layer V with a high number of relatively large pyramids. This cytoachitectual pattern is peculiar of area PEc and is clearly distinguishable from the anterior area PE, located at the level of the posterior tip of the cingulate sulcus. Figure 34 shows that in PE, the size gradient in layer III becomes more evident against a less cellular background; layer V, instead, is characterized by the presence of large pyramids less packed and preset in an almost continuous row. Area V6A is ventral and posterior to area PEc. As described by (Luppino *et al*., 2005) and shown in Figure 34, the dorsal part of area V6A (V6Ad) is characterized by a poorly defined layer II and a less pronounced size gradient in layer III and by the presence of fewer and larger pyramids in layer V with respect to area PEc. The location of the border between area PEc and V6Ad varies from animal to animal from 1 mm posterior to the exposed surface of the SPL to 1.5 mm anterior to it. The ventral part of area V6A (V6Av), shown in Figure 34, is characterized by a well delineated layer II and a size-gradient layer III with relatively large pyramids in its lower part; layer V is populated by medium-sized pyramids. Area V6 is located in the fundus of the parieto-occipital sulcus, with cytoarchitectonic features characterizing it as an occipital area differently from the above-mentioned areas. V6 (Figure 34) shows an evident layer II with densely packed small cells and a dense layer III with relatively small amount of medium-sized pyramids in its lowest part.

2.7 Two-dimensional and Three-dimensional Cortical Maps

The location of each recorded cell and the cytoarchitectonic borders of V6A and PEc were reported on two-dimensional maps of the cortex of the medial parieto-occipital region, similarly to previous studies (Galletti *et al*., 1999b; Van Essen *et al*., 2001; Gamberini *et al*., 2011) (Figure 35). We used as reference markers: the line where the dorsal exposed surface of the caudal part of the PPC bends into the medial surface of the hemisphere, the anterior bank of the POs, the medial wall of the IPs and the line where the anterior bank of the POs bends into the medial surface of the hemisphere. Each recorded cell was marked on this two-dimensional map according to our best estimate of the location of the electrode track as described above. The maps of left hemisphere were then flipped vertically so that all the data were represented on the right hemisphere. By superimposing the maps of the two hemispheres and of all the animals, we obtained a single average map for each population of cells. Before superimposition, each map was rescaled according to the relative size of the whole brain and the dorsoventral extent of the anterior wall of the POs. Note that, because of the averaging process of border position, single cells assigned to an area in one animal could be located a bit outside the limits of this area in the average map. Figure 35, E and F, shows the average map obtained by the superimposition of the maps of all the animals studied in this work. The average map is, in this case, superimposed on a three-dimensional (3D) reconstruction of the atlas brain (Figure 35 B-D) obtained by CARET (Computerized Anatomical Reconstruction and Editing Toolkit, http://brainmap.wustl.edu/caret/) (Van Essen et al., 2001). Despite the misalignments caused by individual differences among single hemispheres, the locations of PEc and V6Ad in the averaged map of the atlas brain results quite clear. All final drawings and digitals images of this thesis were generated and assembled using Adobe Photoshop and Adobe Illustrator software packages (Adobe Systems Incorporated, San Jose, CA).

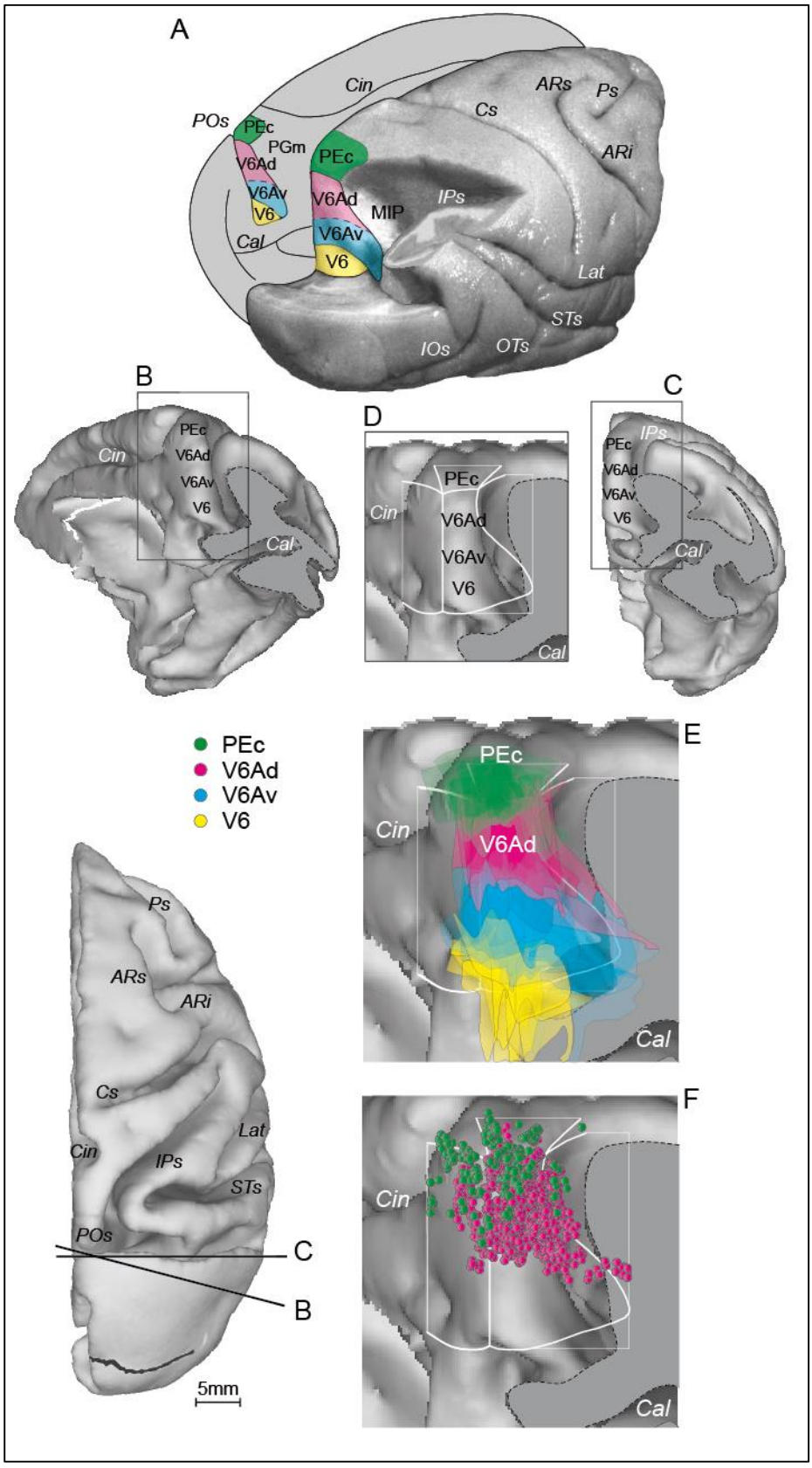
A
Cin
ARs
Ps
Cs
POs
PEc
PGm
V6Ad
ARi
PEc
V6Ad
V6Av
V6
IPs
MIP
Cal
V6Av
V6
Lat
STs
IOs
OTs
B
PEc
Cin
V6Ad
V6Av
V6
Cal
D
PEc
Cin
V6Ad
V6Av
V6
Cal
C
IPs
PEc
V6Ad
V6Av
V6
Cal
PEc
V6Ad
V6Av
V6
E
PEc
Cin
V6Ad
Cal
Ps
ARs
ARi
Cs
Lat
Cin
IPs
STs
POs
C
B
5mm
F
Cin
Cal

Figure 35: Bidimensional map of the recording sites.

A) Posterolateral view of a partially dissected macaque brain (modified from Galletti et al., 1996). The inferior parietal lobule of the right hemisphere has been cut away at the level of the fundud of the itraparietal sulcus (IPs) to show the cortex of the medial bank of this sulcus. The occipital lobe of the same hemisphere has been removed at the level of the fundus of the parieto-occipital (POs) and lunate sulci to show the cortex of the anterior bank of the POs. The mesial surface of the left hemisphere is drawn (gray area). The location of areas V6, V6A (both ventral and dorsal), and PEc are indicated with colors, yellow, blue, pink, and green, respectively.

B) Posteromedial and C) posterior views of the surface-based 3D reconstructions of the ATLAS brain with the posterior part of the occipital lobe cut away (gray area-dashed line) to visualize the entire extent of the anterior bank of POs. The levels of the cut are shown on the bottom left.

D) Anterior bank of POs and, superimposed, the flattened map (white lines) of the part of the SPL.

E) As in D, with the boundaries and extents of the cytoarchitectonically defined area V6 (yellow), V6av (blue), V6Ad (pink), and PEc (green).

F) As in D, with the locations of cells recorded in areas PEc (green circles) and V6Ad (pink circles).

Horizontal scale: 5 mm. Other conventions as in Figure 4.

Adapted from (Gamberini et al., 2011).

3 RESULTS

3.1 V6 and MT Mapping

Data presented here were those collected from the first animal scanned in Lyon, France. The animal performed three anatomical sessions for the cortical surface reconstruction and two functional session (fMRI) using two motion stimuli: Radial-Rings, radial motion to map MT, and Flow-Field, optic flow to map V6. In the first fMRI session, the animal performed 4 runs for each stimulus, in the second functional session the monkey performed 12 runs for the Flow-Field stimulus and 13 runs of Radial-Rings. In the second functional session there were four runs of Flow-Fields stimulus quite noisy which negatively affected the analysis of data so we decided to eliminate from the data analysis these runs and to take into account only the remaining 8 runs (12-4= 8). Data will be firstly presented separately for each functional session and then averaging together the two sessions.

Figure 36 shows the anatomical location of area MT in the fundus of STs in its dorsalmost part. The cyan dot correspond to the center of the map MT. Figure 37 shows the anatomical location of area V6. What emerged from data was a differences between left (LH) and right hemisphere (RH) in the shape and position of the parieto-occipital sulcus (POs) and thus also in the position of V6. In the LH, the POs (yellow line) crossed the medial wall becoming clearly visible in both the folded and inflated brain reconstruction. The location of V6 is indicated with an orange circles and the center of the map is indicated by a dot of the same color, in both the folded (top part) and inflated brain (bottom part). V6 is located at the medial end of the sulcus. On the RH, the POs has a different shape in the sense of 'less medial'. In the inflated brain reconstruction, the POs was clearly visible even with a completely medial view while in the folded brain the surface must be rotated a little to show it, see the close-up view in the right part of figure 37. Above all, there was also a gyrus (indicated by a pink line) which seemed to

correspond to the POs but it was not. The POs starts immediately behind that gyrus. In other words, the cortical region corresponding of area V6 did not involve that gyrus but the sulcus immediately behind, much more difficult to see from the folded surface. The different position of the V6 in the two hemispheres fits with the macaque anatomy.

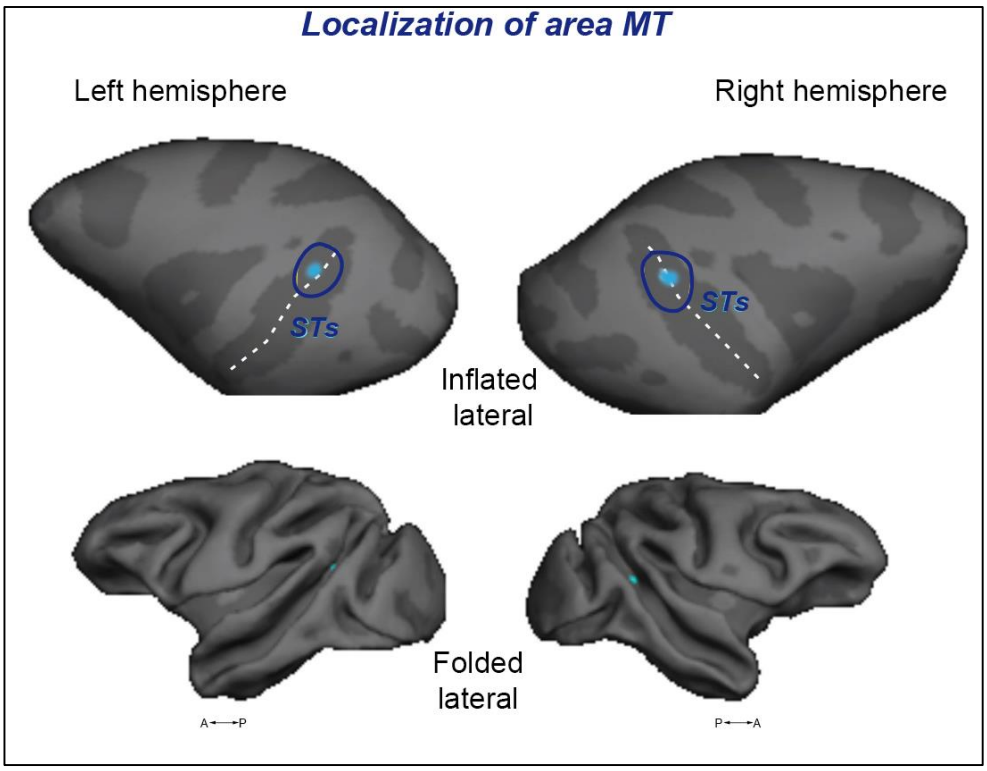

Figure 36: Location of area MT.

Area MT is located in the fundus of the superior temporal sulcus (STs) in its dorsalmost part. The blue dot corresponds to the center of the MT.

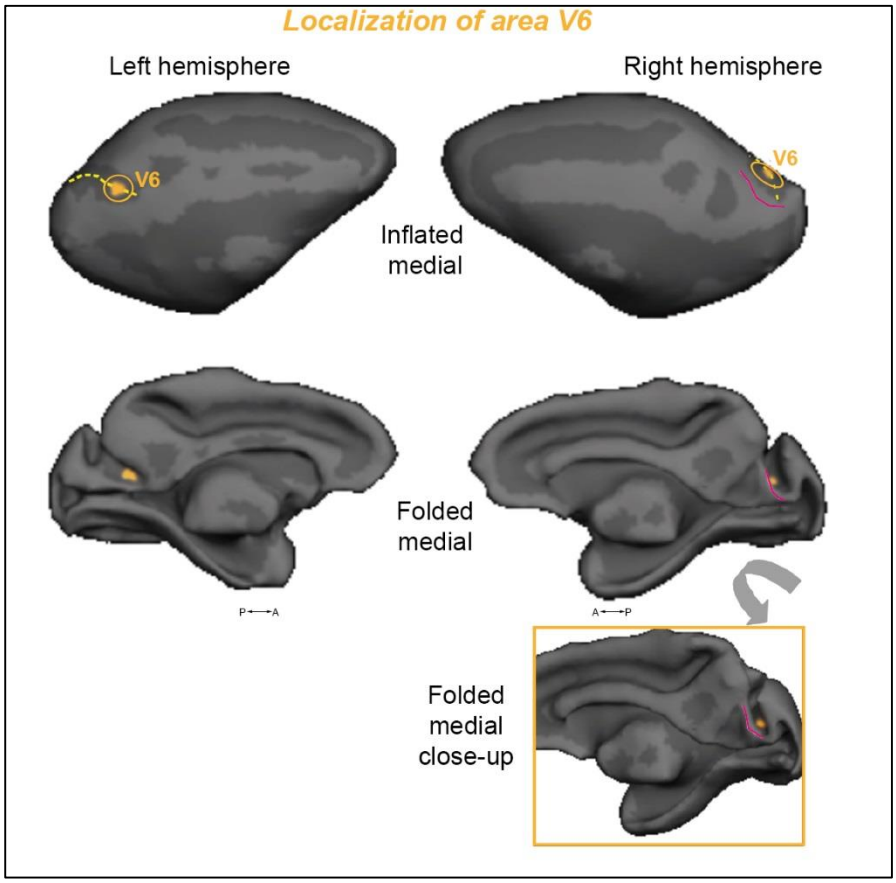

Figure 37: Location of area V6.

The shape and position of the parieto-occipital sulcus (POs) indicated by the yellow-dashed line, is different between the two hemispheres. This results in a different location of area V6 in the left and right hemisphere. In the left hemisphere the POs crossed the medial wall and it is clearly visible in both the folded and inflated brain. The location of V6 in the medial end of the sulcus is indicated by a yellow circle and the center by a yellow dot. In the right hemisphere, the POs has a different shape and there is a gyrus (indicated by the pink dashed line) which seems to correspond to POs, but is not. In reality, the POs starts immediately behind that gyrus. The close-up view allowd to better appreciate the location of the POs and V6.

We tested the responsiveness of monkey area V6 to low contrast radial motion (Radial-Rings), this stimulus was originally used to functionally map human motion middle temporal area (MT+) (Tootell *et al.*, 1995).

Figure 38 shows results from Radial-Rings motion experiment in the first functional session displayed on a folded and inflated brain reconstruction of both left and right hemisphere. The figure shows the differentiated MION activity between moving and stationary conditions. Red-yellow regions indicated higher activity ($p < 0.001$) during radially moving rings with respect to stationary patterns. This stimulus strongly activated area MT in the STs sulcus (blue arrows, top part of the figure), as expected (Tootell *et al*., 1995).

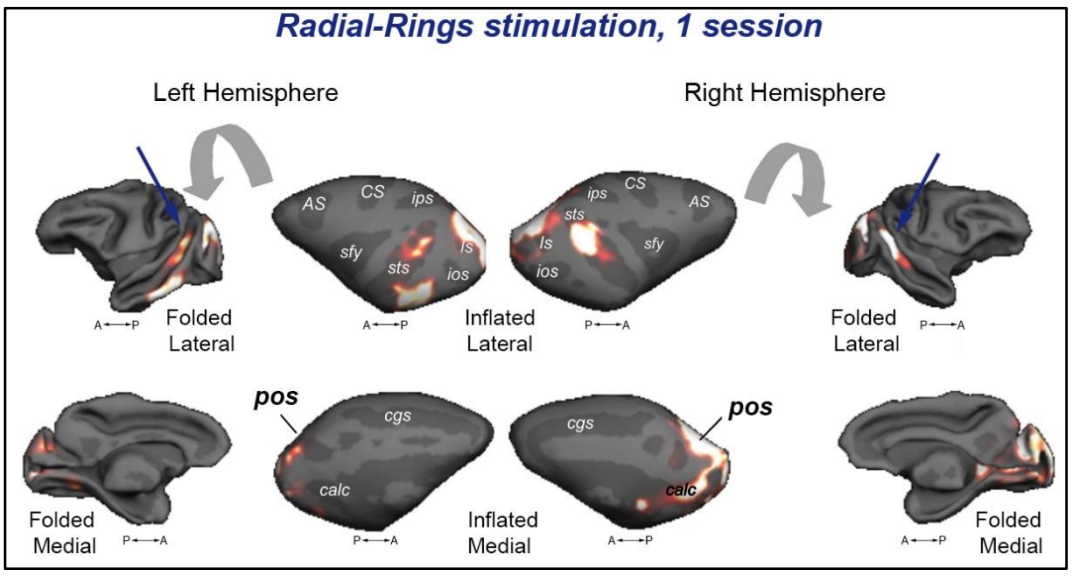

Figure 38: Radial-Rings Stimulation, first functional session.

Radial Rings, first functional session. Average data (n = 4 runs). Results are displayed on lateral and medial views of the folded and inflated brain reconstruction. Differentiated MION activity between moving and stationary conditions is shown. Red-yellow regions indicate higher activity (p< 0.001) during radially moving rings than during stationary phase.

As: arcuate sulcus; calc: calcarine sulcus; cgs: cingulate sulcus; cs: central sulcus; ios: inferior occipital sulcus; ips: intraparietal sulcus; ls: lunate sulcus; pos: parieto-

occipital sulcus; sfy: sylvian fissure (i.e. lateral sulcus); sts: superior temporal sulcus; A: anterior; P: posterior.

This result was consistent across sessions, comparing the results from the first session with those of the second shown in Figure 39 (second scanning session). In both functional sessions area MT was activated bilaterally. Figure 40 illustrated the cross-session average map of all the 17 runs acquired (4+13) from the two fMRI sessions. In summary, area MT+ was activated bilaterally and the signal was extremely high and reliable. On the other hand, area V6 was activated unilaterally in the right hemisphere in both the two scanning sessions, visible on the folded medial view of the right hemisphere (right part of the figure). Motion-selective response was visible also in other cortical areas. We found motion-selective response in the occipital region of areas V1 and V2 and in the lateral occipital region including area V3. Spots of functional activation were also found in the posterior part of area V3A (Fig. 40, folded lateral view of both hemispheres) in the dorsalmost part of Ls. We found quite consistently a motion response in both areas MST and FST in the STs as inferred in both the two functional sessions (see Fig. 38 and Fig. 39 inflated lateral view of both hemispheres).

We also found activation spot in area V4v and in the inferior temporal cortex (areas TEO/TE).

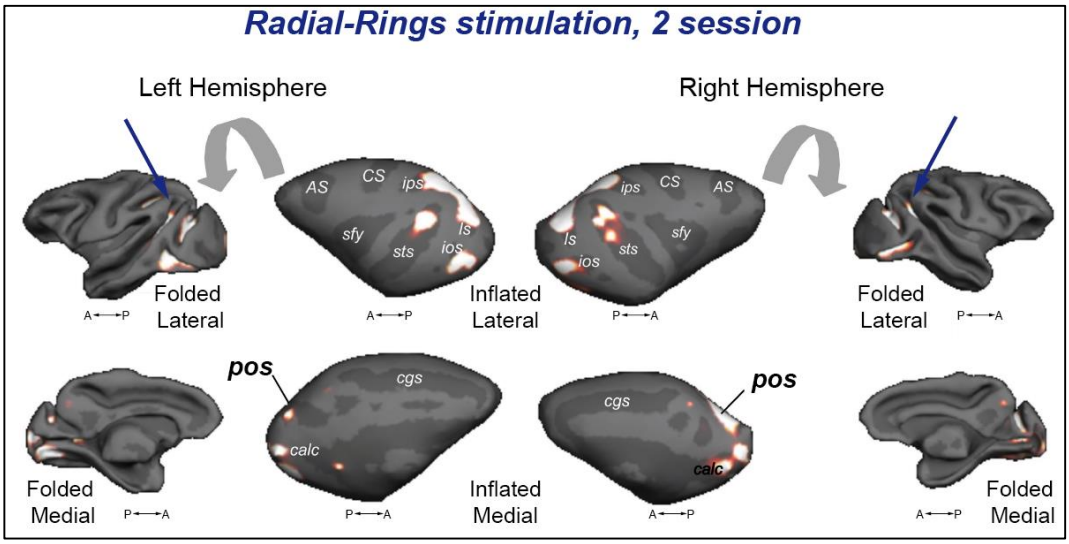

Figure 39: Radial-Rings Stimulation, second functional session.

Radial Rings, first functional session. Average data (n = 13 runs). Other details as in Figure 38.

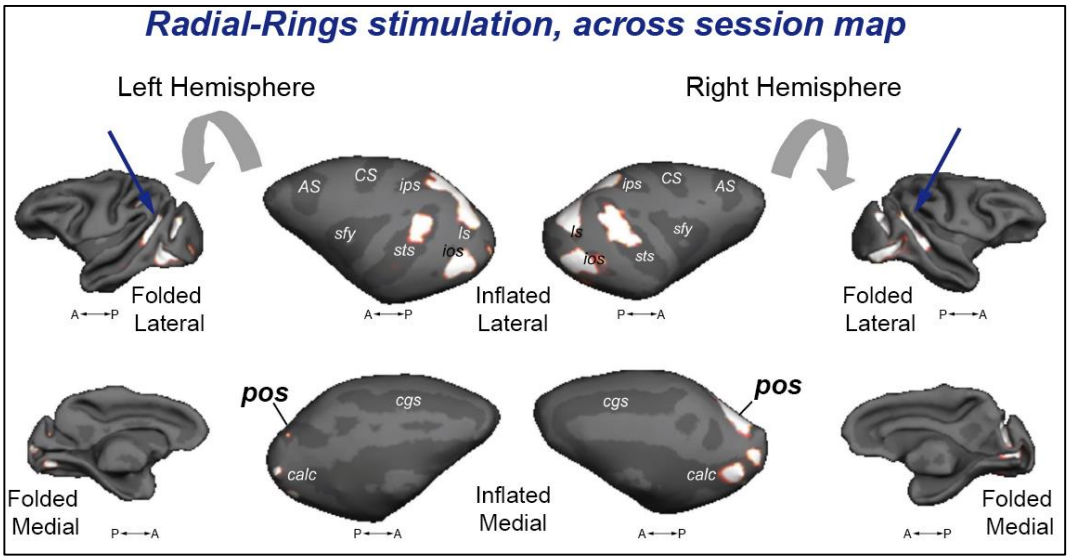

Figure 40: Radial-Rings Stimulation, average map.

Average map of all the 17 runs acquired. The figure shows that area MT was activated bilaterally and the signal was high and reliable. Other detail as in Figure 38.

We then tested V6 sensitivity to another type of motion stimulus, Flow-Fields, which contrasts coherent optical flow stimulation.

Figure 41 shows results from Flow-Fields motion experiment from the first scanning session, displayed on medial and lateral views of the folded and inflated left and right hemispheres of CE monkey brain. Figure 41 shows the differentiated MION activity between ON and OFF conditions. Red—yellow regions indicate higher activity (p< 0.001) during rotating and dilating random dot fields than during scrambled moving random dot fields. In the Figure 41 there was also a close-up of the folded medial right hemisphere, slightly rotated to reveal the activation into the POs. Flow-Fields stimulus strongly activated monkey area V6 in both the two scanning sessions, see also Figure 42 for the second session. In both cases area V6 was activated bilaterally.

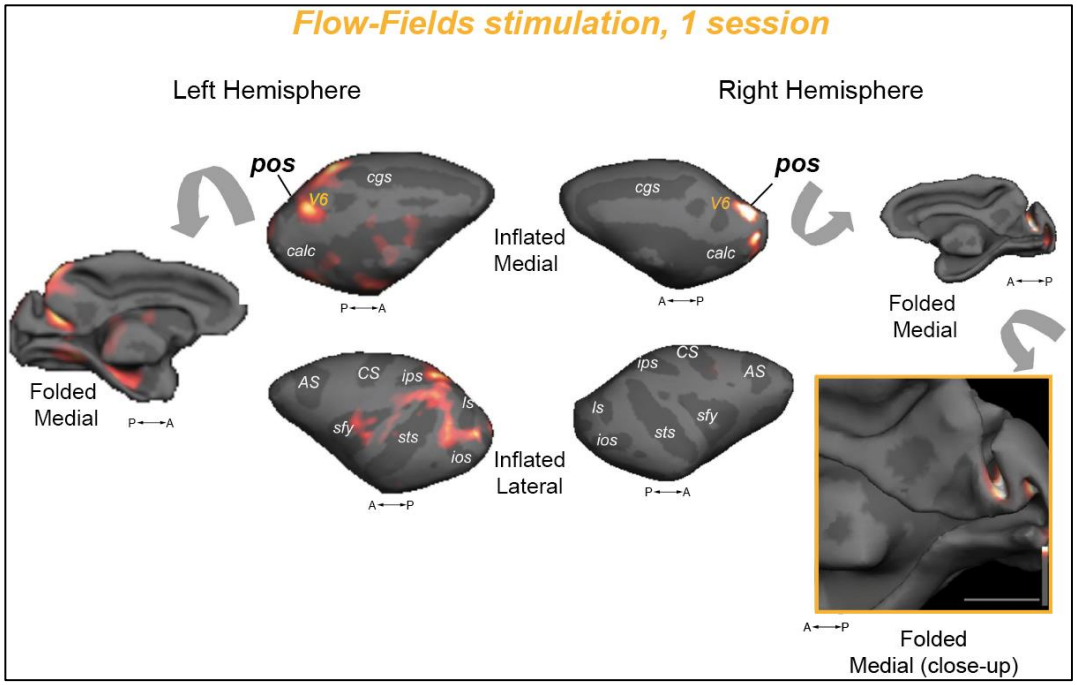

Figure 41: Flow-Fields Stimulation, first functional session.

Flow Fields, first functional session. Average data (n = 4 runs). Results are displayed on lateral and medial views of the inflated and folded left and right

hemispheres of the brain reconstructions. Figure illustrates the differentiated MION activity between coherent and incoherent moving conditions. Red-yellow regions indicate higher activity ($p < 0.001$) during rotating and dilating random dot fields than during scrambled moving random dots. In the box there is a close-up view of the folded medial right hemisphere, slightly rotated to reveal the activation into the POs. Other details as in Fig. 38.

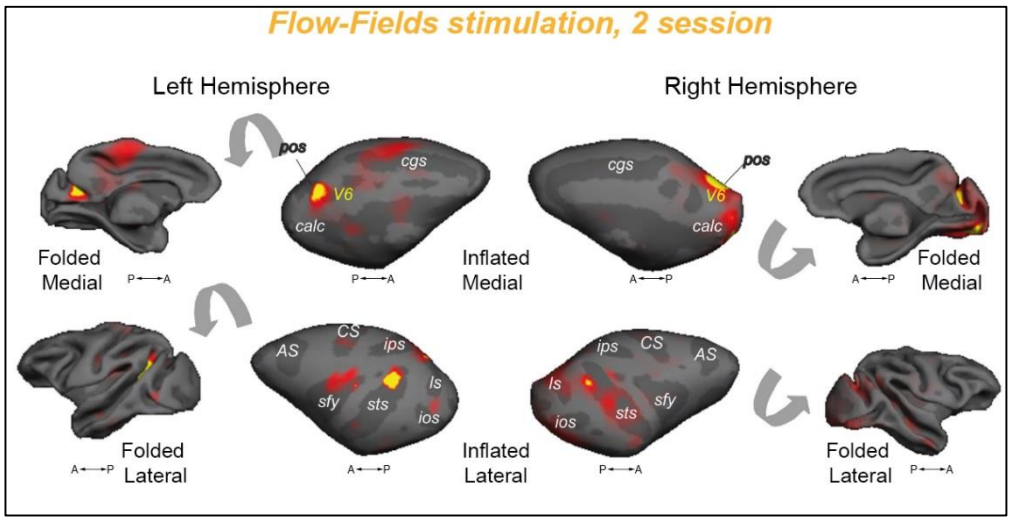

Figure 42: Flow-Fields Stimulation, second functional session.

Average map of 8 runs. Other details as in Figure 38.

Figure 43 illustrates the across-session average map of the two scanning sessions (4+8= 12 runs), in this figure fMRI activation was also shown on a dorsal view of the inflated brain (top view) to show the relationship between V6 position and the other two main sulci, STS and lunate. As expected, this coherent motion activated other motion areas, however area V6 was the most strongly activated focus. We found a less consistent activation in dorsal visual area V2 only in the first scanning session. Activation was also found even though less powerful in the

exposed surface of the SPL, a possibility is area PEc, and in the posterior segment of the IPs involving area LIP and MIP. We found a less consistent motion-selective response in the anterior part of area V3A. We found also focus of activation in the STs in a region involving area MT together with MST, see Fig. 42 lateral view of left hemisphere, and V4T, see Fig. 42 inflated lateral view of right hemisphere.

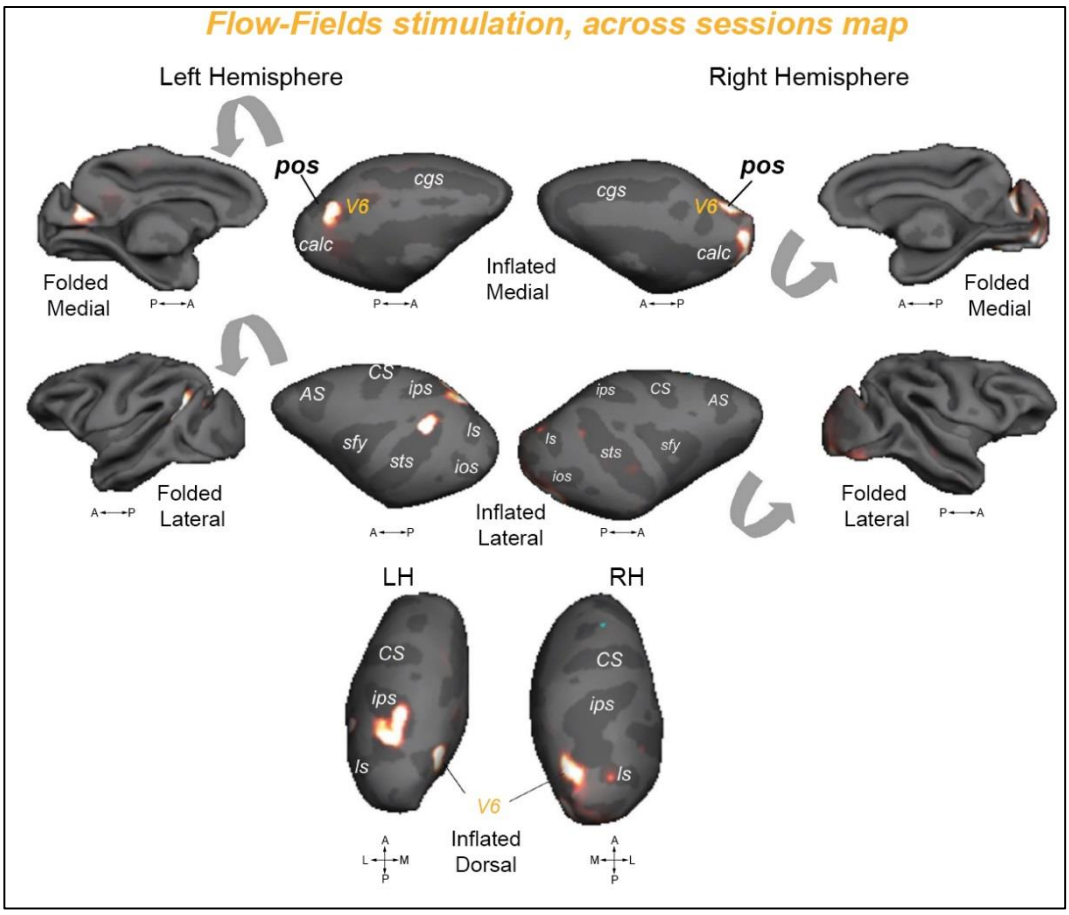

Figure 43: Flow-Fields Stimulation, average maps.

Cross-session maps (n = 12 runs). Area V6 was high activated bilaterally by the Flow-Fields stimulus. Other details as in Figure 38.

Figure 44 shows the average data for a comparison of the two motion mapping. In the V6 mapping (Fig.44, left) using the Flow-Fields stimuli, area V6 was clearly activated in both left and right hemispheres. Conversely, area MT was silent in the right hemisphere but not in the left one, in its most dorsal and anterior part. Other focuses of activation were found in the visual areas V2, V3A and in the IPs. In MT mapping, (right part of Figure 44) area MT was well activated in both hemispheres whereas area V6 was activated only in the right hemisphere. Focus of activation were spread in the superior temporal sulcus, involving area MT and the two neighboring areas MST rostrally and FST caudally. As discussed above, other spots of activation were found in the occipital areas V1 and V2 and in the visual areas V3 and V3A of the lunate sulcus, in the inferior temporal lobe level with area TEO as well as at the level of the intraparietal sulcus, in a region with areas PEc, MIP, LIP and 7a.

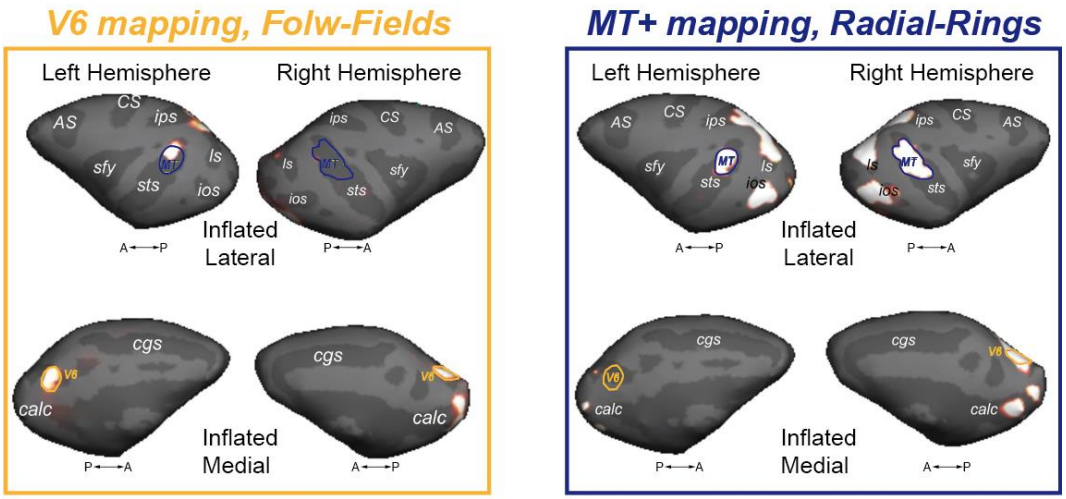

Figure 44: Sum up of the functional activations for Flow-Fields and Radial-Rings stimuli.

It is evident a consistent activation of V6 with Flow-Fields stimuli and a consistent activation of MT with Radial-Rings stimuli.

Other conventions as in above figures.

3.2 *Visual and Somatosensory properties*

Single-cell activity was extracellularly recorded from area V6A and PEc in 22 hemispheres of 12 macaque monkeys (*Macaca fascicularis*). A total of 1496 neurons were studied while the animals performed two different types of behavioral tasks (see Table 1). Recorded cells were assigned to V6A or PEc on the basis of the cytoarchitectual pattern of recording sites (Luppino *et al*., 2005). In this study, we targeted the dorsal sector of area V6A, named area V6Ad, as defined in Luppino (2005) and Gamberini (2011). The functional properties of many neurons have been described in previous work of the group (Galletti *et al*., 1996; 1999b; Fattori *et al*., 2001; Breveglieri *et al*., 2002; Breveglieri *et al*., 2006; Breveglieri *et al*., 2008; Gamberini *et al*., 2011). We checked the sensory related properties, visual and somatic, of the recorded neurons. The motor-related properties of the cells belonging from these two areas will be discussed in the next chapter "*Motor Related Activity*". Each neuron was tested with as many paradigms as possible as far as recording allowed. We did not apply any qualitative criteria to select a particular paradigm for the cell in record as well as to select particular cells for the analysis. The results are summarized in Table 2.

	PEc	V6Ad	**Total**
Visually tested	231	991	**1222**
Somatically tested	178	426	**604**

Table 2: Total numbers of V6Ad and PEc cell tested with sensory tasks.

✓ *Visual Properties*

A total of 1222 neurons were visually tested in area PEc (N =231) and V6Ad (N = 991). Results and relative cell categories are summarized in Table 3. Unclear visual cells were discarded from the analysis (PEc= 231-1=230; V6Ad= 991-42=949).

	PEc	V6Ad
Visual cells	92/230 (40%)	520/949 (55%)
Low-level visual	27/92 (29%)	199/520 (38%)
High-level visual	65/92 (71%)	321/520 (62%)
Unclear visual cells	17	42

Table 3: Incidence of visual cells in the two areas studied.

As shown in the top part of Figure 45A, the neurons sensitive to visual stimulation were significantly more represented in V6Ad (55%) than in PEc (40%, two-proportion z test, $p < 0.0005$). This difference is appreciable also comparing the percentage of visual responsive cells with the unresponsive ones separately for PEc (χ^2 test, $p < 0.01$) and V6Ad (χ^2 test, $p < 0.01$), middle and bottom part of Figure 45A respectively. The flattened map of the caudal SPL (Figure 45, bottom part) shows that visual and nonvisual cells were evenly distributed within area V6Ad, whereas in area PEc visual cells were concentrated in its ventral part.

Figure 45B shows that low-level visual cells were not equally distributed between PEc (29%) and V6Ad (38%, two-proportion z test, $p < 0.05$), with a majority of this tyoe of cell in V6Ad. The high-level visual cells were the majority of visual cells in both PEC (71%) and V6Ad (62%; two-

proportion z test, $p < 0.05$). However, it is evident that low-level visual cells were significantly less represented with respect to high-level visual cells both in area PEc (Fig. 45B middle part, χ^2 test, $p < 0.0005$) and V6Ad (Fig. 45B bottom part, χ^2 test, $p < 0.0005$). The distribution of low-level/high-level visual cells on the flattened map (Fig. 45B, bottom) shows that the two types of cells were evenly distributed within both PEc and V6Ad.

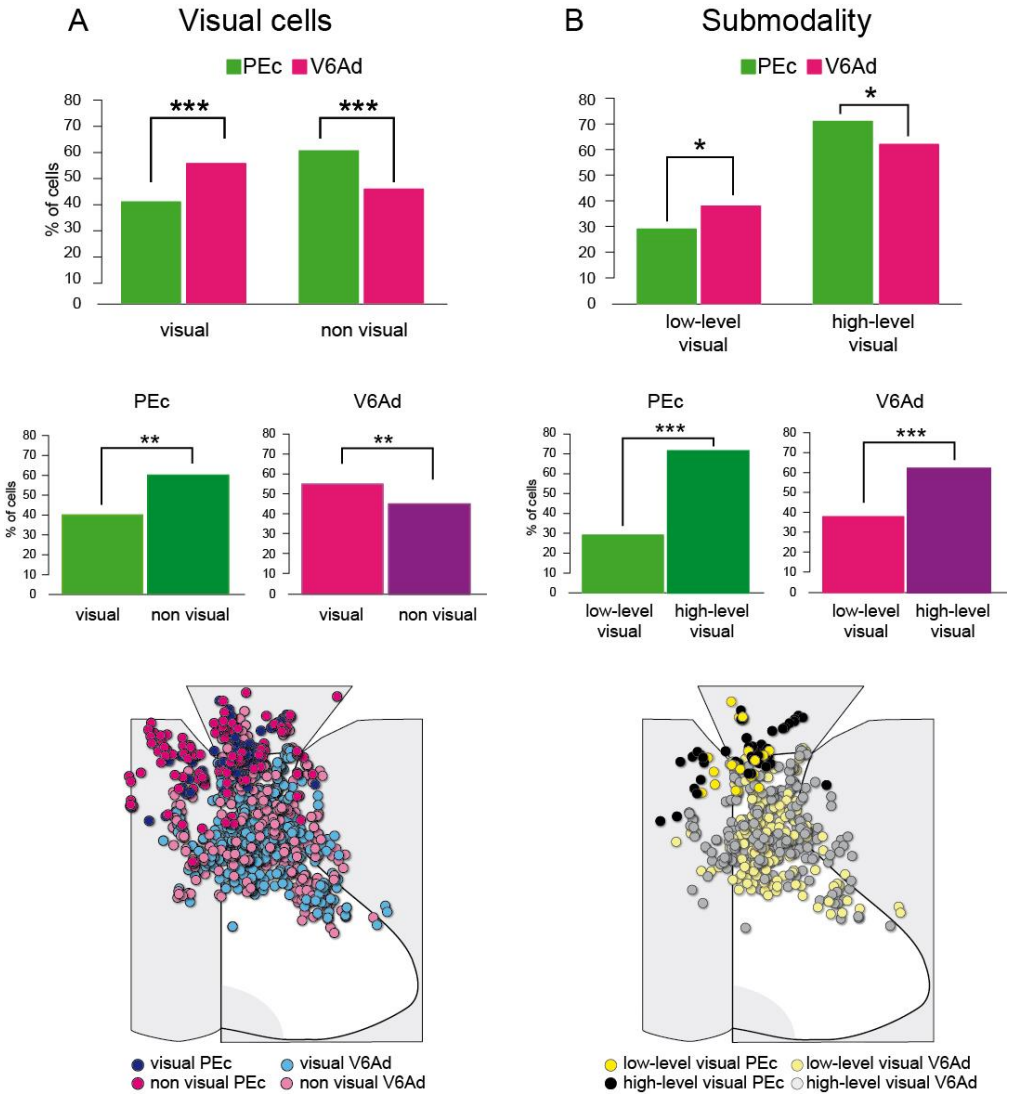

Figure 45: Incidence and distribution of visual responses.

A) Incidence (top and middle) and distribution on the flattened map pf the caudal SPL (bottom) of visual and nonvisual cells

B) Incidence (top and middle) and distribution (bottom) of low-level and high-level visual cells

The results of $\chi 2$ test and two-proportion z test are indicated by asterisks, *p< 0.05; **p< 0.01; ***p< 0.0005.

In the population of visual cells where it was possible to map the entire extent of each RF (in some cases the RF was too large and it extended outside the screen borders), we analyzed the visual field representation in PEc and V6Ad. A total of 67 neurons in area PEc and 364 neurons in area V6Ad were included in this analysis. The difference in the amount of cells included in this analysis reflects the difference in the distribution of visual cells between the two areas. All the RFs of each population were plotted together and a density map of the visual field representation for each area was elaborated as shown in Figure 46. As shown in Figure 46A and more in detail in Figure 46B, both area PEc and V6A represent largely the contralateral lower part of the visual field. The contralateral upper part of the visual field is less represented with respect the lower one both in PEc and V6A. The ipslateral hemifield is represented in both areas but only partially if compared with the contralateral one. The higher density of RFs overlapping (see the coloror full areas in Fig. 46B) is equal between the two areas. The central part of the visual field, especially up to 20°, is equally represented in PEc and V6A. The most external parts of the upper contralateral quadrant is more present in PEc. Figure 47A shows the distribution of the RFs centers in PEc (green circles, top-left part) and V6Ad (pink circles, bottom-left part). In both areas the majority of RFs centers were located in the contralateral lower hemifield within 20° for PEc and 40° for V6Ad of visual field. RFs could be centered also in other part of the visual field altough at a lower rate. We also analyzed wheter there was a difference between the two areas in the relationships between RF size (Square root of

area) and eccentricity. Data were highly scattered, meaning that small as well as large receptive fields can be found at any value of eccentricity. Figure 47B shows that receptive-field size increased with eccentricity in both area PEc and V6Ad, and on average PEc RFs were larger than those of nearby area V6Ad (ANCOVA, $p < 0.01$).

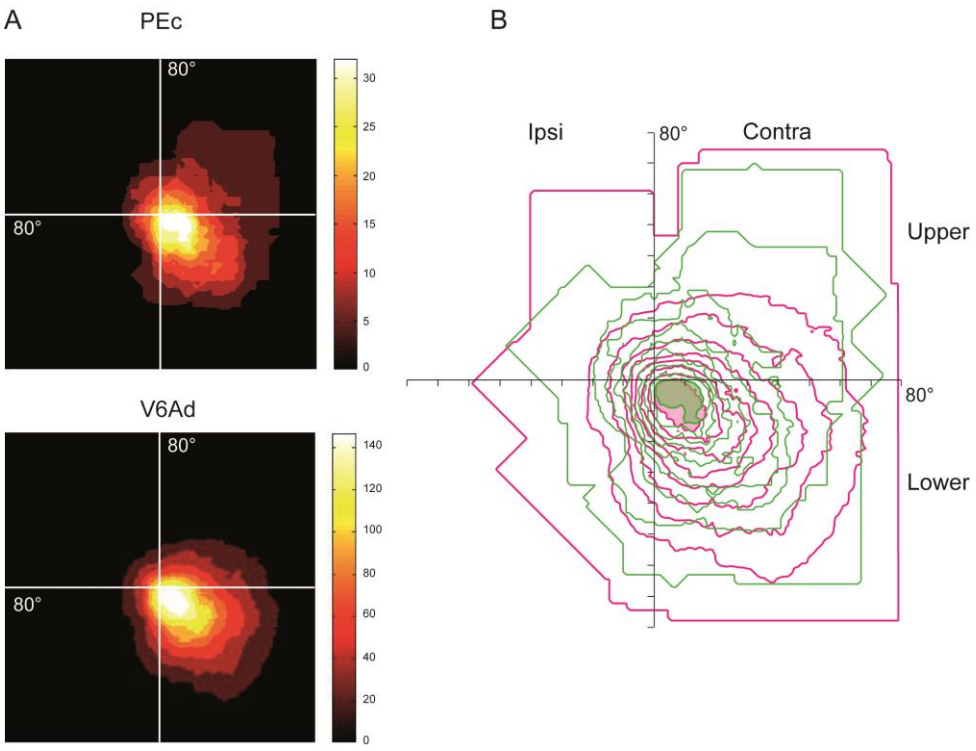

Figure 46: Receptive field distribution in the visual field.

A) Density maps of RFs distribution in areas PEc and V6Ad. Color scale indicates the relative density of RFs covering that specific part of the visual field. In the white region, 30 (PEc) or 80 (V6Ad) are superimposed in the same grid square. The size of the grid square was set to 8 X 8°.

B) Same dataset as in A, but with the data from the two areas superimposed. Green and pink lines are iso-density lines of PEc and V6Ad, respectively. Each isodensity line represents the number of RFs, as reported on the vertical color scale bar of A.The most peripheral isodensity line (not shown in A) represents 1 RF.

Ipsi, ipsilateral visual field; Contra, contralateral visual field; Upper, upper visual field; Lower, lower visual field.

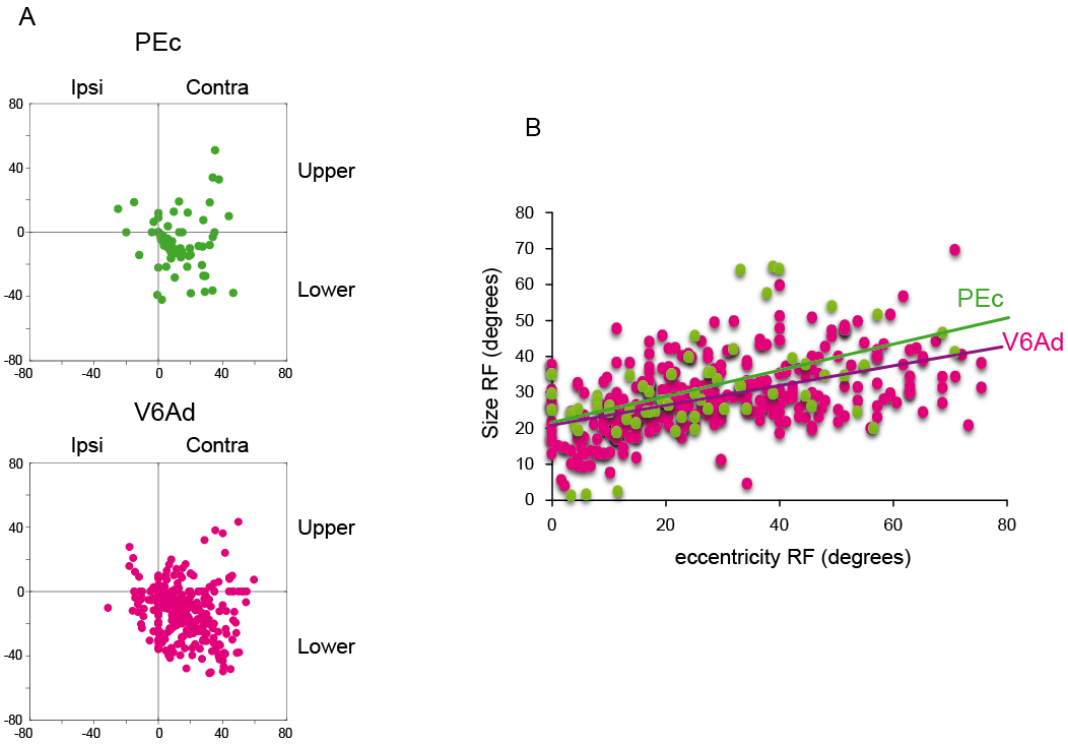

Figure 47: Receptive field center distribution in the visual field.

A) Distribution of the receptive field's center in the visual field, top PEc, green circles and bottom V6Ad, pink circles.

B) Receptive-field size versus eccentricity. Regression plot of RFs size (square root of area) against eccentricity for PEc visual cells, in green, and V6Ad visual cells, in pink. The regression equation are:

RFsize (PEc) = 21.87+0.413 eccentricity R2= 0.26;

RFsize (V6Ad) = 21.13+ 0.312 eccentricity R2= 0.27

ANCOVA analysis established that the two regression lines were not significantly different in slope ($F_{1,425} = 1.76$; $p = 0.2$) but they were significantly different in elevation ($F_{1,425} = 7.05$; $p < 0.01$).

Ipsi, ipsilateral visual field; Contra, contralateral visual field; Upper, upper visual field; Lower, lower visual field.

✓ *Somatic properties*

The somatosensory modulation of neurons was tested in seven animals for area V6Ad and five animals for area PEc, including in this analysis a total of 604 neurons (for details see Table 2). Distribution and sub-modalities of somatic cells are summarized in Table 4.

	PEc	V6Ad
Somatic cells	121/178 (68%)	181/426 (42%)
Submodality		
Skin	16/121 (13%)	26/181 (14%)
Deep	4/121 (3%)	10/181 (6%)
Joint	93/121 (77%)	136/181 (75%)
More	8/121 (7%)	9/181 (5%)
Contralateral	99/121 (82%)	163/181 (90%)
Ipsilateral	4/121 (3%)	9/181 (5%)
Bilateral	18/121 (15%)	9/181 (5%)
Somatotopy		
Arm	82/121 (68%)	160/181 (88%)
Trunk	4/121 (3%)	8/181 (5%)
Leg	19/121 (16%)	4/181 (2%)
Head	3/121 (2%)	4/181 (2%)
Mixed	13/121 (11%)	5/181 (3%)

Table 4: Distribution and sub-modalities of somatic cells.

Sixty-eight percent of cells tested in PEc (χ^2 test, $p < 0.0005$) and 42% of those tested in V6Ad (χ^2 test, $p < 0.01$) were responsive to a somatic stimulation. As shown in Figure 48 (top part of the figure), the percentage of cells responsive to a somatosensory stimulation was explicitly different between the two areas, cells sensitive to a somatic stimulation were clearly more represented in PEc than in V6Ad (two proportion z test, $p < 0.0005$). The distribution on the flattened map of the caudal SPL shows that cells responsive to the somatosensory stimulation were located mostly in the anterior-medial part of area PEc, whereas in area V6A no clear trend was visible.

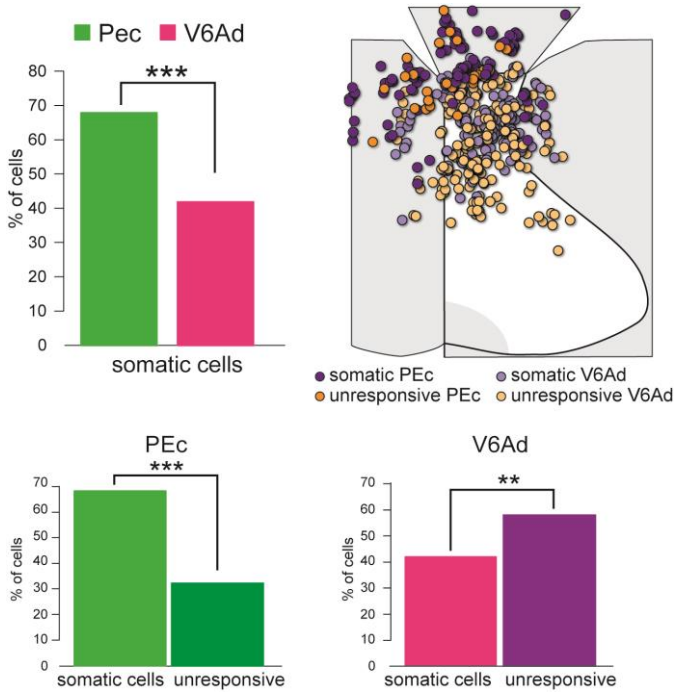

Figure 48: Incidence and distribution of somatosensory responses in PEc and V6Ad.

Top, incidence (left) and distribution (right) of somatic and unresponsive cells comparing area PEc (green bar) and area V6Ad (pink bar). The outcome of two-proportion z test is indicated by asterisks: ***p < 0.0005.

Bottom, incidence of somatic and unresponsive cells in area PEc (green bar graph, left) and in V6Ad (pink bar graph, right). The results of χ2 test are indicated by asterisks, **p < 0.01; ***p < 0.0005.

The majority of soma-sensitive cells in both PEc and V6Ad were modulated by a stimulation on the contralateral part of the body (more than 80% in both areas) and only few cells were activated by a stimulation applied in the ipsilateral (≤5%) or in both sides of the body (5% in V6A and 15% in PEc), as reported in Figure 49. As summarized in Table 4 and in Figure 50, the large majority of somatic cells were modulated by a slow/fast movement of a limb joint both in PEc and V6Ad (≥ 75% of cells) and only a minority of cells were modulated by a tactile stimulation (16% and 20%) or by more than one stimulus simultaneously (less than 10%).

Examples of existence of passive responses in single PEc and V6Ad cells are shown in Figure 51, A and B respectively. The joint neuron in Figure 51A1 is strongly modulated by the passive flextion of the contralateral shoulder, with the arm of the animal in front of it. PEc neuron in Figure 51A2 discharges strongly for an abduction of the shoulder. In Figure 51B1 and 51B2 is shown the same V6Ad neuron tested with a passive extension of the elbow and when the wrist was flexed/extended, respectively.

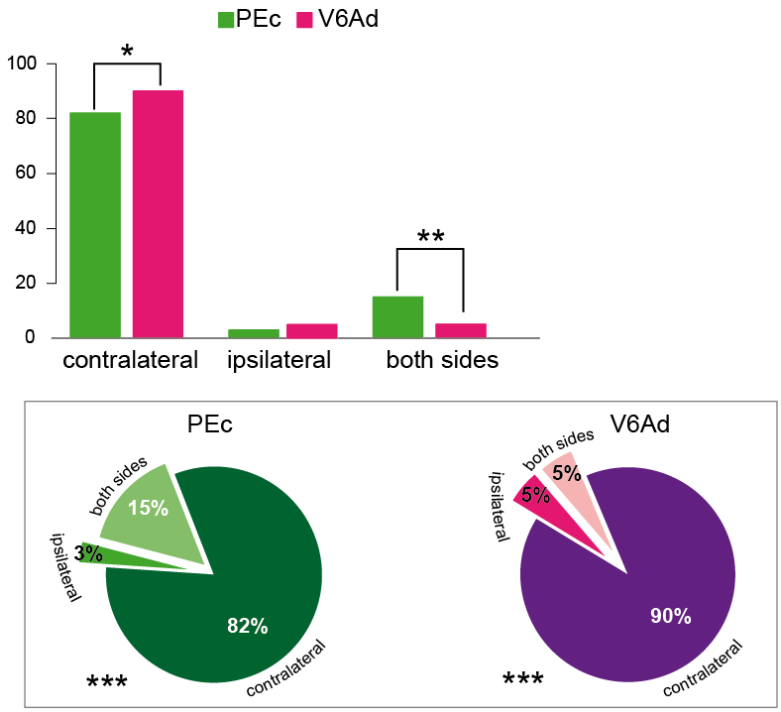

Figure 49: Laterality of somatosensory responses.

Top, incidence of contralateral, ipsilateral and bilateral modulations comparing area PEc (green) and V6ad (pink). The outcome of two-proportion z test is indicated by asterisks: * $p < 0.05$; **$p < 0.01$.

Bottom, incidence of the same modulations in area PEc and V6Ad separately. The results of $\chi 2$ test are indicated by asterisks, ***$p < 0.0005$.

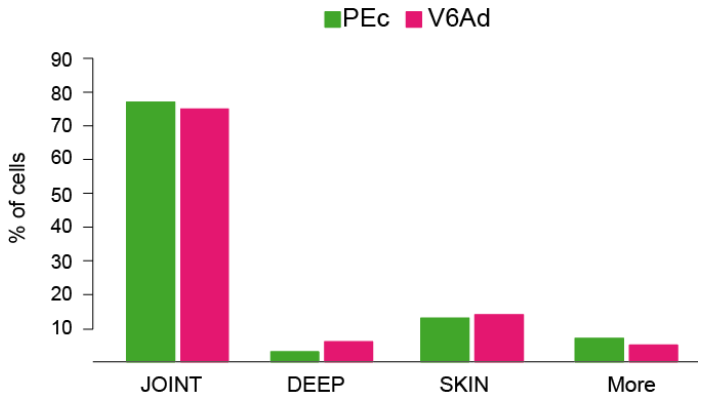

Figure 50: Somatosensory submodality.

Incidence of joint, tactile (depp and skin) and mixed cells in PEc (green) and V6A (pink). No statistical differences between PEc and V6A, $p > 0.05$.

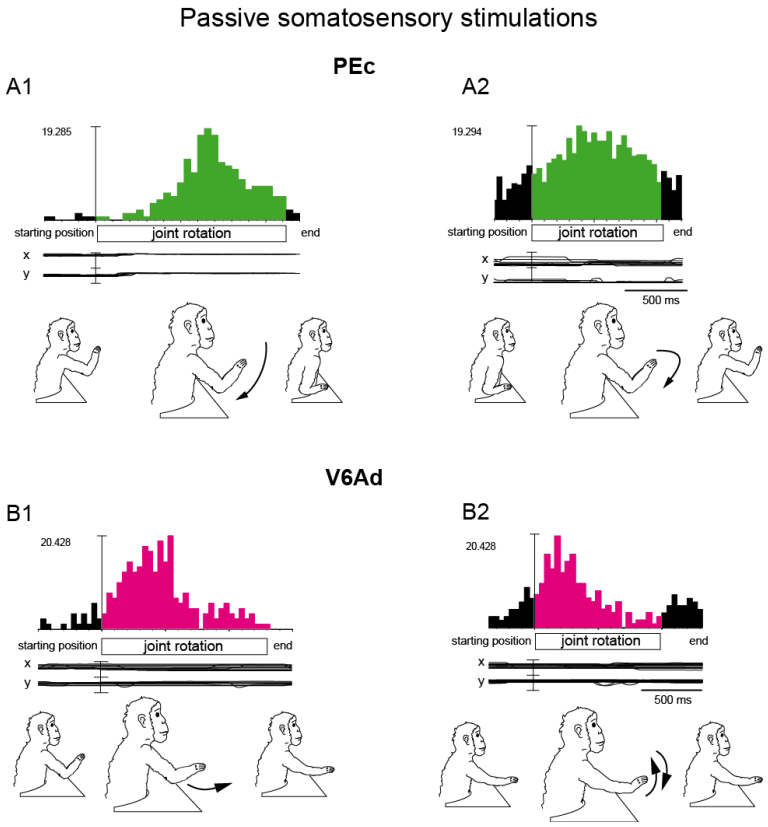

Figure 51: Examples of somatosensory responses.

Top, examples of PEc joints neurons studied with passive stimulations. A1, response of a PEc cell to passive flextion of the shoulder. The elbow before, during, and after the passive movements was mantained with the same angle (90°). A2, activity of another PEc neurons tested with a passive joint rotation of the shoulder. The movement was an abduction of the shoulder from the initial start position with the arm close to the armpit to the arm at shoulder height. Elbow, wrist and hand were controlled and maintained in the same orientation during movements.

Bottom, examples of V6Ad neuron tested with passive stimulations. B1, response of a V6Ad cells to extension of the elbow with the shoulder maintained at 45°. B2, activity of the same V6Ad cell during flextion/extension of the wrist. The shoulder was maintained at 45°, the elbow and the hand were horizontal.

Horizontal (x) and vertical (y) eye traces are reported below each PSTH. The activity and eye traces were aligned at the beginning of the somatosensory stimulation. Vertical scale bars: 86 spikes/s (A1), 170 spikes/s (A2), 46 spikes/s (B1), 40 spikes/s (B2); horizontal scale bars on histograms (500 ms); bin size 40ms, eye traces, 10V per division.

In area V6Ad the large majority of somatic cells (95%) were modulated by a stimulation of the upper half part of the body and particularly for stimulation of the arm (88%, χ^2 test, $p < 0.0005$). Only a small number of cells were affected by a stimulation of the legs (2%). In area PEc, in addition to the large amount of cells affected by a stimulation of the upper limbs (68%) we observed a quite good proportion of cells modulated by the somatic stimulation of the lower limbs (16%), Figure 52 left part. This difference can be better appreciated if we compare the percentages between the two areas, as shown in Figure 52 in the bottom part. While in area V6Ad almost all the cells responded to a somatic stimulation of the arm, in area PEc somatic cells were sensitive to stimulations in the lower part of the body (two proportion z test, $p < 0.0005$). The different body representation between these two areas of the SPL is evident also taking into account the distribution of the different cells categories within area PEc and V6Ad. In fact, cells with RFs located in both arm and leg were not segregated within area PEc covering almost uniformly all its surface. On the contrary, in area V6Ad, the few cells with RFs located on the leg were located rostrally around the border between this area and area PEc.

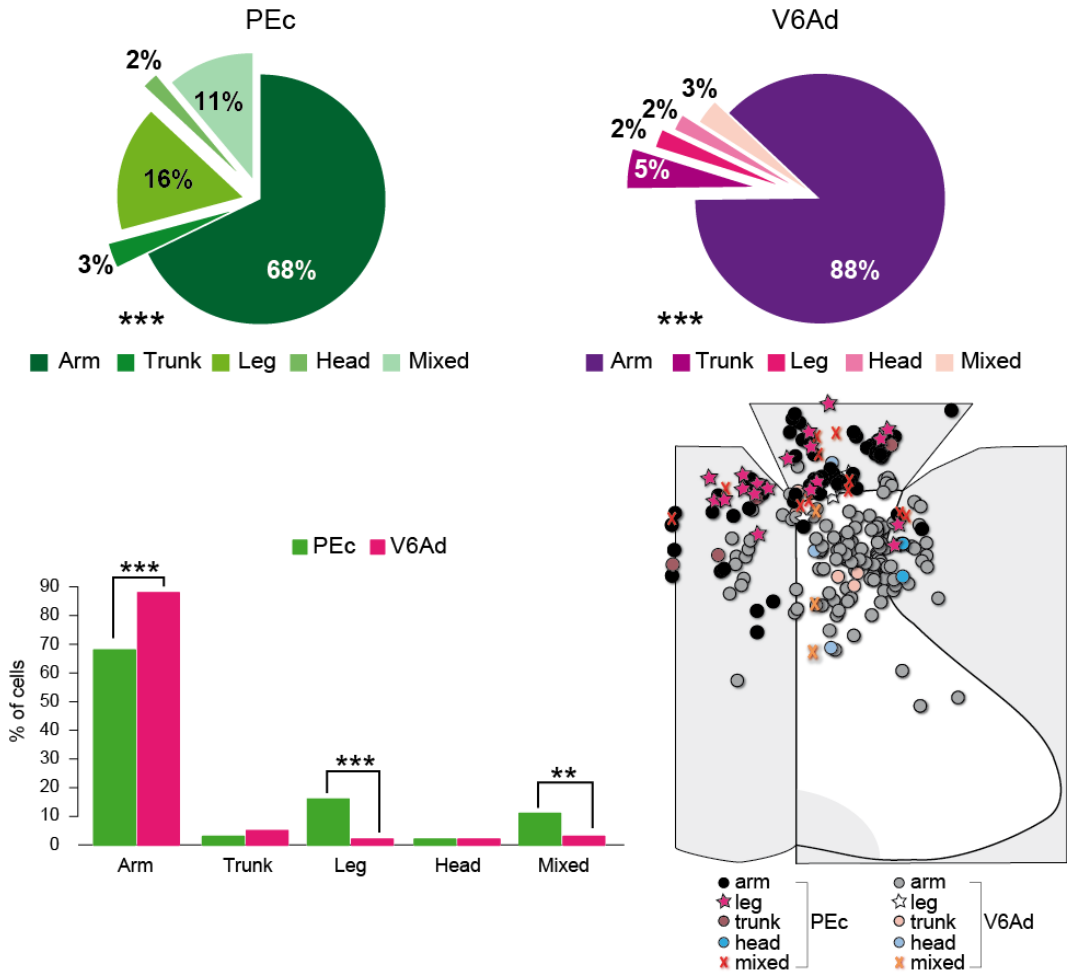

Figure 52: Incidence and distribution of somatic cells with receptive field in different body parts.

Top, incidence of different body representations in PEc, left and V6Ad, right. Mixed cells are those whose RFs were located in two or more body parts.

Bottom, Left, comparison of body representation across PEc (green) and V6Ad (pink). Right, distribution of body representations on a bidimensional map. Bigger circles refers to PEc somatic neurons.

The results of $\chi 2$ test and two-proportion z test are indicated by asterisks, **p< 0.01; ***p < 0.0005.

We then analyzed the somatosensory representation in PEc and V6Ad more in detail. Figure 53 shows the location and distribution of joint and tactile RFs subdivided between the arm (top), leg (middle) and rest of the animal's body (bottom). Analysing the RFs located on the arm, in both area PEc and V6Ad we observed that the majority of joint-modulated cells were mostly activated by the rotation of the shoulder (more than 60 units) and a good number of cell were active also during the rotation of the elbow. Joint-modulated cells were also found after a rotation of the wrist and of the hand fingers, althogh in a smaller number of units. Tactile RFs in area V6Ad covered all the arm, both in the external and internal parts, and extened also on the top and palm of the hand (as shown in the close-up view), on the contrary in area PEc tactile RFs were located mostly around the joints (shoulder, elbow and wrist) and no RFs were found on the top or palm of the hand. Pooling together joint and tactile data with RF located on the arm of both areas (N=303), we observed a clear difference between the two areas in the percentage of cells with RFs located on the shoulder (two proportion z test, $p< 0.0005$) and on the hand (two proportion z test, $p< 0.05$), while no statistical difference was found in the elbow representation (two proportion z test, NS). When we took into account the location of the RFs on the leg we observed a clear difference between PEc and V6A. As shown in Figure 53, middle part, PEc joint-modulated cells were active during passive rotation of the hip, knee and foot (both ankle and foot fingers), whereas in area V6Ad only few neurons were modulated by the rotation of hip and knee (< 5 units). And similarly to the tactile RFs of the arm but in the opposite manner, in area PEc tactile RFs covered the entire extention of the leg while in area V6Ad no tactile RFs were found from the knee down to the foot. In area PEc a good number of cells had their RFs located around the ankle and on the top and palm of the foot. Pooling together joint and tactile data from both area PEc and V6Ad (N=47) we observed a significant difference in the percentages of cells with RFs located in the hip (two proportion z test, $p< 0.0005$), and foot (two proportion

z test, $p< 0.01$). Regarding the proximo-to-distal distribution of somatic receptive fields, it seems that there is a trend for V6Ad to have less distal receptive fields on the lower limbs, with respect to PEc and *viceversa* more distal receptive fields on the upper limbs. Tactile RFs were also found, although less numerous, in the rest of the body both in PEc and V6Ad and no statistically difference was observed (two proportion z test, NS). RFs were found in the back and sides, in the abdomen and in the neck. In area V6Ad very few cells had their RF on the snout of the monkey, on the lips, around the mouth and only one cell responded to the passive movements of the mandible.

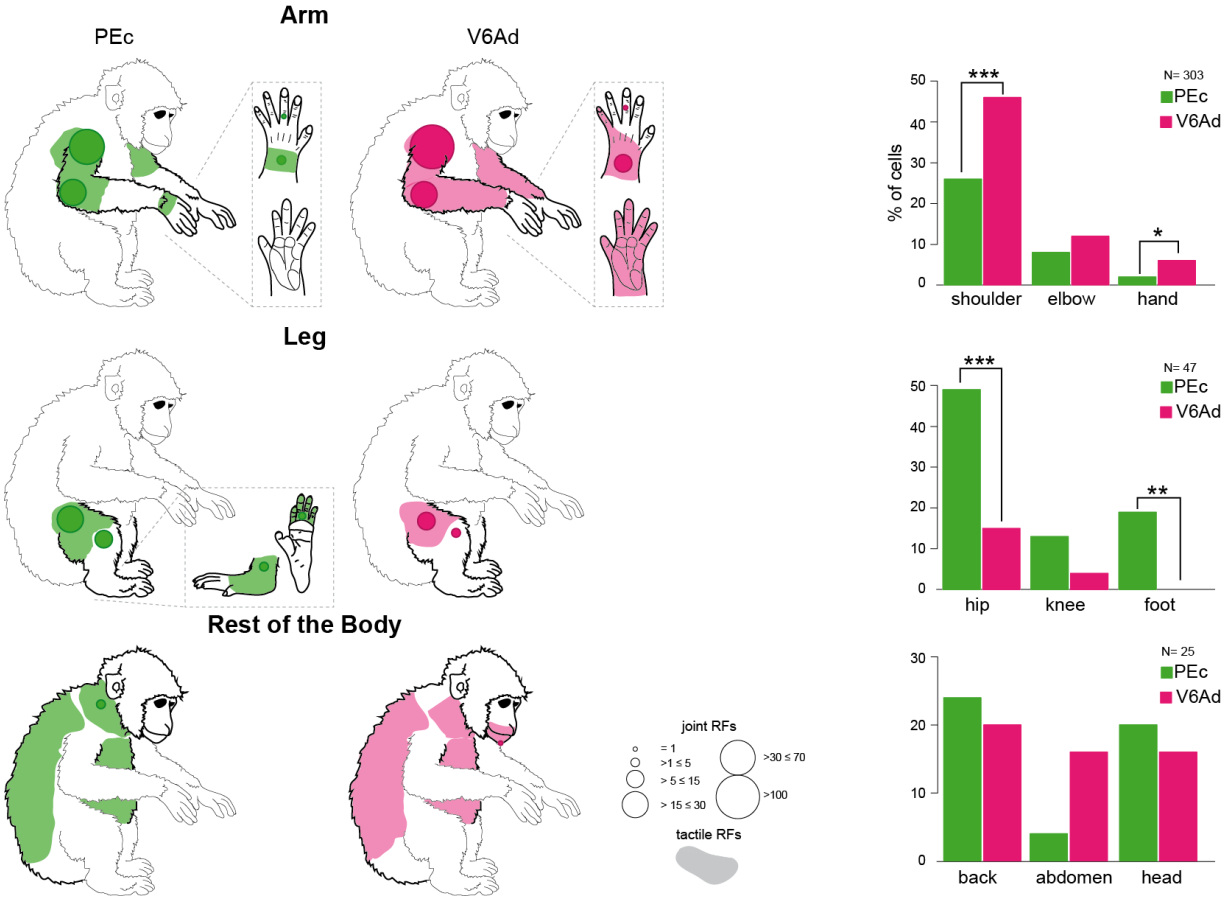

Figure 53: Somatotopy across area PEc and V6Ad.

Left) Locations of somatosensory RFs in PEc (in green) and V6Ad (in pink): joints (dots) and tactile receptive fields (colored patches on the animal body). The size of each dot is proportional to the number of modulated units. All the somatosensory RFs have been reported on animal's body independently to the recording side. Dashed boxes report the close-up view of hand and foot.

Right) Incidence of proximal, middle and distal part of arm and limb representation and of other part of the animal body. The outcome of the two-proportion z test is indicated by asterisks, * p< 0.05; **p< 0.01; ***p < 0.0005.

A subset of neurons (N= 102 for PEc and N= 223 for V6A) was tested for both visual and somatosensory responses to check the distribution of multisensory (bimodal) neurons, as reported in Table 5.

	PEc	V6Ad
Unimodal visual cell	26/102 (25%)	77/223 (35%)
Unimodal somatic cell	45/102 (44%)	50/223 (22%)
Bimodal cells	23/102 (23%)	35/223 (16%)
Somatic low-level visual	4/23 (17%)	12/35 (34%)
Somatic high-level visual	19/23 (83%)	23/35 (66%)
Unresponsive	8/102 (8%)	61/223 (27%)

Table 5: Percentage of bimodal cells.

As shown in Figure 54, the majority of cells were responsive for just one of the two sensory modalities, in area PEc the 44% (χ^2 test, $p < 0.0005$) of cells was modulated by the somatosensory stimulation on the contrary in area V6A the majority of cells were modulated by the visual stimulation (35%, χ^2 test, $p < 0.0005$). These significantly different percentages (two-proportion z test, $p < 0.05$) reflected what already illustrated in the two sections above. As shown in the figure, the bimodal cells were quite equally distributed in the two areas (23% in PEc vs 16% in V6A, two-proportion z test, $p > 0.05$). We investigated also if bimodal cells differred for the kind of visual stimulus used. To do this, we compared the bimodal cells activeted using either simple either complex visual stimuli. As shown in Figure 54 in both areas the majority of cells were activated using the complex visual simulus and were classified as high-level visual/somatic cell (83% in PEc

and 66% in V6A).The different incidence of bimodal cells with complex visual properties is significant between the two areas (Fig. 54, bottom right). These data together supported the overall impression that area PEc and V6Ad share several functional properties but area PEc appears to be more influenced by the somatosensory signals than the visual ones.

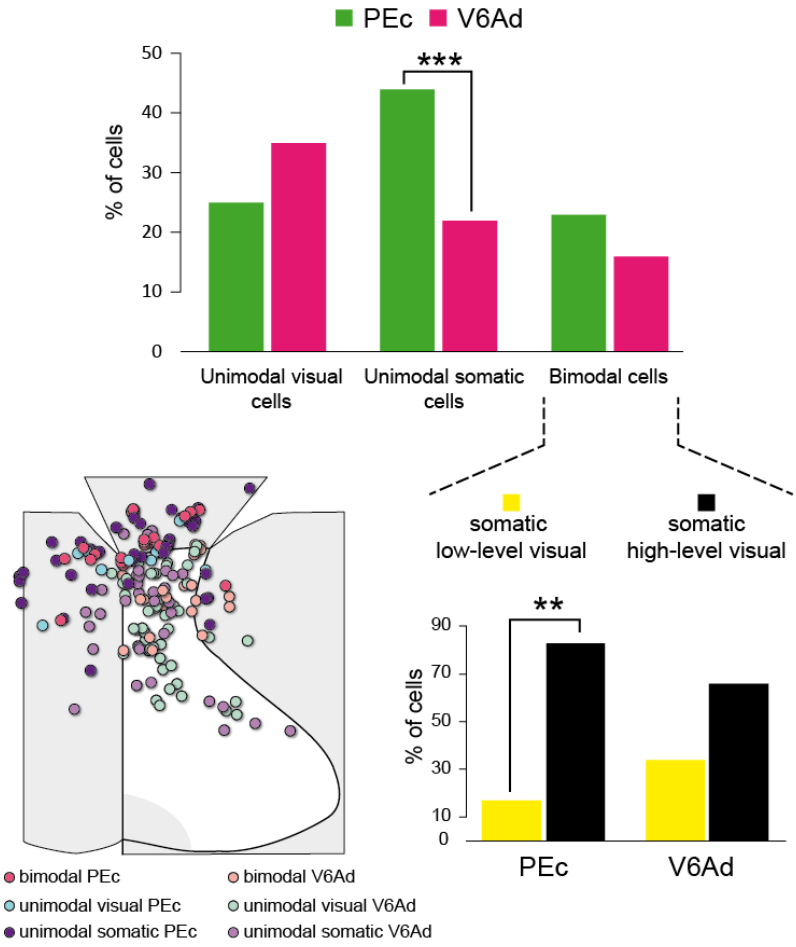

Figure 54: Incidence of unimodal and bimodal visual and somatic cells.

Top) Incidence of unimodal visual, unimodal somatic and bimodal visual/somatic cells in area PEc (green) and V6Ad (pink).

Bottom) Left, distribution of bimodal visual/somatosensory, unimodal visual and unimodal somatosensory neurons. Incidence of bimodal cells split by the complexity/simplicity of visual properties.

The results of $\chi 2$ test and two-proportion z test are indicated by asterisks, *p< 0.05; **p< 0.01; ***p< 0.0005.

3.3 Motor Related Activity in 3D Space

We recorded the neuronal activity from 200 neurons in area PEc from three macaque monkeys (M22, M24, M25). The monkeys were required to execute reaches to foveated targets located at different depths and directions, while the targets' elevation was kept constant at eye level (Fig. 33A). Data from PEc are subsequently compared with a pooled dataset of 388 V6A neurons recorded under the same task conditions that included the neurons (n=288) presented in our recent paper (Hadjidimitrakis *et al*., 2014) and a population (n=100) of newly recorded cells. V6A data were recorded from the same three animals used for PEc recordings

- ✓ *Tuning for depth and direction in the different task epochs*

To quantify the effect of depth and direction on neuronal activity, a two way ANOVA ($p < 0.05$) was performed for each of the several task epochs. As shown in Table 6, the overall effect of depth was moderate (<40%) during the early fixation (FIX), late delay (PLAN) and pre-movement (PreM) periods, increased remarkably and reached its peak (~60%) during the movement execution (MOV), and remained high during the subsequent holding period (HOLD). Differently, the influence of directional signals was more stable (~40%) across the task.

EPOCH	DEPTH		DIRECTION	
	PEc	V6A	PEc	V6A
FIX	32.5%	52%	46%	50.5%
PLAN	39.5%	59.3%	40.5%	46.4%
PreM	38%	54.4%	30.5%	35.6%
MOV	57.5%	57.7%	42%	47.9%
HOLD	47.5%	65.5%	46.5%	51.3%
MEAN	**43%**	**58%**	**41%**	**43%**

Table 6: Numbers and percentages of single cells modulated for depth and direction for each epoch.

Figure 55 shows the tuning of activity of an example PEc neuron. When the animal looked at the contralateral far target (upper left panel in Fig. 55), the neuron started to respond and continued to fire tonically. The activity slightly increased during PLAN, reached its peak in the PreM and MOV epochs, and strongly decreased in HOLD. It is very clear that this activity pattern occurred only when the monkey performed the task for the far, contralateral target, with the neuron's firing being much weaker or absent for the other target locations. The preference for the far contralateral space was evident in all five epochs of analysis, including the epoch HOLD where the activity is inhibited with respect to FIX.

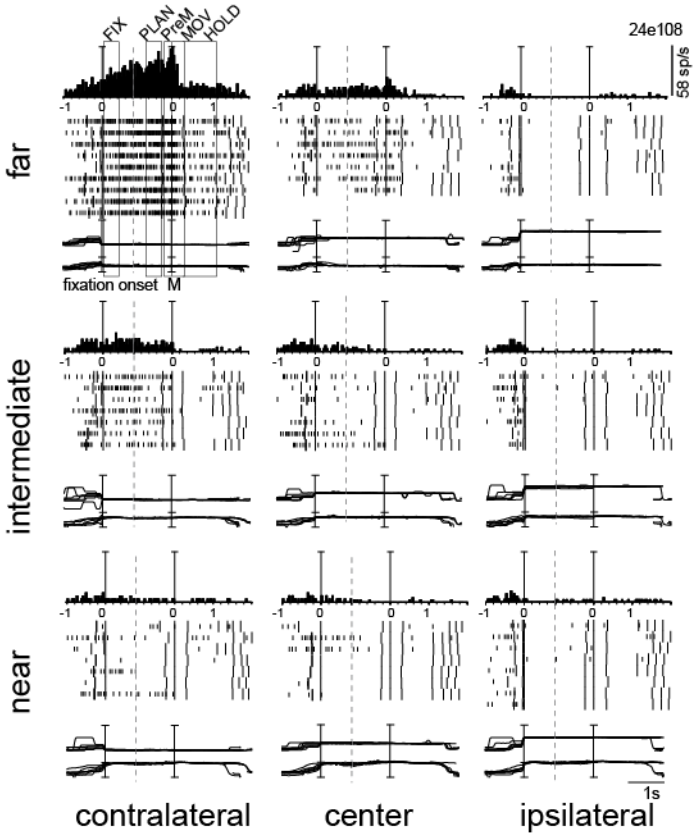

Figure 55: Depth and direction tuning in an example PEc neuron.

Spike histograms, rasters and verion (upper) and vergence (lower) eye position traces for the nine target positions. Rows represent the 3 depths (from top: far/intermediate/near) and columns the 3 directions (from left:

contralateral/center/ipsilateral). Vertical lines indicate the alignment of activity and eye position traces at the onset of fixation and at the onset of arm movement (M). Trial cut is evidenced with a vertical dashed line. This neuron showed a consistent preference in all epochs for far and contralateral space. The epochs duration is indicated in the top-left part. The scale for version and vergence is 100 and 20 deg, respectively.

In the example of Figure 55 depth and direction were processed jointly. In other cases, cell activity was modulated mostly, and in some cases only, by one of the two parameters. To study these effects at population level, we calculated the percentage of PEc cells that encoded both spatial parameters as well as that of cells encoding only one of the two (Fig.56A). The proportion of neurons that showed only depth modulations consistently increased as the task progressed from FIX to MOV epoch. In contrast, the percentage of cells showing only an effect of direction was highest in FIX and decreased in the following epochs. The percentage of cells modulated by both signals (on average the more common behavior) was smaller in the epochs that preceded arm movement with respect to epochs MOV and HOLD. In other words, there was a different temporal pattern in the processing of depth and direction information in PEc. Shortly after the target was fixated, the direction signal modulations were stronger than the depth ones. As the task progressed, the number of neurons carrying depth signals increased significantly and outnumbered those containing directional information. Interestingly, after the onset of arm movement there was a clear increase in the number of neurons coding for both signals.

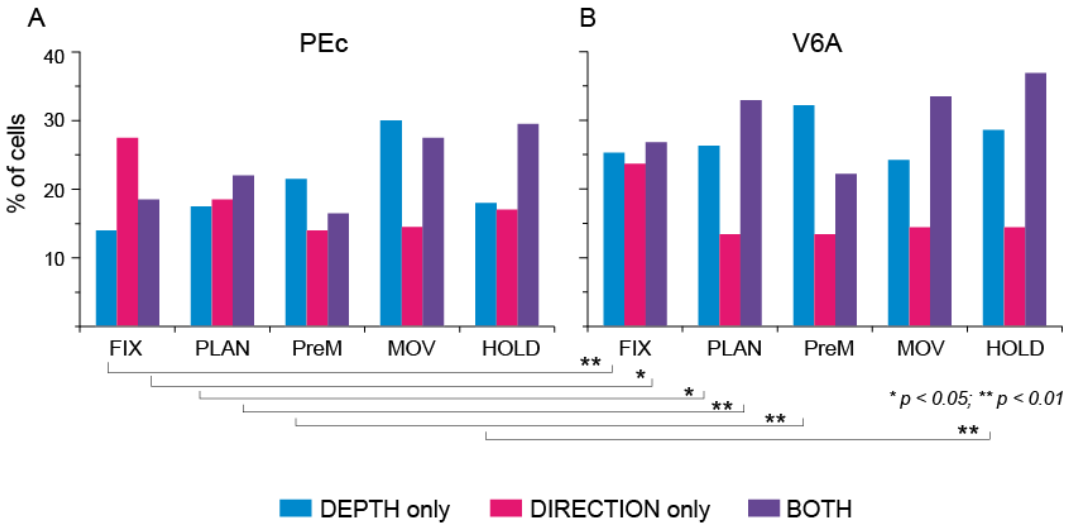

Figure 56: Depth, direction and combined tuning during each task epoch and comparison between PEc and V6A.

Percentage of cells in the population of (A) PEc (n = 200) and (B) V6A (n = 388) with tuning for depth only (cyan), direction only (pink), and for both signals (lilac) during different task epochs (fixation, FIX, planning, PLAN, pre-movement, PreM, movement, MOV, and holding, HOLD). Lines with asterisks indicate significant difference between the two areas in the coding of one or both spatial parameters in a certain epoch (two-proportion z test, * p< 0.05; ** p< 0.01).

✓ *Spatial preference and consistency across epochs*

To define the spatial preference of the modulated neurons, a linear regression analysis was performed with target depth and direction as independent variables. The vast majority (89.5%) of neurons with a depth and/or direction effect showed a monotonic increase of activity for changes of target position in depth (towards near or far space; and these cells were classified as “near” or “far”) and/or in direction (towards contralateral or ipsilateral space; classified as “contra” or “ipsi”, with respect to the recording

hemisphere). Figure 57A shows the percentage of PEc cells falling into the above groups for each epoch.

Neurons tuned only in depth (Fig. 57A, top) did not show any significant preference for near or far locations. Regarding the cells with directional tuning (Fig. 57A, middle) “contra” cells were more numerous than “ipsi” in most epochs, with a significant bias in epochs FIX and PreM (χ^2, $p< 0.05$). In neurons modulated by both signals (Fig. 57A, bottom), the group of “far-contra” cells was the most represented before the movement, especially in FIX (χ^2, $p< 0.05$). In summary, area PEc showed an over-representation of the contralateral space during most of the task phases, especially soon after the target was fixated. This representational bias for contralateral space has not been reported previously for medial PPC, but is consistent with findings from the lateral PPC areas LIP and 7a (Battaglia-Mayer *et al*., 2005; Kagan *et al*., 2010).

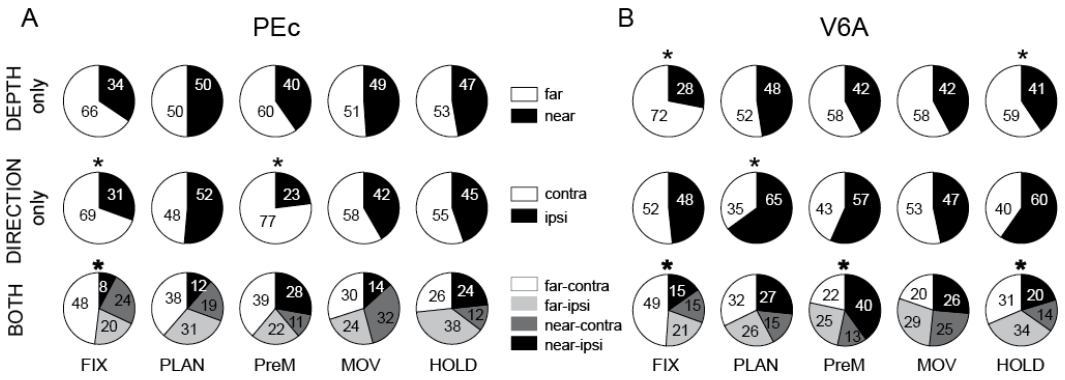

Figure 57: Spatial preference in single epochs

Classification of PEc (A) and V6A (B) neurons with monotonic tuning by depth and direction signals. Top: percentage of neurons that preferred far (white) and near (black) space in each epoch. Middle: percentage of neurons that preferred contralateral (white) and ipsilateral (black) space in each epoch. Bottom: percentage of neurons belonging to the combination of classes in cells linearly modulated by both depth and direction. Asterisks indicate a statistically significant ($\chi 2$, $p< 0.05$) spatial preference.

We then investigated whether the relative similarity in spatial preference between epochs that we observed was due to a single population of cells being active across all task phases, or to different populations recruited in different epochs. In Figure 58A, the percentage of PEc cells that preserved (white), lost (black) or acquired (hatched) their spatial preference as the task progressed from one epoch to the next is shown. About 30-40% of directionally or depth tuned, respectively, cells maintained their spatial preference across consecutive epochs. In either type of modulation, as the task progressed, many neurons lost their tuning and new populations of neurons became tuned. Importantly, the highest percentage (~50%) of neurons that acquired their tuning, either in depth or in direction, was found in the PreM-MOV pair. This suggests that the subpopulation of PEc neurons spatially tuned before the onset of hand movement was quite different with respect to that recruited after movement onset.

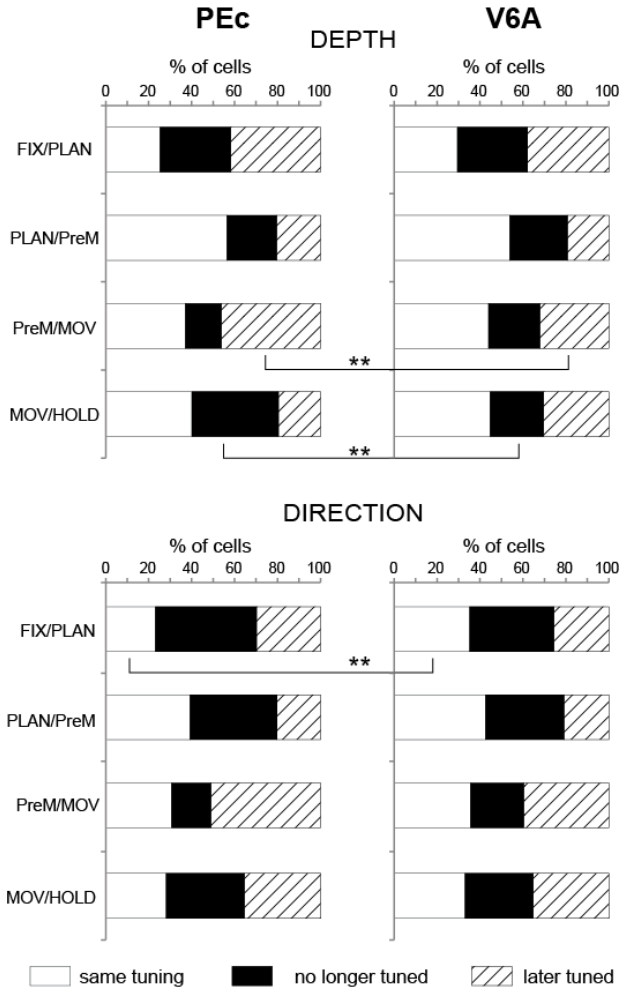

Figure 58: Consistency of spatial preference across epochs.

Percentages of PEc (left) and V6A (right) cells that maintained, lost or acquired their spatial preference in depth (upper panels) and direction (lower panels) from one task epoch to the next. Lines with asterisks indicate statistical differences (two-proportion z test, $p < 0.01$) between the two areas. In PEc there was a larger, compared to V6A, proportion of cells that a) acquired depth tuning in the MOV epoch and b) lost their depth tuning in HOLD epoch. Conversely, more neurons in V6A compared to PEc had a consistent directional tuning between FIX-PLAN epochs.

✓ *Relationship between eye position and arm movement signals*

We analyzed the relationship between modulations of eye- and hand-related activity in single PEc neurons and divided the cells into three main categories : a) 'FIX cells' when they showed spatial tuning in FIX, but not in MOV, b) 'REACH cells' when the opposite condition occurred, and c) 'FIX-REACH cells' when the neurons were spatially tuned in both epochs. The percentage of PEc cells belonging to each category is reported in Figure 59A. Neurons modulated by depth (Fig. 59A, top) fell mostly in the 'REACH cell' category (35%, χ^2, $p< 0.05$), whereas those affected by direction (Fig. 59A, bottom) were almost equally divided between the three categories (χ^2, $p> 0.05$). The fact that in depth there was little tuning of the eye position related activity and a large neural population sensitive to depth only during the hand movement, suggests a more somatomotor compared to visuospatial role of PEc for reaches in depth (see also Discussion).

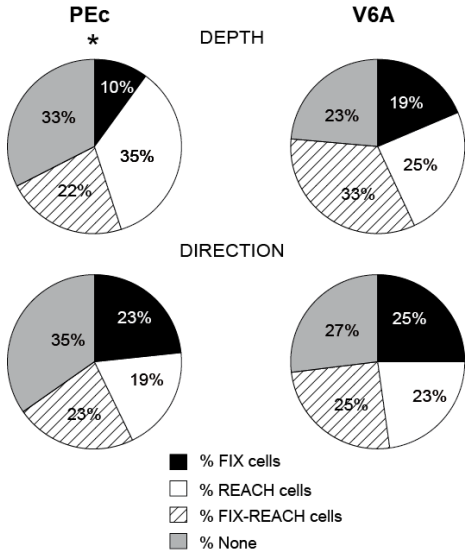

Figure 59: Combination of eye and hand signals in SPL.

Percentage of neurons in PEc (left) and V6A (right) with modulations of activity by eye position ("FIX cells"), hand movement ("REACH cells"), by both signals ("FIX-REACH cells"), or none of them in depth (upper) and direction (lower). The asterisk indicates that depth modulations were not observed with the same frequency in the three categories in PEc ($\chi 2$, $p< 0.05$).

We also investigated the temporal pattern of population activity in the three main categories of cells. Solid/dashed black curves in Fig. 60 are the spike density functions (SDFs) illustrating the average population activity of each category of PEc cells for depth and direction modulations, and for preferred and opposite conditions. All in all, there was a similar trend and time course between depth and direction modulations. Going into detail, the SDFs of preferred and opposite conditions in “FIX” cells diverged slightly before the fixation onset (because many cells showed spatially congruent perisaccadic responses) and their difference was more pronounced during the first part (about 500 ms) of fixation. Interestingly, ‘FIX cells’ showed also arm movement related responses, but these responses had similar magnitude in the preferred and the opposite conditions. In other words, FIX neurons showed spatially tuned fixation activity and received information about the occurrence of an arm movement, regardless of its amplitude and/or direction. This latter behavior is reminiscent of the “pandirectional cells” described in area PE by Acuna and colleagues (Acuña *et al*., 1990) that showed changes in activity during arm movements that was independent of the target’s direction.

In “REACH” cells (Fig. 60, center), FIX modulation was negligible in both preferred and the opposite conditions, whereas a strong activity was observed during the execution of arm movement. The cell activity was also strongly modulated before the hand moved (PLAN epoch), in particular for movements in depth. Interestingly, also the spatial tuning during arm movement was stronger in depth than in direction.

The behavior of “FIX-REACH” cells (Fig. 60, bottom) resembled that of “FIX” cells at the beginning of the task, and that of “REACH” cells during the arm movement. “FIX-REACH” cells showed a strong tuning during movement execution not only for movements in depth, like the “REACH” cells did, but also for movements towards different directions. This finding suggests that neurons carrying both eye and hand signals are engaged in the control of reaches directed everywhere in the peripersonal space,

whereas neurons with only arm signals are more involved in reaches at different depths.

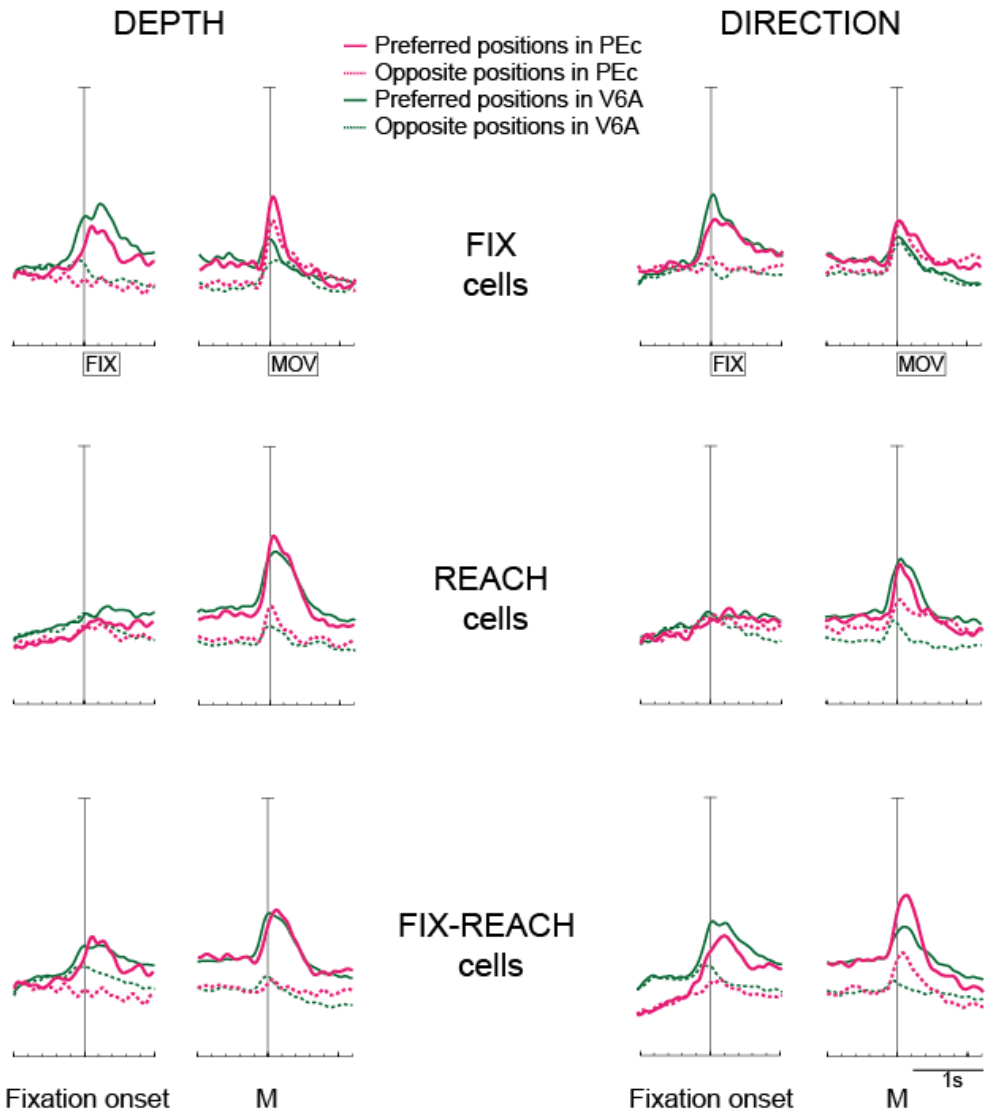

Figure 60: Population average activity of the main categories of cells.

Average normalized spike density functions (SDF) of the cell categories of Fig.56 for areas PEc (pink curves) and V6A (green curves). Top/ Middle/ Bottom: Population activity represented as SDF of 'FIX cells'/ 'REACH cells'/ 'FIX-REACH cells' modulated by depth (left) and direction (right) doubly aligned (grey vertical lines) at the beginning of fixation and at movement onset. For each cell category and type of modulation the average SDF for the preferred (solid) and opposite

(dashed) position are plotted. In “FIX- REACH” cells the preferred condition was defined using the spatial preference of the REACH epoch, which was the same in most of cases (>90%) with the preferred condition in FIX. Scale bar in all SDF plots: 100% of normalized activity. Boxes below the time axis indicate the duration of the FIX and MOV epochs. Sliding permutation tests ($p<0.05$, see Methods) were performed for each category to calculate the time point when the population activity was different in the preferred and opposite conditions. PEc ‘FIX cells’: 140 (depth) and 180 (direction) ms before fixation onset. PEc ‘REACH cells’: 440 ms after fixation onset for depth and 40 ms before movement onset for direction. PEc ‘FIX-REACH cells’: 150 ms before fixation onset for depth and 160 for direction. V6A ‘FIX cells’: 180 ms before fixation onset for depth and 200 for direction. V6A ‘REACH cells’: 240 ms after fixation onset for depth and 400 ms for direction. V6A ‘FIX-REACH cells’: 120 ms before fixation onset for depth and 140 for direction.

- ✓ *Comparison with V6A*

As mentioned above, we examined a large population of V6A neurons recorded under identical conditions for comparison with PEc. Out of the total of 388 V6A neurons here reported, 288 neurons were recorded previously (Hadjidimitrakis *et al.*, 2014), while 100 neurons are newly recorded cells. A summary of the total incidence of depth and direction modulations in V6A neurons across the task epochs is shown in Table 6. It can be seen that, differently from PEc, in V6A the influence of depth information on the neural activity was already strong at the beginning of the task and did not change very much across the epochs. Furthermore, the frequency of modulations, either by depth, or by direction was generally higher in V6A.

Figure 56B shows the proportion of the “pure” effect of depth and direction and the incidence of their convergence on single cells for the same population of V6A cells. Compared to PEc (Fig. 56A), V6A showed a higher incidence of depth-only modulations in all task epochs except MOV (two-

proportion z-test, $p< 0.05$; see connecting lines with asterisks in Fig. 56), and similar incidence of direction-only cells, as well as similar temporal evolution across the task. Interestingly, V6A had a larger proportion of cells than PEc modulated by both depth and direction in all epochs, especially in FIX and PLAN (two-proportion z-test, $p< 0.05$). In summary, the major differences in the encoding of depth and direction information between the two areas involved in particular the pre-movement epochs, with PEc showing a smaller incidence of depth-only tuning and also a smaller convergence on single neurons of depth and direction signals.

Regarding the spatial preference of modulated neurons, V6A cells tuned only in depth showed in most epochs a bias for far space (FIX and HOLD, χ^2, $p< 0.05$) that was also observed in PEc (compare Fig. 57B, top with Fig. 57A, top). Differently, the V6A neurons tuned only in direction (Fig. 57B, middle) did not have the bias for the contralateral space found in PEc. Instead, there was a trend for the ipsilateral space, most evident in PLAN (χ^2, $p< 0.05$). V6A neurons tuned by both depth and direction signals (Fig. 57B, bottom) showed a preference for far and contralateral space in FIX (χ^2, $p< 0.05$) and for far and ipsilateral in HOLD (χ^2, $p< 0.05$), with both findings being consistent with the PEc results (Fig. 57A, bottom). The latter result might reflect the fact that the holding of the targets located at the far and ipsilateral space activated more strongly the neurons receiving proprioceptive input from the contralateral hand. The contralaterality of directional modulations found in PEc, but not in V6A, might be indicative of a functional specialization of the former area for perception and action in the contralateral space.

The analysis of consistency of spatial preference between epochs in V6A (Fig. 58B) gave very similar results to those of PEc (Fig. 58A). Differences between the two areas were found in the proportion of cells that acquired depth tuning in the MOV epoch and in that of cells that lost their depth tuning in HOLD epoch, with the proportion in both cases being larger in PEc (two-proportion z-test, $p< 0.01$, see connecting lines with asterisks

in Fig. 58). In addition, more neurons had consistent directional tuning between FIX-PLAN epochs in V6A compared to PEc (two-proportion z-test, $p< 0.01$). These findings suggest a slightly higher stability of spatial preference in V6A.

Fig. 59B shows that depth and direction modulations in V6A present more or less the same incidence in FIX-, REACH-, and FIX-REACH cells. In PEc, as we have described above and shown in Fig. 59A, we observed a similar situation for direction modulation, but a much higher proportion of "REACH" in comparison to "FIX" cells for depth modulation (χ^2, $p< 0.05$). This findings suggest that V6A neurons are engaged in the control of gazing (visual search) and reaches everywhere in the peripersonal space, whereas PEc neurons are more involved in reaches at different depths.

Figure 60 shows the population SDFs of the three main cell categories for V6A (solid/dashed grey curves) superimposed to those of PEc (solid/dashed black curves). In each cell category, the temporal evolution, the onset, and the peak of the activity was very similar between the two areas. The only difference worth mentioning is the stronger tuning during the hand movement in PEc "REACH" and "FIX-REACH" cells, and the weaker modulations during early fixation in PEc "FIX" cells.

4 DISCUSSION

4.1 Monkey medial PPC: visual motion sensitivity

Two functional experiments carried out on two macaque monkeys were used to test the Flow Field sensitivity in macaque area V6. In this thesis, I analyzed data from the first animal used in this experiment.

Since in macaques both areas MT and V6 contain a high percentage of direction selective cells (Zeki, 1974; Maunsell *&* Van Essen, 1983a; Galletti *et al*., 1999), they are reciprocally interconnected (Ungerleider *&* Desimone, 1986a; b; Galletti *et al*., 2001), and both receive directly from layer IVB of primary visual cortex (Shipp *&* Zeki, 1989a; b), one could have expected that monkey area V6 would be driven by the same stimuli activating area MT. However, we found that the Flow-Fields stimulus powerfully activated monkey V6 and not MT; the Radial-Rings stimulus strongly activated monkey MT and not V6, pararelling the results from humans (Pitzalis *et al*., 2010).

Present data strongly highlighted the role of monkey area V6, like in the homologue human area V6, in motion analysis (Galletti *&* Fattori, 2003; Pitzalis *et al*., 2010). Area V6 powerfully responds to the coherent motion of dot fields (Flow-Fields stimulus), in which direction, speed and the coherence of movement changed every 500ms. The Flow Fields stimulus produces a pattern of coherent motion stimulation similar to the continuously changing optic flow generated by the movement in a complex environment (Koenderink, 1986). Moreover, this stimulus is powerful in inducing a compelling perception of self-motion and this could be clued of the function played by area V6 discussed later.

We are aware that results reported here come from two functional sessions of only one animal, but we feel quite confident to judge the Flow-Fields stimulus as a good localizer for area V6. In fact, in both functional sessions V6 is always activated in response to this stimulus. The focus of

activation is selective, bilateral and segregated from the activation of neighboring areas, in contrast to other stimuli (e.g., Radial Ring stimulus) that also strongly activate surrounding areas. When we will have the results from the second animal used in this study, we will test if the selectivity of fMRI activation resulting from Flow-Fields is consistent between animals.The confidence on V6 activation with Flow-Fields stimuli is enhanced by parallel results obtained from 34 subjects in human fMRI work (Pitzalis et al., 2010).

Present results demonstrate the existence of two distinct motion areas in the monkey dorsal stream, area V6 and the classic motion area MT. These two areas are located in separate parts of the brain and both are activated by moving stimuli. However, the complex visual stimulations used in the present work, highlight a possible functional dissociation between the two areas (see Fig. 44). In particular, MT is constantly and bilaterally activated by Radial Rings but not so constantly by Flow Fields and, conversely, area V6 is strongly and consistently activated by Flow Fields but not by Radial Rings. Indeed in only one functional session, we observed an activation of area MT by Flow Fields stimulus, but it seems that this activation involves the dorsalmost part of the superior temporal sulcus and thus more area MST than MT. Moreover, the activation produced by the Radial Rings seems to be less powerful and specific with respect to that produced by Flow Fields stimulus, and involves more occipital and parietal cortical regions. These results suggest that the two motion areas may perform different functional functions, with area MT encoding visual motion but not strongly distinguishing between coherent and incoherent motion. From this point of view, many authors suggested that lateral motion area MT is engaged in the detection of object motion, whereas the medial motion area V6 is engaged in the detection of self-motion (a more detailed description of the functional properties will follow). This idea is in line with human neuroimaging studies that showed no responses in area MT for coherent motion when incoherent motion was subtracted (Brandt *et al*.,

1998) and with studies that conversely showed the activation of the medial occipital cortex by the coherent motion (Sereno *et al*., 2001).

- ✓ *Comparison with human studies*

Since the macaque V6 was originally described as a retinotopically organized area, the research of a human homolog of monkey area V6 was carried out by a retinotopic mapping. The wide-field retinotopic mapping revealed that the retinotopic organization of human area V6 closely resembles the one reported in monkeys (Pitzalis *et al*., 2006). Moreover, the same authors identified the optimal visual stimulus for quickly localizing this area in fMRI studies (Pitzalis *et al*., 2010). Human V6 is sensitive to coherent Flow Fields motion and flickering stimulation. The Flow Fields stimulus is in fact the most effective visual stimulus in driving human V6 in fMRI experiments, both at individual and group levels. Moreover, human V6, together with VIP and MST areas, is able to distinguish among different types of self-movements. All these three areas have a strong response for translational egomotion, whereas the various types of optic flow do not affect both area MT and V3A. Overall, these results confirmed that human V6 is suitable for the analysis of egomotion (Sdoia et al., 2009), as I will discuss later.

The results of monkey fMRI reported in this thesis, seem to be in line with those of human fMRI. Flow Fields stimulus seems to be the more powerful visual stimulus in activating area V6 both in human and macaque monkey. This also confirms the proposed homology between the two brain regions across different species (Pitzalis *et al*., 2006;2010).

- ✓ *Functional role of area V6*

Human clinical studies reported that electrical stimulation of the PPC, avoiding the superior temporal sulcus, produced hallucinations of visual motion in the contralateral field including a “transparent circle” moving to the periphery, and sustained motion of objects toward the periphery or away

from the subject (Richer *et al*., 1991). Lesions in the same region produced motion related disturbances (Blanke *et al*., 2003). Interestingly, epileptic seizures within the precuneus produced linear self-motion perception (Wiest *et al*., 2004). These evidences support the idea that area V6, both in human and in monkey could be specialized in the analysis of motion related to a self-movement.

As described above, V6 neurons share several properties with areas MT and MST. V6 neurons are direction- and speed-selective and respond to large visual stimuli (Galletti *et al*., 1999a). Like area MSTd, V6 receives strong direct input from V1 and these two areas are directly interconnected (Galletti *et al*., 2001). One difference between V6 and MSTd lies on the receptive field's size, with those of area V6 slightly smaller than in MSTd. From this point of view, V6 may be an earlier processing node with respect to both MT and MSTd, sending motion information. Studies using a combined VEPs/fMRI technique supported this idea. Pitzalis and coworkers (Pitzalis *et al*., 2012; 2013) found that area V6 is one of the most early stations coding the motion coherence. The early timing of V6 activation (onset latency 105 ms) together with the small temporal gap with the V1 (peak latency 75 ms) found in humans is supported by the existence of a direct connection between V1 and V6 reported for macaque brain (Galletti *et al*., 2001). The second late peak of activity in V6 observed by the authors was interpreted as a feedback signal arriving from other extrastriate visual areas, likely V3A which in the macaque is connected with V6 (Galletti *et al*., 2001) and is involved in the analysis of motion. This feedback signal could help V6 in recognizing real motion of objects among the plethora of retinal image movements self-evoked by eye and head movements (Galletti *&* Fattori, 2003).

To understand the role of this area it is important to take into consideration the outputs that this area has with areas of the PPC. These multimodal areas coordinate visual, somatosensory, and motor signals for reaching, grasping (area V6A) and protection of head and face (area VIP,

i.e. is rich in cells sensitive to direction of movement particularly if the stimulation is delivered near the head). These data indicate that V6 distributes visual information on form and motion along fast-conducting routes (Galletti *et al*., 2003) usable by other cortical area to control actions. Among the above-mentioned parietal areas, V6A is the only one that contains cells able to encode object attributes relevant for grasping. In addition, V6A largely represents the central part of the visual field, the part of the visual world where our actions take place. So far, visual information must be continuously collected to monitor the interaction between hand and object during the manipulation of objects of our interest.

In conclusion, area V6 is involved in the recognition of both object- and self-motion across the whole visual field (Galletti *&* Fattori, 2003). The fact that area V6 contains real-motion cells lend us to support its involvement in the real object-motion discrimination in the visual field. On the other hand, the activation due to Flow Fields stimulus that resembles the optic flow (present results and human results) and the strong response to translational egomotion (Sdoia *et al*., 2009) support its second role. This area processes visual egomotion signals to extract information about the relative distance of objects, likely in order to act on them. Moreover, V6 sensitivity to optic flow is enhanced when it is combined with binocular disparity, suggesting that this area is specialized for navigating in dense and cluttered environments (Cardin *&* Smith, 2011). The ability of V6 neurons to recognize the real movement in the visual field and to encode the direction of movements of objects could be useful to monitor the continuously changing spatial location of moving objects, providing the spatial coordinates of the moving object to the controllers of arm reaching movements.

Given its proximity and the anatomical connection with parietal areas involved in motor planning and motor control (Galletti *et al*., 2001), area V6 could be involved not in the perception of egomotion *per se* but in the perception of egomotion specifically related to objects and obstacles that are amenable to motor interventions.

- ✓ *Activations in surrounding areas*

Other spots of activation were found in other cortical areas of occipital, temporal and parietal lobes. Here, I will briefly describe the possible role of these areas in the analysis of motion.

Activations in the occipital areas (V1/V2/V3) are visible with both stimuli used in this work. In area V1, neurons respond well to a stimulus moving in a certain direction but not in the opposite one. All these cortical regions respond to an expanding pattern of dots, but this doesn't imply the encoding of egomotion (Wall *&* Smith, 2008).

Activations were found in the prestriate area V3A. This area is highly motion sensitive and contains many real-motion cells (40%) that are able to distinguish between real object motion and motion of the retinal images self-induced by the eye movements (Galletti *et al*., 1990; Arnoldussen *et al*., 2011), similarly to area V6. This area is involved in the processing of 3D visual information about objects in space (Caplovitz *&* Tse, 2007) and in extracting form information from motion (Vanduffel *et al*., 2002). Apart from motion, area V3A responds to both monocular and binocular depth information and has strong projections to LIP, which processes visual 3D object information and object-related hand actions (Nakamura *et al*., 2001). Importantly strong responses to 3D monocular self-motion stimuli were demonstrated supporting its contribution to motion-in-depth information, for example, for approaching and avoiding objects (Arnoldussen *et al*., 2011). Similar properties were found in the human homolog of area V3A. Human imaging studies revealed a strong involvement of V3A in motion processing, comparable to that of human MT and MST (Tootell *et al*., 1997; Orban *et al*., 2003). The work of Fischer (Fischer *et al*., 2012) demonstrated motion responses entirely driven by real, but not retinal, motion in human V3A. This area is connected with parietal area V6 and V6A, areas associated with the visual control of grasping rather than control of pursuit and estimation of self-motion found in MST. The pattern of anatomical connections strongly

indicates that area V3A and V6 achieve a profound multimodal integration of pursuit eye movements with planar visual motion suggesting a crucial role of both areas in our perception of a stable world (Fischer *et al*., 2012).

Another area located in the temporal lobe activated by both Radial Rings and Flow Fields stimuli is area MST, in the superior temporal sulcus dorsally to area MT. As above-mentioned, area MST contains cells strongly responsive to visual stimuli in motion and selective for the direction and speed of movement. This area contains also cells that respond selectively to complex optical flow fields such as expansion, contraction and rotation (Morrone *et al*., 2000) as well as real-motion cell. Area MST is involved in the encoding of heading, in both monkeys and humans. However, recently Wall and coworkers have shown that strong activity can occur in human MST in response to visual stimuli that are inconsistent with egomotion (Wall *&* Smith, 2008). Our results support this hypothesis, in fact, macaque area MST is activated by both Flow Fields and Radial Rings. Many authors suggest that this area is involved in the 3D motion perception of objects or of the observer in the visual field (IIg, 2008; Bisley *&* Pasternak, 2000).

Area FST is located anteriorly to MT in the fundus of the superior temporal sulcus. About one third of FST neurons are sensitive to direction of motion of the stimulus either in the frontal plane, in depth, or in both (Dubner *&* Zeki, 1971). Together with area MST it can constitute the next station, after MT, in a motion-analysis system. Both areas MST and FST receive major inputs from MT (Boussaoud *et al*., 1990), thus supporting this hypothesis. In additions, MST and FST have also connections with area TEO, and FST has connections with V4 and V4t, all of which are associated with the ventral stream. Thus, it is likely that MST and FST provide information about motion that is useful for object recognition (Boussaoud *et al*., 1990; Sereno *et al*., 2002; Gattass *et al*., 2005).

4.2 Sensory properties

In the present study we characterized visual, somatosensory and bimodal cells in both areas PEc and V6Ad, taking advantage of newly recorded cells in the most anterior part of area PEc with respect to previous studies (Breveglieri *et al*., 2006; 2008). In fact, the present study is based on a large amount of data (seventeen hemispheres from nine animals) collected in the same laboratory in the last 16 years. Moreover, the reconstruction of recording sites, the cytoarchitectural criteria, and the functional classification of neurons were all done in a consistent manner, thus increasing the reliability of the results obtained.

Present results show that visual cells are more common in area V6Ad (55%) than in PEc (40%), whereas the opposite happened for somatosensory cells which are more common in area PEc (68% vs. 42%). This is in line with the functional trend within the SPL regarding visual and somatosensory properties discussed in the Introduction (Battaglia-Mayer *et al*., 2006). Moving anteriorly from V6 to PE, visual sensitivity progressively decreases and *viceversa* somatosensory sensitivity progressively increases. Present data are in line with this trend.

Neurons in both areas are easily activated by simple visual stimuli, such as light/dark bars or spots, preferring more complex visual stimulation for being activated. This visual complexity both in area PEc and V6Ad could be explained with the pattern of cortical connections, which shows that both areas are more strongly connected with other parietal areas as well as with the dorsal premotor cortex with respect to extrastriate visual areas (Gamberini *et al*., 2009; Bakola *et al*., 2010; Passarelli *et al*., 2011). The functional results and the anatomical connections reflect the higher hierarchical role played by PEc and V6Ad in the elaboration of visual information. Recent studies (Battaglia-Mayer *et al*., 2001; Squatrito *et al*., 2001) have reported the presence of visual cells in area PEc in percentages (65% and 45%, respectively) not dissimilar from the one we reported in the

present work. Results are remarkably similar if we take into account the different stimuli used (light bars in previous studies vs. light/dark stimuli here), the different extents of visual field tested (central part <30° vs. central and periphery up to 80° here), and the location and extent of the recording sites (the medial most part in previous studies vs. the full extent here). Also in agreement with previous data is the absence of a retinotopic map. The percentage of visual neurons in area V6Ad is also in good agreement to what previously reported (Gamberini *et al*., 2011).

Somatosensory cells represent the 68% of our PEc population and only the 42% of V6Ad cell. The present study, in good agreement to previous data (Breveglieri *et al*., 2006; 2008), finds a predominance of joint modulations (>70%, Table 4) in both areas. Although more represented than in V6Ad, PEc somatic cells are less representative of the distal parts of the arm. In fact, no receptive fields were found in the back or palm of the hand in area PEc with respect to area V6Ad (see Fig. 53). This data together with other evidences, suggest that PEc is less involved than V6A in the control of grasping movements (the functional role of area PEc is discussed later). Conversely, only the upper limbs are represented in V6Ad leading us to strongly support the idea that area V6A is involved in the control of visually guided actions (Fattori *et al*., 2004; 2005; 2009).

We found a polymodal convergence of visual and somatosensory signals in 23% of PEc cells and 16% of V6Ad cells. The difference in the percentages with respect to what previously found in our laboratory in previous works (Breveglieri *et al*., 2008; Gamberini *et al*., 2011) could be due to the different population of neurons considered.

- ✓ *Comparison with other parietal areas*

A visual and somatosensory organization was described in other parietal areas. Although the comparison with other areas of the PPC is sometimes difficult due to differences in the tasks used, terminology or because information is still missing (as in case of area PGm), I will briefly compare

the results presented here with what found in other parietal areas, moving from the anterior to the posterior border of the parietal lobe.

Area 3a: Area 3a is located immediately rostral to area 3b and contains a topographically organized representation of deep receptors and musculature of the contralateral body (Krubitzer *&* Disbrow, 2008). Studies in awake monkeys reported that neurons in area 3a modulate activity prior to wrist flexion and extension (Nelson, 1987) and are modulated by joint movements (Gardner, 1988). Taken together, data from several studies indicate that area 3a integrates somatic and vestibular inputs with the motor system to control the kinetics of movement, to maintain posture and limb position and to regulate the velocity of limb movement (Krubitzer *&* Disbrow, 2008).

Area 3b: The topographic organization this area, located posteriorly to the central sulcus, has been described in a variety of primates of the Old and New World. Area 3b forms a systematic representation of the contralateral body surface with the tail, genitals and feet represented most medially, followed by the representations of the hindlimb, trunk, forelimb, hand, face and oral structures in a mediolateral progression (Krubitzer *&* Disbrow, 2008). Neurons in this area have small receptive fields compared to other anterior and posterior parietal fields and respond to high frequency stimulations, pressure and flutter (Krubitzer *&* Disbrow, 2008). Functional studies on single 3b cells support the idea that this area is involved in texture and form discrimination, topographic tactile learning, and in generating coordinate tongue and facial movements (Krubitzer *&* Disbrow, 2008).

Areas 1 and 2: The somatosensory cortical field just caudal to area 3b, termed area 1, has been described both in macaque monkeys and in humans. In macaques, this area forms a mirror reversal representation of area 3b and contains, contrary to the more posterior parietal areas, a precise and topographically organized representation of the contralateral body surface (Krubitzer *&* Disbrow, 2008). As in area 3b, there is a

magnification of the hand and oral structures, and receptive fields are small and limited to single digits.

The functional organization of area 2, located between area 1 and area PE, has been investigated only in macaque monkeys (Pons et al., 1985; Toda & Taoka, 2001; 2002). The neurons of this area contain a complete representation of the contralateral body although the somatic organization is not as precise as in the most anterior areas. Differently from areas 3b and 1, but much alike to the most posterior areas, in area 2 the representation of the hand and forelimb is highly magnified (Krubitzer *&* Disbrow, 2008). Neurons in this area respond to deep and cutaneous stimulation as well as to passive and active flexion of joints as reported also in area PEc and V6A. The receptive fields are relatively large and sometimes bilateral when compared to areas 3b and 1. These data indicate that area 2 is involved in the discrimination of shape and in the online maintenance of hand and forelimb movement necessary for reaching and grasping (Krubitzer *&* Disbrow, 2008).

Area 5 (PE): Area 5 was first described as a very large field occupying the entire rostral bank of the IPs and much of the caudal post-central gyrus (Brodmann, 1909).

Several recent studies indicate that area 5 is smaller and resides in the middle and rostral bank of the IPs and folds around the sulcal crown to spread onto the adjacent gyrus (Iwamura, 2000). This area is dominated by the representation of the hand and forelimb. Neurons have contralateral, ipsilateral and bilateral receptive fields are respond to joint and tactile stimulations, similarly to what found in area PEc (Iwamura, 2000). Studies in awake macaque monkeys indicate that area 5 is involved in programming and coordinating a reach and grasp movement (Debowy *et al*., 2001) and in generating a body-centered reference frame (Wise *et al*., 1997). Recently Seelke and coworkers identified a lateral area on the rostral IPs named area 5L distinct from more medial portions of the IPs (Seelke *et al*., 2012). This area 5L contains neurons with receptive fields mostly on the shoulder,

forelimb and digitis, with no apparent representation of other body parts. Moreover, receptive fileds often contain multiple joints of the forelimb or multiple digits, resulting in imprecise and fractured topographical organization.

Areas PG/PFG/PF: These areas of the inferior parietal lobe show a similar functional trend reported here for PEc and V6Ad (Rozzi *et al*., 2008). The posterior area PG, located more closely to the occipital pole, shows the highest percentage of visual cells, whereas the rostralmost area PF, that borders with the somatic area 2, shows the highest number of somatic cells, with area PFG showing intermediate trend. Under this point of view, we can suppose that areas V6Av/V6Ad/PEc could reflect the same trend of areas PG/PFG/PF. In fact, area V6Av, not analyzed here, shows the highest percentage of visual cells with respect to both V6Ad and PEc (Gamberini *et al*., 2011), and could be seen as the area PG of the superior parietal lobule. Areas V6Ad containing both visual and somatosensory cells could be the equivalent of PFG and PEc with the somatic preponderance the PF area of the SPL.

Area MIP: This area located on the medial bank of the intraparietal sulcus (Colby *et al*., 1988), borders V6A laterally and anteriorly. Colby and Duhamel (Colby *&* Duhamel, 1991) reported a large proportion of arm reaching cells in its dorsal part (although an extensive study of passive somatosensory properties is lacking), which gradually gave way to an increasing number of visual cells moving ventrally. Here again data of the anatomical connections could reflect the similarities in the dichotomy observed between PEc and V6Ad. The dorsal part of MIP (named also dMIP) is strongly connected with the somatically dominated area PEc (Bakola *et al*., 2010) whereas the ventral part of MIP is connected with the extrastriate visual area V6 which is directly connected with V6A (Galletti *et al*., 2001; Passarelli *et al*., 2011).

Area PGm: Area PGm (named also 7m) borders area PEc ventrally on the mesial surface of the hemisphere (Pandya *&* Seltzer, 1982). The role of

PGm in elaborating somatosensory information was inferred from the anatomical connections of this area (Cavada, 2001).

Area PEci: This area, also known as the supplementary sensory area, is located on the mesial surface around the cingulate sulcus. It contains cells sensitive to passive somatosensory stimulations (Murray *&* Coulter, 1981) and shows a complete representation of the body similarly to what found here in area PEc. Moreover, area PEci shows a quite clear somatotopic organization not present in PEc.

After this briefly overview, we demonstrate that the maps in area PEc and V6Ad, such as the anterior area 5/PE, are not topographic but fractured and complex compared to the simple maps of the body in the early stages of the somatosensory processing in the anterior somatosensory fields (3b, 1 and 2).

The magnification of upper limb representation found here in both areas PEc and V6Ad was described also in area 5 of cebus and macaque monkeys (Padberg *et al*., 2007). This phenomenon is not surprising given the increases of the amount of parietal cortex devoted to visually manual behaviors in humans and non-human primates (Rosa *&* Tweedale, 2005; Krubitzer *&* Disbrow, 2008). Other examples of this phenomenon are the expansion of auditory cortex linked to echolocation in dolphins (Marino *et al*., 2007) and the emergence of motor areas associated with the elaboration of the tongue and lips in humans (Krubitzer *&* Kahn, 2003).

- ✓ *Functional Role of area PEc*

The coexistence of visual and somatosensory neurons observed in area PEc and the presence of bimodal visual/somatic cells as well, supportes the role of this area in controlling body movements and posture. As the somatosensory activity is mainly referred to the limbs both the upper and the lower ones, we suggest that this area is involved in a complete control of lower and upper limb movements. The integration between visual and somatosensory signals appears useful to coordinate motor activity during

locomotion in a complex visual environment, which requires a continuous interaction between body parts and objects in the visual word. The particular sensitivity of the visual cells to complex stimuli continuously changing in size and speed (Breveglieri *et al*., 2008), and the presence of cells sensitive to joint rotations and tactile stimulations and of reach-related cells in 2D and 3D space (Battaglia-Mayer *et al*., 2001; Ferraina *et al*., 2001; Breveglieri *et al*., 2006; 2008), fully agree with this view.

During locomotion, the brain has to relate body movements with the flow of visual information coming from the entire visual environment. The analysis of visual scene during locomotion is deeply different from that required during the visual manipulation of objects in which we need specific information about features and spatial location of that object. In locomotion, the global interaction between body and visual environment is the crucial cue. Thus, the nontopographic organization of visual information, the presence of somatosensory signals from the entire body (upper and lower limbs), the coexistence of visual and somatic input upon single cells and the anatomical pattern of connections observed in PEc seem to strongly support the suggested functional role of this area. In particular the projection from the parietal area 2, a field present only on those primates with a skillful use of their hands (Padberg *et al*., 2007), is consistent with the use of limbs in macaque in grasping and manipulating objects with both hands and feet.

Another support for the role suggested for PEc is provided by a study on a patient reporting topographical disorientation and abnormalities of body movement after damage of the posterior part of the SPL, region likely containing the homolog of monkey area PEc (Kase *et al*., 1977). Kase's patient M.V.V in the short period showed oculomotor disorders and visuo-motor incordination. Surprisingly, when she started walking 3 weeks later a completely different set of abnormalities became apparent. She was not particularly impaired in reaching and grasping objects under visual guidance, but when she walked her behavior was like a blind person. She had a severe spatial disorientation impairing the whole-body interaction with

both the familiar and unfamiliar surroundings. She was not able to find her bed, to lie on it in the appropriate orientation, or to modify her body posture in order to sit on a chair (which she immediately recognized as such). These spatial abnormalities were still present 2 months and a half after. The post-mortem investigation showed that the infarcted area implicated the parieto-occipital fissure, both on the medial and lateral aspects of the hemispheres, leaving the occipital lobes completely intact. The anterior margin of the infarct involved the precuneus and the posterior one-third of the gyrus cingulus. These spatial abnormalities described by Kase and coworkers due to a lesion in a region likely homolog to monkey area PEc, seem to support the role of PEc in controlling locomotion and whole-body interaction with the visual world.

More recent studies of human brain imaging reported activations in the parietal regions likely including human homologues of area PEc in experiments where the subjects had to use vision in order to judge self-motion, to control postural balance and to guide vehicles (de Jong *et al*., 1994; Brandt *et al*., 1998; Kleinschmidt *et al*., 2002). More investigations are necessary to verify whether this brain region could be considered as the human homolog of area PEc.

4.3 Motor Related Activity in 3D Space within SPL

The main purposes of the analysis of reach-related discharges were: 1) to investigate the spatial tuning of reaches in depth in PEc, an issue never addressed before, and 2) to compare the processing of distance and direction in PEc with that of the nearby area V6A during the same reaching task in 3D space.

In PEc, the modulations of neural activity by depth and direction had on average a similar incidence across the task. Nevertheless, the effect of each spatial parameter varied in the different epochs. Directional tuning prevailed early in the task, i.e. when the target was initially fixated. Depth tuning became much stronger during and after movement execution. Convergence of direction and depth information on single neurons was not frequently observed in the early stages, but it gradually increased and became prominent during the holding phase. PEc neurons with depth modulations showed a slight preference for far peripersonal space. The cells with direction tuning preferred the contralateral space, especially during early fixation and pre-movement period. Many individual PEc cells showed tuning of the hand movement-related activity, or of both the eye position- and hand movement-related activity, while neurons carrying only eye position signals -especially in depth- were a minority.

The comparison between PEc and V6A revealed both common and distinct properties. During the early phases of the task, a significantly smaller number of neurons coding exclusively depth information, or combining depth and direction information were found in PEc compared to V6A. As the task progressed towards movement execution, the two areas showed a more similar pattern of spatial encoding, with depth information becoming much more influential than direction, and with increased convergence of depth and direction signals on single cells. The differences in the processing of spatial information early in the task might reflect a functional organization in SPL, with PEc and V6A involved in more local and

global, respectively, visuospatial processing. Area PEc has been studied in the past using center-out reaching tasks (Battaglia-Mayer *et al*., 2001; Ferraina *et al*.,2001) that reported numerous directional modulations of the arm movement-related activity and less frequent modulations of the gaze-related activity. Differently with respect to the above studies, here the directional tuning of gaze- and hand movement-related activity had a similar frequency, thus resulting in three comparable subpopulations of neurons called “FIX”, “REACH” and “FIX-REACH” cells (Fig.59A, bottom). The discrepancy between ours and previous results could be attributed to the smaller number of directions tested in our task compared to the center-out tasks.

- ✓ *Role of PEc in arm movements in 3D space*

In the present study, we compared the effects of direction and depth information on PEc neuronal activity and found the former to be predominant in the early task epochs. The stronger effect of direction versus depth well before the onset of arm movement is reminiscent of findings in the dorsal premotor cortex (PMd) (Fu *et al.*, 1993; Fu *et al.*, 1995; Messier *&* Kalaska, 2000). Similar to PEc, the encoding of direction in PMd appeared early, i.e. during the target cue or movement planning period, whereas movement distance exerted its effect mostly during movement execution. Given the well-established anatomical connection between PEc and PMd (Johnson *et al*., 1996; Matelli *et al*., 1998; Marconi *et al*., 2001; Bakola *et al*., 2010), signals about the target direction could be transmitted directly, i.e. without interacting with vergence signals, to PMd in order to first specify the movement direction that is more pivotal in the initial stages of movement planning and execution (Fu *et al.*, 1995; Messier *&* Kalaska, 2000).

Another similarity between PEc and PMd is the temporal evolution of the convergence of direction and depth signals. As it was reported for PMd (Fu *et al.*, 1993; Fu *et al.*, 1995; Messier *&* Kalaska, 2000), we found here that the convergence of direction and depth signals in the activity of

individual PEc neurons increased as the task progressed. This convergence on single neurons is in contrast with the view that the depth and direction of reaching targets are processed by separate visuomotor channels (Flanders *et al*., 1992), a view supported by many behavioral studies (Soechting *&* Flanders, 1989; Flanders *&* Soechting, 1990; Gordon *et al*., 1994; Sainburg *et al*., 2003; Vindras *et al*., 2005; Bagesteiro *et al*., 2006; Van Pelt *&* Medendorp, 2008). However, we have also observed in PEc a different temporal course of depth and direction processing, and large numbers of cells coding only for one spatial parameter, even in the late stages of the task (e.g. depth-only cells in MOV). These findings suggest that there is both temporal and spatial segregation in the processing of depth and direction information, that is implemented on overlapping populations of PEc cells. The difference in the degree of convergence of depth and direction information between the early and late task phases might be related to the different representations of movement (Flanders *et al*., 1992; Crawford *et al.*, 2011). Before the onset of movement, depth and direction are defined in extrinsic reference frames, so they are more likely to be independent. However, during and after the movement, depth and direction are transformed into the intrinsic coordinates of the elbow and shoulder joint angles and become more tightly coupled. Consistent with this context, the maximum degree of convergence in PEc was observed during the holding the target epoch (Fig.56A), i.e. when the arm was kept still at various locations in 3D space.

- ✓ *Comparison of PEc with V6A and other PPC areas*

Vergence angle information has strong influence on the activity of many neurons in the medial posterior parietal areas V6A (Breveglieri *et al*., 2012) and parietal reach region PRR (Bhattacharyya *et al*., 2009). Present results show a weaker depth tuning in PEc during fixation. This is a new finding since no studies have investigated vergence signals in this area to date. In area PE, vergence angle has an even weaker effect (Ferraina *et al*., 2009).

Taken together, these findings hint at the existence of a rostral to caudal gradient of increased vergence sensitivity in medial PPC.

During the initial target fixation and planning periods, significantly less PEc than V6A neurons showed convergence of depth and direction information. This implies that PEc is not much involved in encoding the 3D location of the reaching target in space. This finding adds to other evidence suggesting that caudal SPL areas, like V6A and PRR, encode the goal of the reaching movement, whereas more rostral areas like PE are more related to the implementation of the movement plan (Cui *&* Andersen, 2011; Li *&* Cui, 2013; Breveglieri *et al*., 2014). Overall, the differences in spatial processing between PEc and V6A, combined with the similarities between PEc and PMd mentioned in the previous section, place PEc closer to the premotor circuit compared to V6A.

During pre-movement, movement execution and holding periods, PEc and V6A demonstrated a similar profile of depth and direction processing. In the movement period, a significantly larger -compared to V6A- proportion of PEc neurons tuned in depth was recruited. This difference might be related to the fact that PEc contains much more cells modulated by somatosensory inputs (present results) and receives much more somatosensory input compared to V6A (Breveglieri *et al*., 2002; Bakola *et al*., 2010).

A conceptual framework for the processing of depth and direction signals in SPL reaching areas proposed by our group well explained the dichotomy in the processing of target depth and direction based on visual and proprioceptive information (Hadjidimitrakis *et al*., 2014). This framework, shown in Figure 61, is based on behavioral and computational evidence. Visual signals and eye position information interact with somatosensory signals related to arm position at intermediate levels of this network, to generate the motor output. The first source of visual and eye position signals is represented by the striate and extrastriate cortex. This information is then sent to PPC areas MIP, V6A and PEc through area V6

(Galletti *et al*., 2001; Gamberini *et al*., 2009; Passarelli *et al*., 2011). These areas send the 3D spatial information about target location to the dorsal premotor cortex (PMd), and then from PMd this information is transmitted to the primary motor cortex (M1) (Gamberini *et al*., 2009). The other major contribution to this circuit regards the proprioceptive information about the hand position. This input arises from the anterior areas of the parietal lobe and enters the circuit mainly at the level of area PE. Importantly, in the primary somatosensory area (SI), neurons are more sensitive to movement amplitude than to direction of movement (Tillery *et al*., 1996) and the same happens in area PE, in which neurons modulated by distance are twice as much as those modulated by direction and elevation (Lacquaniti *et al*., 1995). Furthermore, PE is strongly and reciprocally connected with M1 (Johnson *et al.*, 1996; Bakola *et al*., 2013). The proprioceptive signals are sent to MIP, V6A and PEc, where they can be combined with visual- and vergence-related signals in order to establish a jointly processing of information on direction and depth. On the contrary area PE does not receive visual input (Johnson *et al.*, 1996; Bakola *et al*., 2013), and vergence angle influences the reaching activity only in a small fraction of cells (Ferraina *et al*., 2009). This could explain why in PE depth and direction signals are represented by distinct subsets of neurons (Lacquaniti *et al*., 1995).

As above mentioned, area PMd encodes both the movement distance and direction (Messier *&* Kalaska, 2000) but in different times during the task. Directional information are specified during target cue or movement planning period, whereas movement distance effects mostly movement execution. This difference in time could be advantageous in the online control of arm movement, when parietal and frontal regions must interact more closely (Wise *et al*., 1997), and highlights the importance of a feedback mechanisms in the encoding of reach direction and depth. Moving toward targets in depth is more demanding computationally and requires a better control (Danckert *et al*., 2009). As described in the Introduction,

several studies showed that the variability of endpoints in arm movements in 3D space is larger along the depth axis where visual uncertainty is higher (Gordon *et al*., 1994). A way to better control arm movement in depth could be to recruit neurons receiving inputs other than visual (proprioceptive, efference copy). Under this view, areas of the SPL, containing these signals, are presumably well suited in controlling movement, especially in depth as supported by patients with lesions in this region showing stronger deficit in depth than in direction during arm movements (Baylis *&* Baylis, 2001; Danckert *et al*., 2009). The framework proposed is consistent also with the evidence that when vision is available, humans compare the target to both visual and proprioceptive sensation of hand position and optimally integrate these signals depending on the stage of the movement planning (Sober *&* Sabes, 2005; Crawford *et al*., 2011). This framework supports the idea that movement in depth relies on proprioceptive information, whereas vision is more important for the specification of reach direction (van Beers *et al*., 1998; 2002; 2004; Monaco *et al*., 2010).

Based on the above evidence, we suggested that the relative proportion of visual versus proprioceptive inputs of a given SPL area could be critical for its contribution to the specification of the reach direction and depth. PEc primarily processes somatosensory information about the movement and static posture of the hand (Ferraina *et al*., 2001; Breveglieri *et al*., 2006; Bakola *et al*., 2010) and in the SPL circuitry, it occupies a position closer to PE than to V6A. As visual sensitivity increases towards area V6A, and somatosensory sensitivity increases in the opposite direction, towards area PE, PEc was expected to show a pattern of increased depth modulations during the hand movement and static posture. Our findings are consistent with this framework and provide further neurophysiological support to the link between proprioception and movement in depth that has been suggested by other lines of evidence.

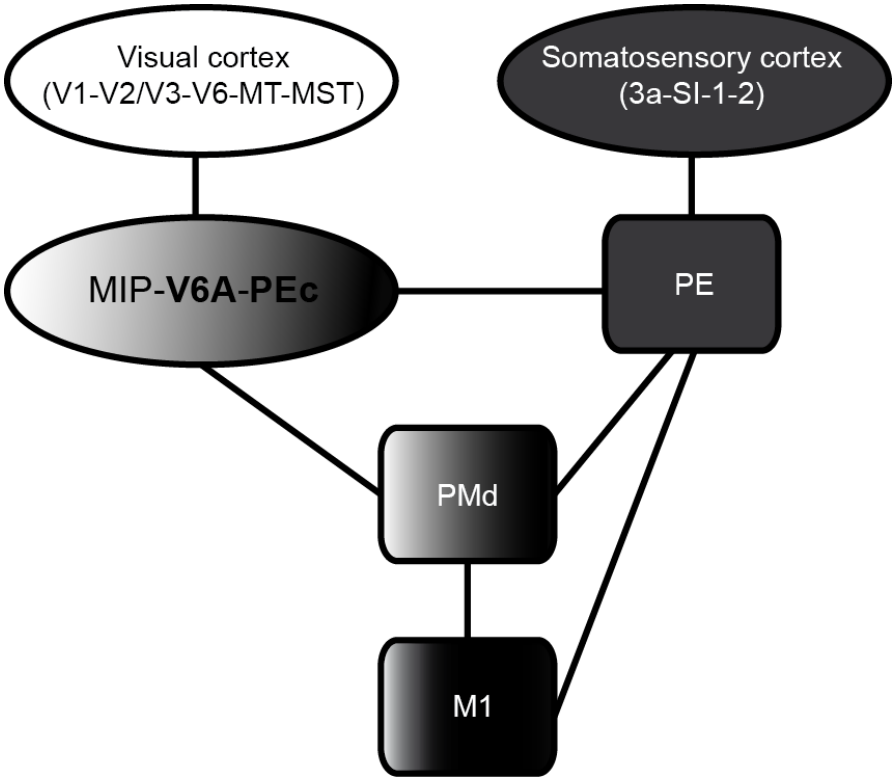

Figure 61: Depth and direction coding in the cortical reach-related areas.

Areas are depicted in different grayscale gradients according to the relative proportion of visual (white) and somatosensory (black) information they receive. Areas receiving predominantly visual input tend to process jointly target depth and direction information, whereas those that receive mainly somatosensory input are more likely to represent spatial parameters separately and show greater sensitivity for depth encoding. *Adapted from (Hadjidimitrakis et al., 2014)*.

- ✓ *Are PEc and V6A the same functional area?*

Area PEc contains both visual and somatosensory cells. As reported here the same happened in area V6Ad with which PEc shares borders in its caudal part. In addition, both areas show reach-related discharges sensitive to depth and direction of reaching. Thus, the question migh arise of wheter

PEc is an indipendednt area or is part or a subfiled of the nearby area V6A. The main arguments in favor of PEc as an independent area centered on its distinctive architecture (Luppino *et al*., 2005) and a different set of anatomical connections (Gamberini *et al*., 2009; Bakola *et al.,* 2010). Moreover, present functional data stressed the functional differences between the two. First of all area PEc contains a lower number of visual cells with respect to V6Ad, and the minority of PEc cells shows responses to simple visual stimuli in comparison with V6Ad (see Fig. 45). Visual receptive fields are on average larger than those of V6Ad for the same given eccentricity (see Fig. 47B). The incidence of somatosensory cells in PEc (68%) is higher than that in V6Ad (42%) and PEc somatosensory receptive fields are located both on the upper and lower limbs, whereas in area V6Ad they are located exclusively on the upper limbs, both in the proximal and distal parts of the arms.

Taking into account the motor-related properties in 3D space, PEc and V6A share some important characteristics, but some differences are clearly visible. Firstly the number of neurons modulated, less in PEc with respect to V6A, secondly the temporal pattern of modulation for depth and direction present in PEc. In fact, in area PEc, the effect of direction is prevalent before the reaching execution, whereas depth modulations become prominent as soon as the arm movement started. In area V6A, on the contrary, the joint encoding of direction and depth is evident during all phases of the task. These observations support the putative role of both areas in the control of arm reaching movements in the three-dimensional space highlighting, however, a possible temporal/spatial segregation within the fronto-parietal network.

In summary all the evidences argues against PEc and V6Ad being part or subfileds of a same cortical area. We believe that PEc and the adjoining areas in the caudal part of the superior parietal lobule are different cortical areas differently involved in the transformation necessary to guided action such as manipulate objects or moving on the external environment.

✓ *Clarifications*

The abundance of projection neurons in zones that represent the lower limbs contrast with the reported overrepresentation of the upper limbs in PEc (Breveglieri *et al*., 2006; 2008) as well as in its involvement in manual tasks. Such a contrast could be due to a methodological bias. Experiments are usually conducted in animals trained to sit quietly in the primate chair, and it may be the case that types of tasks to reveal a role in control of legs have not been tested so far. It could also be due to a more limited neuronal sampling used in the past (Breveglieri *et al*., 2006), data reported here agree with this point. Data analyzed here were collected from the more anterior part of PEc, where lower limbs are more represented, and reveal the presence of the representation of the legs more consistent with respect to previous work (Breveglieri *et al*., 2006). In line with this view, data of the anatomical connection demonstrated that after injections in PEc, the areal distribution of labeled cells is not uniform, with the anterior part of PEc being more strongly targeted by somatosensory and motor areas than the caudal part (Bakola *et al*., 2010). This is consistent also with the asymmetrical connections of area 2, with foot representation displaying wider connections with the motor regions than arm representation (Pons *&* Kaas, 1986).

About the motor related activity tested in the present work we have to clarify that we did not test which frame of reference was used (i.e. eyes- or body-centered). Reaches were performed towards foveated targets and this choice was done for different reasons. Firstly, foveal reaching is a common behavior in natural environments in primates (Land *&* Hayhoe, 2001), and secondly, the issue of reference frame was not the scope of our study.

We have to report also that in the experimental setup used, the depth range explored was larger than the range of directions. Although the 30° range of visual angles is much smaller than the entire direction range (180°) we believe that it comprises most of the central visual field where naturally eyes and hands interact with objects in everyday life.

Overall, despite the limitations listed above, we are quite sure to support the above-mentioned functional role of the areas objects of this thesis.

Taking into account the data presented here, we could suggest that the caudal pole of the superior parietal lobe, taken as a whole, contains the neuronal machinery to help in controlling body movements. For macaques, interactions between these fields would probably be very important during locomotion though complex environments, where coordination between arm and legs is essential.

5 FUTURE DIRECTIONS

The present work highlights the important role played by the posterior parietal cortex in integrating information coming from different sources (vision, somatosensory and motor) to control and coordinate movements in complex environments.

Signals recorded from areas beyond the motor cortex, such as areas of the posterior parietal cortex, will be the new frontiers in brain machine interface. Brain machine interface is a system that can interface brain with computers or other electronics, like prosthetics, and can be used to assist paralyzed patients and subjects with neurological deficits. A brain machine interface may record brain activity from a population of neurons, decodes the subject's intent and then uses this processed intention signal to control external devices, such as computers or robotic limbs. The source of control signals to areas outside the motor cortex, such as the areas of the posterior parietal lobule, that carry out not only the intention to make movements but also somatosensory signals in a higher cognitive level, could allow a more intuitive and versatile control (Andersen *et al*., 2014b). Recent advances and successes in neurophysiology will support, hopefully, the research and the clinical testing of this brain machine interface in order to become a device to enhance the quality of life of the affected clinical population. This will be not only of help for patients, but will give a boost to the knowledge of the human brain.

6 ACKNOWLEDGEMENTS

I would like to express my heartfelt thanks to those who directly or indirectly contributed to the realization of this work.

First, I am deeply grateful to my supervisor Professor Patrizia Fattori who gave me the opportunity to work in her laboratory. I grew personally and professionally thanks to her support, her encouragement and her teaching.

I want to express my deep gratitude to Professor Claudio Galletti for the unique opportunity to work with him and learn from him. Thanks to both for your trust in me.

Thanks to all the people of the laboratory, Rossella, Michela, Annalisa, Lauretta, Konstantinos, Sophia and Valentina.

Thanks to all the students for the help during experiments and data analysis, Paola, Francesca, Stella, Nunzia, Valentina, Emilia, Gloria, Federica, Andrea, Domenico, Beatrice, Benedetta, Marina, Silvia.

I would like to thank the researchers of the INSERM Unit 1028 of the University Claude Bernard of Lyon. I express my special thanks to Alessandro Farné, Martine Meunier and Fadila Hadj-Bouziane for the opportunity to work with them and learn incredible things.

Thanks to Carole and Aurélie for the time spent in the laboratory.

Thanks to Mattia, the happiness of my life.

I dedicate this work to my dad, Franco, without you this would not have been possible. Thank to be on my side.

7 REFERENCES

Acuna C., Cudeiro J., Gonzalez F., Alonso JM., Perez R., (1990) Lateral-posterior and pulvinar reaching cells: comparison with parietal area 5a: a study in behaving Macaca nemestrina monkeys. *Exp Brain Res, 82:158-166*.

Allman J., Miezin F., McGuinness E., (1985) Direction- and velocity-specific responses from beyond the classical receptive field in the middle temporal visual area (MT). *Perception, 14:105-26.*

Andersen RA., (2011) Inferior parietal lobule function in spatial perception and visuomotor integration. *Comprehensive Physiology, handbook of Physiology, The Nervous System, higher functions of the Brain, doi:10.1002/cphy.cp010512*.

Andersen RA., Andersen KN., Hwang EJ., Hauschild M., (2014a) Optic ataxia: from Balint's syndrome to the parietal reach region. *Neuron, 81:967-983*.

Andersen RA., Kellis S., Klaes C., Aflalo T., (2014b) Toward more versatile and intuitive cortical brain-machine interfaces. *Curr Biol, 24:885-897*.

Arnoldussen DM., Goossens J., Van Den Berg AV., (2011) Adjacent visual representations of self-motion in different reference frames. *PNAS, 108:11668-11673*.

Archambault PS., Ferrari-Toniolo S., Caminiti R., Battaglia-Mayer A., (2014) Visually-guided correction of hand reaching movements: The neurophysiological bases in the cerebral cortex. *Vision Res, doi:10.1016/j.visres.2014.09.009*.

Bagesteiro L., Sarlegna F., Sainburg R., (2006) Differential influence of vision and proprioception on control of movement distance. *Exp Brain Res, 171: 358-370*.

Baker CL., Hess RF., Zihl J., (1991) Residual motion perception in a "motion-blind" patient, assessed with limited-lifetime random dot stimuli. *J Neurosci, 11:454-461*.

Bakola S., Gamberini M., Passarelli P., Fattori P., Galletti C., (2010) Cortical connections of parietal field PEc in the macaque: linking vision and somatic sensation for the control of limb action. *Cereb Cortex, 20: 2592-2604*.

Bakola S., Passarelli L., Gamberini M., Fattori P., Galletti C., (2013) Cortical connectivity suggests a role in limb coordination for macaque area PE of the superior parietal cortex. *J Neurosci, 33:6648-6658*.

Barlow HB., Blakemore C., Pettigrew JD., (1967) The neural mechanism of binocular depth discrimination. *J Physiol, 193:327-342*.

Battaglia-Mayer A., Ferraina S., Mitsuda T., Marconi B., Genovesio A., Onorati P., Lacquaniti F., Caminiti R., (2000) Early coding of reaching in the parietooccipital cortex. *J Neurophysiol, 83:2374-2391*.

Battaglia-Mayer A., Ferraina S., Genovesio A., Marconi B., Squatrito S., Molinari M., Lacquaniti F., Caminiti R., (2001) Eye-hand coordination during reaching. II. An analysis of the relationships between visuomanual signals in parietal cortex and parieto-frontal association projections. *Cereb Cortex, 11:528-544*.

Battaglia-Mayer A., Mascaro M., Brunamonti E., Caminiti R., (2005) The over-representation of contralateral space in parietal cortex: a positive image of directional motor components of neglect? *Cereb Cortex, 15:514-25*.

Battaglia-Mayer A., Archambault PS., Caminiti R., (2006) The cortical network for eye-hand coordination and its relevance to understanding motor disorders of parietal patients. *Neuropsychologia, 44:2607-2620*.

Battaglia-Mayer A., Ferrari-Toniolo S., Visco-Comandini F., Archambault PS., Saberi-Moghadam S., Caminiti R., (2013) Impairment of online control of hand and eye movements in a monkey model of optic ataxia. *Cereb Cortex, 23:2644-2656*.

Battaglini PP., Muzur A., Galletti C., Skrap M., Brovelli A., Fattori P., (2002) Effects of lesions to area V6A in monkeys. *Exp Brain Res, 144:419-422*.

Baylis GC., Baylis LL., (2001) Visually misguided reaching in Balint's syndrome. *Neuropsychologia, 39:865-875*.

Bhat RB., Sanes JN., (1998) Cognitive channels computing action distance and direction. *J Neurosci, 18:7566-7580*.

Bhattacharyya R., Musallam S., Andersen RA., (2009) Parietal Reach Region encodes reach depth using retinal disparity and vergence angle signals. *J Neurophysiol, 102:805-816*.

Bisiach E., Luzzatti C., (1978) Unilateral neglect of representational space, *Cortex, 14:129-133*.

Bisley JW., Pasternak T., (2000) The multiple roles of visual cortical areas MT/MST in remembering the direction of visual motion. *Cereb Cortex, 10:1053-1065*.

Blangero A., Ota H., Delporte L., Revol P., Vindras P., Rode G., Boisson D., Vighetto A., Rossetti Y., Pisella L., (2007) Optic ataxia is not only 'optic': impaired spatial integration of proprioceptive information. *Neuroimage, 36:Suppl 2:T61-68*.

Blanke O., Landis T., Mermoud C., Spinelli L., Safran AB., (2003) Direction-selective motion blindness after unilateral posterior brain damage. *Eur J Neurosci, 18:709-722*.

Blatt GJ., Andersen RA., Stoner GR., (1990) Visual receptive field organization and cortico-cortical connections of the lateral intraparietal area (area LIP) in the macaque. *J Comp Neurol, 299:421-445*.

Bloom FE., Lazerson A., Hofstadter L., (1988) Brain, mind, and behavior. *Freeman New York, 1988. ISBN 0716718634*.

Born RT., Bradley DC., (2005) Structure and function of visual area MT. *Annu Rev Neurosci, 28:157-189*.

Boussaoud D., Ungerleider LG., Desimone R., (1990) Pathways for motion analysis: cortical connections of the medial superior temporal and fundus of the superior temporal visual areas in the macaque. *J Comp Neurol, 296:462-495*.

Brandt T., Bartenstein P., Janek A., Dieterich M., (1998) Reciprocal inhibitory visual-vestibular interaction. Visual motion stimulation deactivates the parieto-insular vestibular cortex. *Brain, 121:1749-1758*.

Breveglieri R., Kutz DF., Fattori P., Gamberini M., Galletti C., (2002) Somatosensory cells in the parieto-occipital area V6A of the macaque. *Neuroreport, 13:2113-2116*.

Breveglieri R., Galletti C., Gamberini M., Passarelli L., Fattori P., (2006) Somatosensory cells in area PEc of macaque posterior parietal cortex. *J Neurosci, 26:3679-3684.*

Breveglieri R., Galletti C., Monaco S., Fattori P., (2008) Visual, somatosensory, and bimodal activities in the macaque parietal area PEc. *Cereb Cortex, 18:806-816*.

Breveglieri R., Hadjidimitrakis K., Bosco A., Sabatini SP., Galletti C., Fattori P., (2012) Eye position encoding in three-dimensional space: integration of version and vergence signals in the medial posterior parietal cortex. *J Neurosci, 32:159-169*.

Breveglieri R., Galletti C., Dal Bò G., Hadjidimitrakis K., Fattori P., (2014) Multiple aspects of neural activity during reaching preparation in the medial posterior parietal area V6A. *J Cogn Neurosci, 26:878-895*.

Brodmann K., (1909) Vergleichende lokalisationslehre der grosshirnrinde in ihren prinzipien dargestellt auf grund des zellenbaues. *Barth*.

Bruce V., Green PR., Georgeson MA., (1996) Visual perception: physiology, psychology, and ecology. *Lawrence Earlbaum Associates, Hove*.

Caplovitz GP., Tse PU., (2007) V3A processes contour curvature as a trackable feature for the perception of rotational motion. *Cereb Cortex, 17:1179-1189*.

Cardin V., Smith AT., (2011) Sensitivity of human visual cortical area V6 to stereoscopic depth gradients associated with self-motion. *J Neurophysiol, 106:1240-9*.

Cavada C., Goldman-Rakic PS., (1989a) Posterior parietal cortex in Rhesus monkey: I. Parcellation of areas based on distinctive limbic and sensory corticocortical connections. *J Comp Neurol, 287:393-421*.

Cavada C., Goldman-Rakic PS., (1989b) Posterior parietal cortex in Rhesus monkey: II. Evidence for segregated corticocortical networks linking sensory and limbic areas with the frontal lobe. *J Comp Neurol, 287:422-445*.

Cavada C., (2001) The visual parietal areas in the macaque monkey: current structural knowledge and ignorance. *Neuroimage, 14:S21-S26*.

Chen G., Wang F., Dillenburger BC., Friedman RM., Chen LM., Gore JC., Avison MJ., Roe AW., (2012) Functional magnetic resonance imaging of awake monkeys: some approaches for improving imaging quality. *Magn Reson Imaging, 30:36-47*.

Cheng K., Fujita H., Kanno I., Miura S., Tanaka K., (1995) Human cortical regions activated by wide-field visual motion: an H2(15)O PET study. *J Neurophysiol, 74:413-427*.

Colby CL., Gattass R., Olson CR., Gross CG., (1988) Topographical organization of cortical afferents to extrastriate visual area PO in the macaque: a dual tracer study. *J Comp Neurol, 269:392-413*.

Colby CL., Duhamel JR., (1991) Heterogeneity of extrastriate visual areas and multiple parietal areas in the macaque monkey. *Neuropsychologia, 29:517-537*.

Cox RW., (1996) AFNI: software for analysis and visualization of functional magnetic resonance neuroimages. *Comput Biomed Res, 29:162-173*.

Crawford JD., Henriques DY., Medendorp WP., (2011) Three-dimensional transformations for goal-directed action. *Annu Rev Neurosci, 34:309-331*.

Cui H., Andersen RA., (2011) Different representations of potential and selected motor plans by distinct parietal areas. *J Neurosci, 31:18130-6*.

Cumming BG., Johnston EB., Parker AJ., (1991) Vertical disparities and perception of three-dimensional shape. *Nature, 349:411-3*.

Cumming BG., DeAngelis GC., (2001) The physiology of stereopsis. *Annu Rev Neurosci, 24:203-38*.

Curtis CE., (2006) Prefrontal and parietal contributions to spatial working memory. *Neuroscience, 139:173-80*.

Dale AM., (1999) Optimal experimental design for event-related fMRI. *Hum Brain Mapp, 8:109-14*.

Dale AM., Fischl B., Sereno MI., (1999) Cortical surface-based analysis. I. Segmentation and surface reconstruction. *Neuroimage, 9:179-94*.

Danckert J., Goldberg L., Broderick C., (2009) Damage to superior parietal cortex impairs pointing in the sagittal plane. *Exp Brain Res, 195:183-91*.

de Jong BM., Shipp S., Skidmore B., Frackowiak RS., Zeki S., (1994) The cerebral activity related to the visual perception of forward motion in depth. *Brain, 117:1039-54*.

Debowy DJ., Ghosh S., Ro JY., Gardner EP., (2001) Comparison of neuronal firing rates in somatosensory and posterior parietal cortex during prehension. *Exp Brain Res, 137:269-91*.

Desmurget M., Epstein CM., Turner RS., Prablanc C., Alexander GE., Grafton ST., (1999) Role of the posterior parietal cortex in updating reaching movements to a visual target. *Nat Neurosci, 2:563-7*.

Doeller CF., Barry C., Burgess N., (2010) Evidence for grid cells in a human memory network. *Nature, 463:657-61*.

Dubner R., Zeki SM., (1971) Response properties and receptive fields of cells in an anatomically defined region of the superior temporal sulcus in the monkey. *Brain Res, 35:528-32*.

Duffy CJ., Wurtz RH., (1995) Response of monkey MST neurons to optic flow stimuli with shifted centers of motion. *J Neurosci, 15: 5192-208*.

Duffy CJ., (1998) MST neurons respond to optic flow and translational movement. *J Neurophysiol, 80:1816-27*.

Fattori P., Gamberini M., Kutz DF., Galletti C., (2001) 'Arm-Reaching' neurons in the parietal area V6A of the macaque monkey. *Eur J Neurosci, 13:2309-13*.

Fattori P., Breveglieri R., Amoroso K., Galletti C., (2004) Evidence for both reaching and grasping activity in the medial parieto-occipital cortex of the macaque. *Eur J Neurosci, 20:2457-66*.

Fattori P., Kutz DF., Breveglieri R., Marzocchi N., Galletti C., (2005) Spatial tuning of reaching activity in the medial parieto-occipital cortex (area V6A) of macaque monkey. *Eur J Neurosci, 22:956-72*.

Fattori P., Breveglieri R., Marzocchi N., Filippini D., Bosco A., Galletti C., (2009) Hand orientation during reach-to-grasp movements modulates neuronal activity in the medial posterior parietal area V6A. *J Neurosci, 29:1928-36*.

Fattori P., Raos V., Breveglieri R., Bosco A., Marzocchi N., Galletti C., (2010) The dorsomedial pathway is not just for reaching: grasping neurons in the medial parieto-occipital cortex of the macaque monkey. *J Neurosci, 30:342-9*.

Felleman DJ., Kaas J. H., (1984) Receptive-field properties of neurons in middle temporal visual area (MT) of owl monkeys. *J Neurophysiol, 52:488-513*.

Ferraina S., Garasto MR., Battaglia-Mayer A., Ferraresi P., Johnson PB., Lacquaniti F., Caminiti R., (1997) Visual control of hand-reaching movement: activity in parietal area 7m. *Eur J Neurosci, 9:1090-5*.

Ferraina S., Battaglia-Mayer A., Genovesio A., Marconi B., Onorati P., Caminiti R., (2001) Early coding of visuomanual coordination during reaching in parietal area PEc. *J Neurophysiol, 85:462-7*.

Ferraina S., Brunamonti E., Giusti MA., Costa S., Genovesio A., Caminiti R., (2009) Reaching in depth: hand position dominates over binocular eye position in the rostral superior parietal lobule. *J Neurosci, 29:11461-70*.

Filimon F., (2010) Human cortical control of hand movements: parietofrontal networks for reaching, grasping, and pointing. *Neuroscientist, 16:388-407*.

Fischer E., Bulthoff HH., Logothetis NK., Bartels A., (2012) Human areas V3A and V6 compensate for self-induced planar visual motion. *Neuron, 73:1228-40*.

Fischl B., Sereno MI., Dale AM., (1999) Cortical surface-based analysis. II: Inflation, flattening, and a surface-based coordinate system. *Neuroimage, 9:195-207*.

Flanders M., Soechting JF., (1990) Parcellation of sensorimotor transformations for arm movements. *J Neurosci, 10: 2420-7*.

Flanders M., Helms Tillery SI, Soechting JF., (1992) Early stages in a sensorinotor transformation. *Behav. Brain Sci., 15:309-362*.

Fluet MC., Baumann MA., Scherberger H., (2010) Context-specific grasp movement representation in macaque ventral premotor cortex. *J Neurosci, 30:15175-84*.

Foley JM., (1980) Binocular distance perception. *Psychol Rev, 87:411-34*.

Fu QG., Suarez JI., Ebner TJ., (1993) Neuronal specification of direction and distance during reaching movements in the superior precentral

premotor area and primary motor cortex of monkeys. *J Neurophysiol, 70:2097-116*.

Fu QG., Flament D., Coltz JD., Ebner TJ., (1995) Temporal encoding of movement kinematics in the discharge of primate primary motor and premotor neurons. *J Neurophysiol, 73:836-54*.

Galati G., Pappata S., Pantano P., Lenzi GL., Samson Y., Pizzamiglio L., (1999) Cortical control of optokinetic nystagmus in humans: a positron emission tomography study. *Exp Brain Res, 126:149-59*.

Galletti C., Battaglini PP., Squatrito S., Maioli MG., Aicardi G., Rapisarda C., (1984) Single unit activity and visual perception of motion. *Boll Soc Ital Biol Sper, 60:(Suppl4):59-64*.

Galletti C., Battaglini PP., Aicardi G., (1988) 'Real-motion' cells in visual area V2 of behaving macaque monkeys. *Exp Brain Res, 69:279-88*.

Galletti C., Battaglini PP., Fattori P., (1990) 'Real-motion' cells in area V3A of macaque visual cortex. *Exp Brain Res, 82:67-76.*

Galletti C., Battaglini PP., Fattori P., (1991) Functional properties of neurons in the anterior bank of the parieto-occipital sulcus of the macaque monkey. *Eur J Neurosci, 3:452-461.*

Galletti C., Battaglini PP., Fattori P., (1995) Eye position influence on the parieto-occipital area PO (V6) of the macaque monkey. *Eur J Neurosci, 7:2486-501*.

Galletti C., Fattori P., Battaglini PP., Shipp S., Zeki S., (1996) Functional demarcation of a border between areas V6 and V6A in the superior parietal gyrus of the macaque monkey. *Eur J Neurosci, 8:30-52*.

Galletti C., Fattori P., Kutz DF., Battaglini PP., (1997) Arm movement-related neurons in the visual area V6A of the macaque superior parietal lobule. *Eur J Neurosci, 9:410-3*.

Galletti C., Fattori P., Gamberini M., Kutz DF., (1999a) The cortical visual area V6: brain location and visual topography. *Eur J Neurosci, 11:3922-36*.

Galletti C., Fattori P., Kutz DF., Gamberini M., (1999b) Brain location and visual topography of cortical area V6A in the macaque monkey. *Eur J Neurosci, 11:575-82*.

Galletti C., Gamberini M., Kutz DF., Fattori P., Luppino G., Matelli M., (2001) The cortical connections of area V6: an occipito-parietal network processing visual information. *Eur J Neurosci, 13:1572-88*.

Galletti C., Kutz DF., Gamberini M., Breveglieri R., Fattori P., (2003) Role of the medial parieto-occipital cortex in the control of reaching and grasping movements. *Exp Brain Res, 153:158-70*.

Galletti C., Fattori P., (2003) Neuronal mechanisms for detection of motion in the field of view. *Neuropsychologia, 41:1717-27*.

Galletti C., Fattori P., Gamberini M., Kutz DF., (2004) The most direct visual pathway to the frontal cortex. *Cortex, 40:216-217*.

Galletti C., Gamberini M., Kutz DF., Baldinotti I., Fattori P., (2005) The relationship between V6 and PO in macaque extrastriate cortex. *Eur J Neurosci, 21:959-70*.

Galletti C., Breveglieri R., Lappe M., Bosco A., Ciavarro M., Fattori P., (2010) Covert shift of attention modulates the ongoing neural activity in a reaching area of the macaque dorsomedial visual stream. *Plos one 5(11):e15078*.

Gamberini M., Passarelli L., Fattori P., Zucchelli M., Bakola S., Luppino G., Galletti C., (2009) Cortical connections of the visuomotor parietooccipital area V6Ad of the macaque monkey. *J Comp Neurol, 513: 622-42*.

Gamberini M., Galletti C., Bosco A., Breveglieri R., Fattori P., (2011) Is the medial posterior parietal area V6A a single functional area? *J Neurosci, 31:5145-57*.

Gardner E., (1988) Somatosensory cortical mechanisms of feature detection in tactile and kinesthetic discrimination. *Canadian Journal of Physiology & Pharmacology,66:439-454*.

Gattass R., Nascimento-Silva S., Soares JG., Lima B., Jansen AK., Diogo AC., Farias MF., Botelho MM., Mariani OS., Azzi J., Fiorani M., (2005) Cortical visual areas in monkeys: location, topography, connections, columns, plasticity and cortical dynamics. *Philos Trans R Soc Lond B Biol Sci, 360:709-31*.

Genovesio A., Ferraina S., (2004) Integration of retinal disparity and fixation-distance related signals toward an egocentric coding of distance in the posterior parietal cortex of primates. *J Neurophysiol, 91:2670-84*.

Gibson JJ., (1950) The perception of the visual world. *Houghton Mifflin*.

Goense JB., Whittingstall K., Logothetis NK., (2010) Functional magnetic resonance imaging of awake behaving macaques. *Methods, 50:178-88*.

Goodale MA., Milner AD., Jakobson LS., Carey DP., (1991) A neurological dissociation between perceiving objects and grasping them. *Nature, 349:0028-0836*.

Goodale MA., Milner AD., (1992) Separate visual pathways for perception and action. *Trends Neurosci,15:0166-2236*.

Goodale MA., Jakobson LS., Milner AD., Perret DI., Benson PJ., Hietanen JK. (1994a) The nature and limits of orientation and pattern

processing supporting visuomotor control in a visual form agnosic. *J Cogn Neurosci, 6:46-56*.

Goodale MA. (1994b) Perceiving the world and grasping it: is there a difference?. *Lancet 343:930-1*.

Goodale MA., Meenan JP., Bülthoff HH., Nicolle DA., Murphy KJ., Racicot CI., (1994c) Separate neural pathways for the visual analysis of object shape in perception and prehension. *Curr Biol, 4:0960-9822*.

Goodale MA., (2011) Transforming vision into action. *Vision Res, 51:1567-87*.

Goodale MA., (2014) How (and why) the visual control of action differs from visual perception. *Proc Biol Sci, 281:1471-2954*.

Gordon J., Ghilardi MF., Ghez C., (1994). Accuracy of planar reaching movements. I. Independence of direction and extent variability. *Exp Brain Res, 99:97-111*.

Graziano MS., Andersen RA., Snowden RJ. (1994) Tuning of MST neurons to spiral motions. *J Neurosci, 14:54-67*.

Guariglia C., Piccardi., Ilaria G., Nico D., Pizzamiglio L., (2005). Representational neglect and navigation in real space. *Neuropsychologia. 43:1138-43*.

Haarmeier T., Their P., Repnow M., Petersen D. (1997) False perception of motion in a patient who cannot compensate for eye movements. *Nature 389:849-52*.

Hadj-Bouziane F., Bell AH., Knusten TA., Ungerleider LG., Tootell RB., (2008) Perception of emotional expressions is independent of face selectivity in monkey inferior temporal cortex. *Proc Natl Acad Sci U S A, 105:5591-6*.

Hadj-Bouziane F. Liu N., Bell AH., Gothard KM., Luh WM., Ungerleider LG., Tootell RB., Murray EA., (2012) Amygdala lesions disrupt modulation of functional MRI activity evoked by facial expression in the monkey inferior temporal cortex. *Proc Natl Acad Sci U S A, 109:3640-8*.

Hadj-Bouziane F. Monfardini E., Guedj C., Gardechaux G., Hynaux C., Farnè., Meunier M., (2014) The helmet head restraint system: a viable solution for resting state fMRI in awake monkeys. *Neuroimage, 86:536-43*.

Hadjidimitrakis K., Breveglieri R., Placenti G., Bosco A., Sabatini SP. Fattori P., (2011) Fix your eyes in the space you could reach: neurons in the macaque medial parietal cortex prefer gaze positions in peripersonal space. *Plos One, 6-E23335*.

Hadjidimitrakis K., Bertozzi F., Breveglieri R., Bosco A., Galletti C., Fattori P., (2014) Common neural substrate for processing depth and direction signals for reaching in the monkey medial posterior parietal cortex. *Cereb Cortex, 24:1645-57*.

Hikosaka O., Tanaka M., Sakamoto M., Iwamura Y., (1985) Manipulative behaviors induced by local injections of muscimol in the first somatosensory cortex of the conscious monkey. *Brain Research, 325:375-380*.

Holmes G., (1918) Disturbances of visual orientation. *Br J Ophthalmol, 2-449-68*.

Hwang EJ., Hauschild M., Wilke M., Andersen RA., (2012) inactivation of the Parietal Reach Region causes optic ataxia, impairing reaches but not saccades. *Neuron, 76:1021-9*.

Ilg UJ., Schumann S., Their P., (2004) Posterior parietal cortex neurons encode target motion in world-centered coordinates. *Neuron, 43:145-151*.

Ilg UJ., (2008) The role of areas MT and MST in coding of visual motion underlying the execution of smooth pursuit. *Vision Res, 48:2062-2069*.

Iwamura Y., (2000) Bilateral receptive field neurons and callosal connections in the somatosensory cortex. *Philos Trans R Soc Lond B Biol Sci, 355:267-73*.

Jeannerod M., (1994) The representing brain: neural correlates of motor intention and imagery. *Behavioral And Brain Sciences. 17:187-202*.

Johnson PB., Ferraina S., Bianchi., Caminiti R., (1996) Cortical networks for visual reaching: physiological and anatomical organization of frontal and parietal lobe arm regions. *Cereb Cortex, 6-102-19*.

Kagan I., Iyer A., Lindner A., Andersen RA., (2010) Space representation for eye movements is more contralateral in monkeys than in humans. *Proc Natl Acad Sci U S A. 107:7933-8*.

Kandel ER., Schwartz JH., Jessell TM., (2000) Principles of neural science. *Appleton & Lange, McGraw-Hill New York, 2000*.

Kase CS., Troncoso JF., Court JE., Tapia JF., Mohr JP. (1977) Global spatial disorientation. Clinico-pathologic correlations. *J Neurol Sci, 34: 267-78*.

Kleinschmidt A., Thilo KV., Büchel C., Gresty MA., Bronstein AM., Frackowiak RS., (2002) Neural correlates of visual-motion perception as object- or self-motion. *Neuroimage, 16:873-82*.

Koenderink JJ., (1986) Optic flow. *Vision Res, 26:161-79*.

Kravitz DJ., Saleem KS., Baker CI., Mishkin M., (2011) A new neural framework for visuospatial processing. *Nat Rev Neurosci, 12:217-30*.

Krubitzer L., Kahn DM., (2003) Nature versus nurture revisited: an old idea with a new twist. *Prog Neurobiol, 70:33-52*.

Krubitzer L., Disbrow E., (2008) The evolution of parietal areas involved in hand use in primates. *Somatosensation. London: Elsevier, 183-214*.

Kutz DF., Fattori P., Gamberini M., Breveglieri R., Galletti C., (2003) Early- and late-responding cells to saccadic eye movements in the cortical area V6A of macaque monkey. *Exp Brain Res, 149:83-95*.

Kutz DF., Marzocchi N., Fattori P., Cavalcanti S., Galletti C. (2005) Real-time supervisor system based on trinary logic to control experiments with behaving animals and humans. *J Neurophysiol, 93:3674-86*.

Lacquaniti F., Guigon E., Bianchi L., Ferraina S., Caminiti R., (1995) Representing spatial information for limb movement: role of area 5 in the monkey. *Cereb Cortex, 5:391-409*.

Lacquaniti F., Caminiti R., (1998) Visuo-motor transformations for arm reaching. *Eur J Neurosci,10:195-203*.

Land MF., Hayhoe M., (2001) In what ways do eye movements contribute to everyday activities? *Vision Res, 41:3559-65*.

Land MF., (2009) Vision, eye movements, and natural behavior. *Vis Neurosci, 26:51-62*.

Li Y., Cui H., (2013) Dorsal parietal area 5 encodes immediate reach in sequential arm movements. *J Neurosci, 33:14455-65*.

Logothetis NK., (1999) Functional imaging of the monkey brain. *Nat Neurosci, 2:555-62*.

Logothetis NK., (2008) What we can do and what we cannot do with fMRI. *Nature, 453:869-78*.

Luppino G., Ben Hamed S., Gamberini M., Matelli M., Galletti C., (2005) Occipital (V6) and parietal (V6A) areas in the anterior wall of the parieto-occipital sulcus of the macaque: a cytoarchitectonic study. *Eur J Neurosci, 21:3056-76*.

Macko KA., Jarvis CD., Kennedy C., Miyaoka M., Shinohara M., Sololoff L., Mishkin M., (1982) mapping the primate visual system with [2-14C] deoxyglucose. *Science 218:394-7*.

Marconi B., Genovesio A., Battaglia-Mayer A., Ferraina S., Squatrito S., Molinari M., Lacquaniti F., Caminiti R., (2001) Eye-hand coordination during reaching. I. Anatomical relationships between parietal and frontal cortex. *Cereb Cortex, 11: 513-27*.

Marino L., Connor RC., Fordyce RE., Herman LM., Hof PR., Lefebvre L., Lusseau D., McCowan B., Nimchinsky EA., Pack AA., Rendell L., Reidenberg JS., Reiss D., Uhen MD., Van Der Gucht E., Whitehead H., (2007) Cetaceans have complex brains for complex cognition. *Plos Biol, 5:E139*.

Marshall JC., Halligan PW., (1995) Seeing the forest but only half the trees? *Nature, 373:521-523*.

Marzocchi N., Breveglieri R., Galletti C., Fattori P., (2008) Reaching activity in parietal area V6A of macaque: eye influence on arm activity or retinocentric coding of reaching movements? *Eur J Neurosci, 27:775-89*.

Matelli M., Govoni P., Galletti C., Kutz DF., Luppino G., (1998) Superior area 6 afferents from the superior parietal lobule in the macaque monkey. *J Comp Neurol, 402:327-52*.

Maunsell JH., Van Essen DC., (1983a) Functional properties of neurons in middle temporal visual area of the macaque monkey. I. selectivity for stimulus direction, speed, and orientation. *J Neurophysiol, 49:1127-47*.

Maunsell JH., Van Essen DC., (1983b) Functional properties of neurons in middle temporal visual area of the macaque monkey. II. Binocular interactions and sensitivity to binocular disparity. *J Neurophysiol, 49:1148-67*.

Maunsell JH., Van Essen DC., (1983c) The connections of the middle temporal visual area (MT) and their relationship to a cortical hierarchy in the macaque monkey. *J Neurosci, 3:2563-86*.

McLaren DG., Kosmatka KJ., Oakes TR., Kroenke CD., Kohama SG., Matochik JA., Ingram DK., Johonson Sc. (2009) A population-average MRI-based atlas collection of the Rhesus macaque. *Neuroimage, 45:52-9*.

Messier J., Kalaska J F., (2000) Covariation of primate dorsal premotor cell activity with direction and amplitude during a memorized-delay reaching task. *J Neurophysiol, 84:152-65*.

Milner AD., Perrett DI., Johnston RS., Benson PJ., Jordan TR., Heeley DW., Bettucci D., Mortara F., Mutani R., Terazzi E., (1991). Perception and action in 'visual form agnosia'. *Brain, 114:405-28*.

Mishkin M., Ungerleider LG., Macko KA., (1983) Object vision and spatial vision: two cortical pathways. *Trends In Neurosciences, 6:414-417*.

Moffett A., Ettlinger G., Morton HB., Piercy MF., (1967) Tactile discrimination performance in the monkey: the effect of ablation of various subdivisions of posterior parietal cortex. *Cortex, 3:59-96*.

Monaco S., Kròlickaz G., Quinlan DJ., Fattori P., Galletti P., Goodale MA., Culham JC., (2010) Contribution of visual and proprioceptive information to the precision of reaching movements. *Exp Brain Res, 202:15-32*.

Morrone MC., Tosetti M., Montanaro D., Fiorentini A., Cioni G., Burr DC., (2000) A Cortical area that responds specifically to optic flow, revealed by fMRI. *Nat Neurosci, 3:1322-8*.

Mountcastle VB., Andersen RA., Motter BC., (1981) The influence of attentive fixation upon the excitability of the light-sensitive neurons of the posterior parietal cortex. *J Neurosci, 1:1218-25*.

Murray EA., Coulter J. (1981) Supplementary sensory area. *Cortical Sensory Organization, Multiple somatic areas (Woolsey CN, ed) Clifton, NJ: Humana, 1:167-195*.

Nakamura K., Chung HH., Graziano MS., Gross CG., (1999). Dynamic representation of eye position in the parieto-occipital sulcus. *J Neurophysiol, 81:2374-85*.

Nakamura H., Kuroda T., Wakita M., Kusunoki M., Kato A., Mikami A., Sakata H., Itoh K. (2001) From three-dimensional space vision to prehensile hand movements: the lateral intraparietal area links the area V3A and the anterior intraparietal area in macaques. *J Neurosci, 21:8174-87*.

Newsome WT., Paré EB., (1988) Selective impairment of motion perception following lesions of the middle temporal visual area (MT). *J Neurosci, 8:2201-11*.

Nelson R., Activity of monkey primary somatosensory cortical neurons changes prior to active movement. *Brain Research, 406:402-407*.

O'Mara SM., Rolls ET., Berthoz A., Kesner RP., (1994) Neurons responding to whole-body motion in the primate hippocampus. *J Neurosci, 14:6511-23*.

Orban GA., (2002) Functional MRI in the awake monkey: the missing link. *J Cogn Neurosci, 14:965-9*.

Orban GA., Fize D., Peuskens H., Denys K., Nelissen K., Sunaert S., Todd J., Vanduffel W., (2003) Similarities and differences in motion processing between the human and macaque brain: evidence from fMRI. *Neuropsychologia, 41:1757-68*.

Orban GA., Janssen P., Vogels R., (2006) Extracting 3D structure from disparity. *Trends Neurosci, 29:466-73*.

Padberg J., Franca JG., Cooke DF., Soares JG., Rosa MG., Fiorani M., Gattass R., Krubitzer L., (2007) Parallel evolution of cortical areas involved in skilled hand use. *J Neurosci, 27:10106-15*.

Pandya DN., Seltzer B., (1982) Intrinsic connections and architectonics of posterior parietal cortex in the Rhesus monkey. *J Comp Neurol, 204:196-210*.

Passarelli L., Rosa MG., Gamberini M., Bakola S., Burman KJ., Fattori P., Galletti C., (2011) Cortical connections of area V6Av in the macaque: a visual-input node to the eye/hand coordination system. *J Neurosci, 31:1790-801*.

Perenin MT., Vighetto A., (1988) Optic ataxia: a specific disruption in visuomotor mechanisms. I. Different aspects of the deficit in reaching for objects. *Brain, 111:643-74*.

Pisella L., Gréa H., Tilikete C., Vighetto A., Desmurget M., Rode G., Boisson D., Rossetti Y., (2000) An 'automatic pilot' for the hand in human posterior parietal cortex: toward reinterpreting optic ataxia. *Nat Neurosci, 3:729-36*.

Pitzalis S., Galletti C., Huang RS., Patria F., Committeri G., Galati G., Fattori P., Sereno MI., (2006) Wide-field retinotopy defines human cortical visual area V6. *J Neurosci, 26:7962-73*.

Pitzalis S., Sereno MI., Committeri G., Fattori P., Galati G., Patria F., Galletti C., (2010) Human V6: the medial motion area. *Cereb Cortex, 20:411-24*.

Pitzalis S., Fattori P., Galletti C., (2012a) The functional role of the medial motion area V6. *Front Behav Neurosci, 6:91:1-13*.

Pitzalis S., Strappini F., De Gasperis M., Bultrini A., Di Russo F., (2012b) Spatio-temporal brain mapping of motion-onset VEPs combined with fMRI and retinotopic maps. *Plos One, 7:E35771*.

Pitzalis S., Bozzacchi C., Bultrini A., Fattori P., Galletti C., Di Russo F., (2013) Parallel motion signals to the medial and lateral motion areas V6 and MT+. *Neuroimage, 67:89-100*.

Poggio GE., (1995) Mechanisms of stereopsis in monkey visual cortex. *Cereb Cortex, 5:193-204*.

Pons TP., Garraghty PE., Cusick CG., Kaas JH., (1985) the somatotopic organization of area 2 in macaque monkeys. *J Comp Neurol, 241:445-466*.

Pons TP., Kaas JH., (1986) Corticocortical connections of area 2 of somatosensory cortex in macaque monkeys: a correlative anatomical and electrophysiological study. *J Comp Neurol, 248: 313-35*.

Pouget A., Sejnowski TJ., (1994) A neural model of the cortical representation of egocentric distance. *Cereb Cortex, 4:314-29*.

Raffi M., Squatrito S., Maioli MG., (2002) neuronal responses to optic flow in the monkey parietal area PEc. *Cereb Cortex, 12:639-46*.

Raffi M., Ballabeni A., Maioli MG., Squatrito S., (2008) Neuronal responses in macaque area PEc to saccades and eye position. *Neuroscience, 156:413-24*.

Richer F., Martinez M., Cohen H., Saint-Hilaire JM., (1991) Visual motion perception from stimulation of the human medial parieto-occipital cortex. *Exp Brain Res, 87:649-52*.

Rizzolatti G., Cattaneo L., Fabbri-Destro M., Rozzi S., (2014) Cortical mechanisms underlying the organization of goal-directed actions and mirror neuron-based action understanding. *Physiol Rev, 94:655-706*.

Rosa MG., Tweedale R., (2005) Brain maps, great and small: lessons from comparative studies of primate visual cortical organization. *Philos Trans R Soc Lond B Biol Sci, 360:665-91*.

Rosenbaum DA., (1980) Human movement initiation: specification of arm, direction, and extent. *J Exp Psychol Gen, 109:444-74*.

Rossetti Y., Pisella L., Vighetto A., (2003) Optic ataxia revisited: visually guided action versus immediate visuomotor control. *Exp Brain Res, 153:171-9.*

Rozzi S., Calzavara R., Belmalih A., Borra E., Gregoriou GG., Matelli M., Luppino G., (2006) Cortical connections of the inferior parietal cortical convexity of the macaque monkey. *Cereb Cortex, 16:1389-417*.

Rozzi S., Ferrari PF., Bonini L., Rizzolatti G., Fogassi L., (2008) Functional organization of inferior parietal lobule convexity in the macaque monkey: electrophysiological characterization of motor, sensory and mirror responses and their correlation with cytoarchitectonic areas. *Eur J Neurosci, 28:1569-88*.

Rushworth MF., Nixon PD., Passingham RE., (1997a) Parietal Cortex and movement. I. Movement selection and reaching. *Exp Brain Res, 117:292-310*.

Rushworth MF., Nixon PD., Passingham RE., (1997b) Parietal cortex and movement. II. Spatial representation. *Exp Brain Res, 117:311-23*.

Rushworth MF., Johansen-Berg H., Young SA., (1998) Parietal Cortex And Spatial-Postural transformation during arm movements. *J Neurophysiol, 79:478-82*.

Sainburg RL., Lateiner JE., Latash ML., Bagesteiro LB., (2003) Effects of altering initial position on movement direction and extent. *J Neurophysiol, 89:401-15*.

Sakata H., Shibutani H., Kawano K., (1980) Spatial properties of visual fixation neurons in posterior parietal association cortex of the Monkey. *J Neurophysiol, 43:1654-72*.

Saleem KS., Logothetis NK., (2012) A combined MRI and histology atlas of the Rhesus monkey brain in stereotaxic coordinates. *Academic Press, 2nd edition*.

Schall JD., Morel A., King DJ., Bullier J., (1995) Topography of visual cortex connections with frontal eye field in macaque: convergence and segregation of processing streams. *J Neurosci, 15:4464-87*.

Sdoia S., Pitzalis S., Bultrini A., Di Russo F., Fattori P., Galati G., Galletti C., (2009) Sensitivity to optic flow components in human cortical area V6 and other cortical motion areas. *Neuroimage, 47:S86*.

Seelke AM., Padberg JJ., Disbrow E., Purnell SM., Recanzone G., Krubitzer L., (2012) Topographic maps within brodmann's area 5 of macaque monkeys. *Cereb Cortex, 22:1834-50*.

Sereno MI., Dale AM., Reppas JB., Kwong KK., Belliveau JW., Brady TJ., Rosen BR., Tootell RB., (1995) Borders of multiple visual areas in humans revealed by functional magnetic resonance imaging. *Science, 268:889-93*.

Sereno MI., Pitzalis S., Martinez A., (2001) Mapping of contralateral space in retinotopic coordinates by a parietal cortical area in humans. *Science, 294:1350-4*.

Sereno MI., Trinath T., Augath M., Logothetis NK., (2002) Three-dimensional shape representation in monkey cortex. *Neuron, 33: 635-52*.

Shipp S., Zeki S., (1989a) The organization of connections between areas V5 and V1 in macaque monkey visual cortex. *Eur J Neurosci, 1:309-32*.

Shipp S., Zeki S., (1989b) The organization of connections between areas V5 and V2 in macaque monkey visual cortex. *Eur J Neurosci, 1:333-54*.

Snyder LH., Batista AP., Andersen RA., (1997) Coding of intention in the posterior parietal cortex. *Nature, 386:167-70*.

Snyder LH., Batista AP., Andersen RA., (1998) Change in motor plan, without a change in the spatial locus of attention, modulates activity in posterior parietal cortex. *J Neurophysiol, 79:2814-9*.

Snyder LH., Batista AP., Andersen RA., (2000) Saccade-related activity in the Parietal Reach Region. *J Neurophysiol, 83:1099-102*.

Sober SJ., Sabes PN., (2005) Flexible strategies for sensory integration during motor planning. *Nat Neurosci, 8:490-7*.

Soechting JF., Flanders M., (1989) Sensorimotor representations for pointing to targets in three-dimensional space. *J Neurophysiol, 62:582-94*.

Squatrito S., Raffi M., Maioli MG., Battaglia-Mayer A., (2001) Visual motion responses of neurons in the caudal area PE of macaque monkeys. *J Neurosci, 21:RC130*.

Stark M., (1996) Impairment of an egocentric map of locations: implications for perception and action. *Cognitive Neuropsychology, 13:481-524*.

Stefanacci L., Reber P., Costanza J., Wong E., Buxton R., Zola S., Squire L., Albright T., (1998) fMRI of monkey visual cortex. *Neuron, 20:1051-7*.

Stoewer S., Goense J., Keliris GA., Bartels A., Logothetis NK., Duncan J., Sigala N., (2012) An analysis approach for high-field fMRI data from awake non-human primates. *Plos One, 7:E29697*.

Sugita Y., (2004) Contextual modulation in the V1 real motion cells. *Neuroreport, 15:2219-22*.

Suzuki H., Azuma M., (1976) A glass-insulated "Elgiloy" microelectrode for recording unit activity in chronic monkey experiments. *Electroencephalogr Clin Neurophysiol, 41:93-5*.

Their P., Erickson RG., (1992) Responses of visual-tracking neurons from cortical area MST-I to visual, eye and head motion. *Eur J Neurosci, 4:539-553*.

Tillery SI., Soechting JF., Ebner TJ., (1996) Somatosensory Cortical activity in relation to arm posture: nonuniform spatial tuning. *J Neurophysiol, 76:2423-38*.

Toda T., Taoka M., (2001) The complexity of receptive fields of periodontal mechanoreceptive neurons in the postcentral area 2 of conscious macaque monkey brains. *Archives of Oral Biology, 46:1079-1084.*

Toda T., Taoka M., (2002) Integration of the upper and lower lips in the postcentral area 2 of conscious macaque monkeys (Macaca fuscata). *Archives of Oral Biology, 47:449-456*.

Tootell RB., Reppas JB., Kwong KK., Malach R., Born RT., Brady TJ., Rosen BR., Belliveau JW., (1995) Functional analysis of human MT and related visual cortical areas using magnetic resonance imaging. *J Neurosci, 15:3215-30*.

Tootell RB., Mendola JD., Hadjikhani NK., Ledden PJ., Liu AK., Reppas JB., Sereno MI., Dale AM, (1997) Functional analysis of V3A and related areas in human visual cortex. *J Neurosci, 17:7060-78*.

Treue S., Andersen RA., (1996) Neural responses to velocity gradients in macaque cortical area MT. *Vis Neurosci, 13:797-804*.

Trotter Y., Celebrini S., Stricanne B., Thorpe S., Imbert M., (1992) Modulation of neural stereoscopic processing in primate area V1 by the viewing distance. *Science, 257:1279-81*.

Trotter Y., Celebrini S., (1999) Gaze direction controls response gain in primary visual-cortex neurons. *Nature, 398:239-42*.

Ungerleider LG., Mishkin M., (1982) Two cortical visual systems. Analysis Of Visual Behavior, *(eds Ingle DJ, Goodale MA, Mansfield RJW) 549-586: MIT Press, Cambridge, MA*.

Ungerleider LG., Desimone R., (1986a) Cortical connections of visual area MT in the macaque. *J Comp Neurol, 248:190-222*.

Ungerleider LG., Desimone R., (1986b) Projections to the superior temporal sulcus from the central and peripheral field representations of V1 and V2. *J Comp Neurol, 248:147-63*.

van Beers RJ., Sittig AC., Denier van der Gon JJ., (1998) The precision of proprioceptive position sense. *Exp Brain Res, 122:367-77*.

van Beers RJ., Wolpert DM., Haggard P., (2002) When feeling is more important than seeing in sensorimotor adaptation. *Curr Biol, 12:834-7*.

van Beers RJ., Haggard P., Wolpert DM., (2004) The role of execution noise in movement variability. *J Neurophysiol, 91:1050-63*.

Van Essen DC., Drury HA., Dickson J., Harwell J., Hanlon D., Anderson CH., (2001) An integrated software suite for surface-based analyses of cerebral cortex. *J Am Med Inform Assoc, 8:443-59*.

Van Pelt S., Medendorp WP., (2008) Updating target distance across eye movements in depth. *J Neurophysiol, 99:2281-22*90.

Vanduffel W., Fize D., Mandeville JB., Nelissen K., Van Hecke P., Rosen BR., Tootell RB., Orban GA., (2001) Visual motion processing investigated using contrast agent-enhanced fMRI in awake behaving monkeys. *Neuron, 32:565-77*.

Vanduffel W., Fize D., Peuskens H., Denys K., Sunaert S., Todd JT., Orban GA., (2002) Extracting 3D from motion: differences in human and monkey intraparietal cortex. *Science, 298:413-5*.

Verdon V., Schwartz S., Lovblad KO., Hauert CA., Vuilleumier P., (2010) Neuroanatomy of hemispatial neglect and its functional

components: a study using voxel-based lesion-symptom mapping. *Brain, 133:880-94*.

Vindras P., Desmurget M., Viviani P., (2005) Error parsing in visuomotor pointing reveals independent processing of amplitude and direction. *J Neurophysiol, 94:1212-24*.

Vingerhoets G., (2014) Contribution of the posterior parietal cortex in reaching, grasping, and using objects and tools. *Front Psychol, 5:2-17*.

Vogt BA., Pandya DN., (1987) Cingulate cortex of the Rhesus monkey: II. Cortical afferents. *J Comp Neurol, 262:271-89*.

Wall MB., Smith AT., (2008) The representation of egomotion in the human brain. *Curr Biol, 18:191-4*.

Wandell BA., Dumoulin SO., Brewer AA., (2007) Visual field maps in human cortex. *Neuron, 56:366-83*.

Wiest G., Zimprich F., Prayer D., Czech T., Serles W., Baumgartner C., (2004) Vestibular processing in human paramedian precuneus as shown by electrical cortical stimulation. *Neurology, 62:473-5*.

Wise SP., Boussaoud D., Johnson PB., Caminiti R., (1997) Premotor and parietal cortex: corticocortical connectivity and combinatorial computations. *Annu Rev Neurosci, 20:25-42*.

Zar JH., (1999) Biostatistical analysis. *Upper Saddle River, New Jersey: Prentice-Hall: Xi, V. 661, 212:11*.

Zeki SM., (1974) Functional organization of a visual area in the posterior bank of the superior temporal sulcus of the Rhesus monkey. *J Physiol, 236:549-73*.

Zihl J., von Cramon D., Mai N., (1983) Selective disturbance of movement vision after bilateral brain damage. *Brain, 106:(Pt 2):313-40*.